LBL-11865
SAC-48
UC-70

SWEDISH-AMERICAN COOPERATIVE PROGRAM ON RADIOACTIVE WASTE STORAGE IN MINED CAVERNS IN CRYSTALLINE ROCK

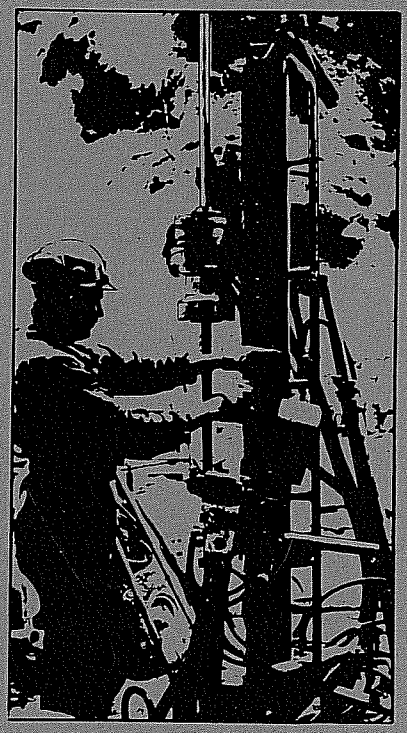

Technical Information Report No. 48

EFFECTS OF SAMPLE SIZE ON THE STRESS-PERMEABILITY RELATIONSHIP FOR NATURAL FRACTURES

J.E. Gale and K.G. Raven

Department of Earth Sciences
University of Waterloo
Waterloo, Ontario, Canada

October 1980

A Joint Project of

Swedish Nuclear Fuel Supply Co.
Fack 10240 Stockholm, Sweden

Operated for the Swedish
Nuclear Power Utility Industry

Lawrence Berkeley Laboratory
Earth Sciences Division
University of California
Berkeley, California 94720, USA

Operated for the U.S. Department of
Energy under Contract DE-AC03-76SF00098

This report was prepared as an account of work sponsored by the United States Government and/or the Swedish Nuclear Fuel Supply Company. Neither the United States nor the U.S. Department of Energy, nor the Swedish Nuclear Fuel Supply Company, nor any of their employees, nor any of their contractors, subcontractors, or their employees, makes any warranty, express or implied or assumes any legal liability or responsibility for the accuracy, completeness or usefulness of any information, apparatus, product or process disclosed, or represents that its use would not infringe privately owned rights.

Printed in the United States of America
Available from
National Technical Information Service
U.S. Department of Commerce
5285 Port Royal Road
Springfield, VA 22161
Price Code: A06

Lawrence Berkeley Laboratory is an equal opportunity employer.

LBL-11865
SAC-48
UC-70

EFFECTS OF SAMPLE SIZE ON THE STRESS-PERMEABILITY RELATIONSHIP FOR NATURAL FRACTURES

J. E. Gale[1] and K. G. Raven

Department of Earth Sciences
University of Waterloo
Waterloo, Ontario, Canada

Prepared for
Lawrence Berkeley Laboratory
University of California
Berkeley, California 94720

[1]Now at:

Department of Earth Sciences
Memorial University of Newfoundland
St. John's, Newfoundland, Canada A1B 3X5

October, 1980

This work was supported by the Assistant Secretary for Nuclear Energy, Office of Civilian Work Management, U.S. Department of Energy under Contract No. DE-AC03-76SF00098. Funding for this project was administered by the Office of Crystalline Repository Development at Battelle Memorial Institute.

PREFACE

This report is one of a series documenting the results of the Swedish-American cooperative research program in which the cooperating scientists explore the geological, geophysical, hydrological, geochemical, and structural effects anticipated from the use of a large crystalline rock mass as a geologic repository for nuclear waste. This program has been sponsored by the Swedish Nuclear Power Utilities through the Swedish Nuclear Fuel Supply Company (SKBF), and the U.S. Department of Energy (DOE) through the Lawrence Berkeley Laboratory.

The principal investigators are L.B. Nilsson and O. Degerman for SKBF, and N.G.W. Cook, P.A. Witherspoon, and J.E. Gale for LBL. Other participants will appear as authors of the individual reports.

Previous technical reports in this series are listed below.

1. Swedish-American Cooperative Program on Radioactive Waste Storage in Mined Caverns by P.A. Witherspoon and O. Degerman. (LBL-7049, SAC-01).

2. Large Scale Permeability Test of the Granite in the Stripa Mine and Thermal Conductivity Test by Lars Lundstrom and Haken Stille. (LBL-7052, SAC-02).

3. The Mechanical Properties of the Stripa Granite by Graham Swan. (LBL-7074, SAC-03).

4. Stress Measurements in the Stripa Granite by Hans Carlsson. (LBL-7078, SAC-04).

5. Borehole Drilling and Related Activities at the Stripa Mine by P.J. Kurfurst, T. Hugo-Persson, and G. Rudolph. (LBL-7080, SAC-05).

6. A Pilot Heater Test in the Stripa Granite by Hans Carlsson. (LBL-7086, SAC-06).

7. An Analysis of Measured Values for the State of Stress in the Earth's Crust by Dennis B. Jamison and Neville G.W. Cook. (LBL-7071, SAC-07).

8. Mining Methods Used in the Underground Tunnels and Test Rooms at Stripa by B. Andersson and P.A. Halen. (LBL-7081, SAC-08).

9. Theoretical Temperature Fields for the Stripa Heater Project by T. Chan, Neville G.W. Cook, and C.F. Tsang. (LBL-7082, SAC-09).

10. Mechanical and Thermal Design Considerations for Radioactive Waste Repositories in Hard Rock. Part I: An Appraisal of Hard Rock for Potential Underground Repositories of Radioactive Waste by N.G.W. Cook; Part II: In Situ Heating Experiments in Hard Rock: Their Objectives and Design by N.G.W. Cook and P.A. Witherspoon. (LBL-7073, SAC-10).

11. Full-Scale and Time-Scale Heating Experiments at Stripa: Preliminary Results by N.G.W. Cook and M. Hood. (LBL-7072, SAC-11).

12. Geochemistry and Isotope Hydrology of Groundwaters in the Stripa Granite: Results and Preliminary Interpretation by P. Fritz, J.F. Barker, and J.E. Gale. (LBL-8285, SAC-12).

13. Electrical Heaters for Thermo-Mechanical Tests at the Stripa Mine by R.H. Burleigh, E.P. Binnall, A.O. DuBois, D.O. Norgren, and A.R. Ortiz. (LBL-7063, SAC-13).

14. Data Acquisition, Handling, and Display for the Heater Experiments at Stripa by Maurice B. McEvoy. (LBL-7063, SAC-14).

15. An Approach to the Fracture Hydrology at Stripa: Preliminary Results by J.E. Gale and P.A. Witherspoon. (LBL-7079, SAC-15).

16. Preliminary Report on Geophysical and Mechanical Borehole Measurements at Stripa by P. Nelson, B. Paulsson, R. Rachiele, L. Andersson, T. Schrauf, W. Hustrulid, O. Duran, and K.A. Magnussen. (LBL-8280, SAC-16).

17. Observations of a Potential Size-Effect in Experimental Determination of the Hydraulic Properties of Fractures by P.A. Witherspoon, C.H. Amick, J.E. Gale, and K. Iwai. (LBL-8571, SAC-17).

18. Rock Mass Characterization for Storage in Nucler Waste in Granite by P.A. Witherspoon, P. Nelson, T. Doe, R. Thorpe, B. Paulsson, J.E. Gale, and C. Forster. (LBL-8570, SAC-18).

19. Fracture Detection in Crystalline Rock Using Ultrasonic Shear Waves by K.H. Waters, S.P. Palmer, and W.F. Farrell. (LBL-7051, SAC-19).

20. Characterization of Discontinuities in the Stripa Granite--Time Scale Heater Experiment by R. Thorpe. (LBL-7083, SAC-20).

21. Geology and Fracture System at Stripa by A. Okliewicz, J.E. Gale, R. Thorpe, and B. Paulsson. (LBL-8907, SAC-21).

22. Calculated Thermally Induced Displacements and Stresses for Heater Experiements at Stripa by T. Chan and N.G.W. Cook. (LBL-7061, SAC-22).

23. Validity of Cubic Law for Fluid Flow in a Deformable Rock Fracture by P.A. Witherspoon, J. Wang, K. Iwai, and J.E. Gale. (LBL-9557, SAC-23).

24. Determination of In-Situ Thermal Properties of Stripa Granite from Temperature Measurements in the Full-Scale Heater Experiments: Methods and Primary Results by J. Jeffry, T. Chan, N.G.W. Cook and P.A. Witherspoon. (LBL-8424, SAC-24).

25. Instrumentation Evaluation, Calibration, and Installation for Heater Tests Simulating Nuclear Waste in Crystalline Rock, Sweden by T. Schrauf, H. Pratt, E. Simonson, W. Hustrulid, P. Nelson, A. DuBois, E. Binnall, and R. Haught. (LBL-8313, SAC-25)

26. Part I: Some Results From a Field Investigation of Thermo-Mechanical Loading of a Rock Mass When Heater Canisters are Emplaced in the Rock by M. Hood. Part II: The Application of Field Data from Heater Experiments Conducted at Stripa, Sweden for Repository Design by M. Hood, H. Carlsson, and P.H. Nelson. (LBL-9392, SAC-26).

27. Progress with Field Investigations at Stripa by P.A. Witherspoon, N.G.W. Cook, and J.E. Gale (LBL-10559, SAC-27).

28. A Laboratory Assessment of the Use of Borehole Pressure Transients to Measure the Permeability of Fractured Rock Masses by C.B. Forster and J.E. Gale. (LBL-8674, SAC-28).

29. Thermal and Thermomechanical Data for In Situ Heater Experiments at Stripa, Sweden by T. Chan, E. Binnall, P. Nelson, O. Wan, C. Weaver, K. Ang, J. Braley, and M. McEvoy. (LBL-11477, SAC-29).

30. The Effect of Radon Transport in Groundwater Upon Gamma Ray Borehole Logs by P.H. Nelson, R. Rachiele, and A. Smith. (LBL-11180, SAC-30).

31. Strength and Permeability Tests on Ultra-Large Stripa Granite Core by R. Thorpe, D.J. Watkins, W.E. Ralph, R. Hsu, and S. Flexser. (LBL-11203, SAC-31).

32. Ultrasonic and Acoustic Emission Results from the Stripa Heater Experiments. Part I: A Cross-Hole Investigation of a Rock Mass Subjected to Heating by B.N.P. Paulsson and M.S. King. Part II: Acoustic Emission Monitoring During Cool-Down of the Stripa Heater Experiment by R. Rachiele. (LBL-10975, SAC-32).

33. Numerical Modeling to Assess Possible Influence of the Mine Openings on Far-Field In Situ Stress Measurements at Stripa by T. Chan, V. Guvanasen, and N. Littlestone (LBL-12469, SAC-33).

34. A Field Assessment of the Use of Borehole Pressure Transients to Measure the Permeability of Fractured Rock Masses by C.B. Forster and J.E. Gale. (LBL-11829, SAC-34).

35. Water Inflow into Boreholes During the Stripa Experiments by P.H. Nelson, R. Rachiele, J.S. Remer and H.S. Carlsson. (LBL-12547, SAC-35).

36. Petrology and Radiogeology of the Stripa Pluton by H. Wollenberg, S. Flexser, and L. Andersson. (LBL-11654, SAC-36).

37. Geohydrological Data from the Macopermeability Experiment at Stripa, Sweden by C.R. Wilson, J.C.S. Long, R.M. Galbraith, K. Karasaki, H.K. Endo, A.O. DuBois, M.J. McPherson, and G. Ramqvist. (LBL-12520, SAC-37).

38. Characterization of Discontinuities in the Stripa Granite--Full-Scale Heater Experiments by B.N.P. Paulsson, P.H. Nelson, and P.J. Kurfurst. (LBL-9063, SAC-38).

39. Application of Borehole Geophysics at an Experimental Waste Storage Site by P.H. Nelson, K.A. Magnusson, and R. Rachiele. (LBL-11982, SAC-39).

40. Laboratory Investigations of Thermomechanical Properties of Stripa Granite by L. Myer and R. Rachiele. (LBL-13435, SAC-40)

41. Petrologic Changes and Damage in the Stripa Quartz Monzonite in Response to Heater Tests by S. Flexser, H. Wollenberg, and D.E. Wedge. (LBL-14929, SAC-41).

42. Fracture Mapping in the Ventilation Drift at Stripa: Procedures and Results by A. Rouleau, J.E. Gale, and J. Baleshta. (LBL-13071, SAC-42).

43. Thermal Analysis of the Stripa Heater Test Data from the Full Scale Drift by I. Javandel and P.A. Witherspoon. (LBL-13217, SAC-43).

44. In Situ Stress Measurements at the Stripa Mine, Sweden by T.W. Doe, K. Ingevald, L. Strindell, B. Leijon, W. Hustrulid, A. Tarikka, M. Holmberg, E. Majer, and H. Carlsson. (LBL-15009, SAC-44).

45. Fracture Detection in Crystalline Rock Using Ultrasonic Reflection Techniques by S.P. Palmer. (LBL-16347, SAC-45).

46. Fracture and Hydrology Data from Field Studies at Stripa, Sweden by J.E. Gale. (LBL-13101, SAC-46).

47. Equipment Design, Installation, and Operation for the Macropermeability Experiment at Stripa, Sweden by R.M. Galbraith, C.R. Wilson, A.O. DuBois, S.A. Lundgren, M.J. McPherson and G.W. West. (LBL-13392, SAC-47).

48. Effects of Sample Size on the Stress Permeability Relationship for Natural Fractures by J.E. Gale and K.G. Raven. (LBL-11865, SAC-48).

49. Progress with Hydrogeological Characterization of the Stripa Site by J.E. Gale, A. Rouleau, P.A. Witherspoon and C.R. Wilson. (LBL-14878, SAC-49).

50. Extensometer Performance During Heater Experiments at Stripa by A.O. DuBois, M. Hood, E.P. Binnall and L. Andersson. (LBL-13531, SAC-50).

51. Seismic Velocities and Attenuation in a Heated Underground Granitic Repository by B.N.P. Paulsson (LBL-16346 1/2, SAC-51).

CONTENTS

Page

LIST OF FIGURES ix

LIST OF TABLES xiii

ABSTRACT xv

1. INTRODUCTION 1
   1.1 The Problem: Stress-Permeability Relationships and Sample Size 1
   1.2 Previous Work 2

2. SAMPLE COLLECTION, PREPARATION, AND TESTING PROCEDURES 13

3. EXPERIMENTAL RESULTS 21
   3.1 Rock and Fracture Deformation Versus Normal Stress 21
   3.2 Fracture Flowrate and Hydraulic Conductivity Versus Normal Stress 26
   3.3 Regression Analyses 37

4. DISCUSSION 45

5. CONCLUSIONS AND RECOMMENDATIONS 55

ACKNOWLEDGMENTS 57

REFERENCES 59

APPENDIX A: SAMPLE COLLECTION, TESTING, AND MAPPING 61
   A.1 Collection and Preparation 62
   A.2 Instrumentation and Testing Procedures 65
   A.3 Surface Maps 70

APPENDIX B: REFORMATORY GRANITE AND CORE DEFORMATION DATA 77

APPENDIX C: PLOTS OF FRACTURE FLOWRATE PER UNIT HEAD AND OF HYDRAULIC CONDUCTIVITY VERSUS NORMAL STRESS FOR SAMPLES 2-4 83

APPENDIX D: STRESS-PERMEABILITY DATA 97

LIST OF FIGURES

		Page
1.1	Variation of hydraulic conductivity with normal stress across fracture in three rock specimens.	8
1.2	Effect of contact area on fracture permeability, as proposed by Witherspoon et al. (1979a).	9
1.3	The "representative elementary volume" concept.	11
2.1	Generalized bedrock geology of the St. Cloud area	14
2.2	Schematic of instrumented sample placed within loading frame and ready for testing	16
2.3	Schematic of laboratory test configuration.	18
3.1	Fracture and rock displacement as a function of normal stress; sample 1, cycles 1, 2, and 3	22
3.2	Fracture and rock displacement as a function of normal stress; sample 5, cycles 1, 2, and 3	23
3.3	Vertical stress concentration profiles above fracture plane at applied normal stress of 25 MPa, for all five samples	25
3.4	Fracture flowrate per unit head as a function of normal stress, sample 1: (a) cycle 1, (b) cycle 2, (c) cycle 3	28
3.5	Fracture flowrate per unit head as a function of normal stress, sample 5: (a) cycle 1, (b) cycle 2, (c) cycle 3	31
3.6	Fracture hydrology conductivity as a function of normal stress, sample 1, loading cycles 1, 2, and 3.	35
3.7	Fracture hydraulic conductivity as a function of normal stress, sample 5, loading cycles 1, 2, and 3.	36
4.1	Fracture hydraulic conductivity as a function of normal stress, samples 1 to 5, loading cycle 3	51

Page

4.2 Comparison of the variation of fracture hydraulic conductivity with normal stress, samples 1 and 5, with published data 53

A.1 Surface map of sample 1. 71

A.2 Surface map of sample 2. 72

A.3 Surface map of sample 3. 73

A.4 Surface map of sample 4. 74

A.5 Surface map of sample 5. 75

B.1 Fracture and rock displacement as a function of normal stress, sample 2, cycles 1, 2, and 3. 80

B.2 Fracture and rock displacement as a function of normal stress, sample 3, cycles 1, 2, and 3. 81

B.3 Fracture and rock displacement as a function of normal stress, sample 4, cycles 1, 2, and 3. 82

C.1 Fracture flowrate per unit head as a function of normal stress, sample 2, cycle 1 84

C.2 Fracture flowrate per unit head as a function of normal stress, sample 2, cycle 2 85

C.3 Fracture flowrate per unit head as a function of normal stress, sample 2, cycle 3 86

C.4 Fracture flowrate per unit head as a function of normal stress, sample 3, cycle 1 87

C.5 Fracture flowrate per unit head as a function of normal stress, sample 3, cycle 2 88

C.6 Fracture flowrate per unit head as a function of normal stress, sample 3, cycle 3 89

C.7 Fracture flowrate per unit head as a function of normal stress, sample 4, cycle 1 90

C.8 Fracture flowrate per unit head as a function of normal stress, sample 4, cycle 2 91

Page

C.9 Fracture flowrate per unit head as a function of normal stress, sample 4, cycle 3 92

C.10 Fracture hydraulic conductivity as a function of normal stress, sample 2, loading cycles 1, 2, and 3 93

C.11 Fracture hydraulic conductivity as a function of normal stress, sample 3, loading cycles 1, 2, and 3 94

C.12 Fracture hydraulic conductivity as a function of normal stress, sample 4, loading cycles 1, 2, and 3 95

LIST OF TABLES

Page

2.1 Average modal composition of Reformatory granite, St. Cloud, Minnesota 15

2.2 Dimensions of samples tested 15

3.1 Average fracture closure at maximum normal stress. 27

3.2 Summary of flowrate per unit head. 34

3.3 Constants α and β derived from regresssion analyses for the empirical relation $K_f = \beta\sigma^{-\alpha}$ 38

3.4 Constants A, α, and β, and Rss (residual sum of squares) derived from regression analyses for the empirical relation $K_f = A + \beta\sigma^{-\alpha}$. 40

3.5 Nonlinear least-squares regression with log transformation; $\log (Q/H) = \log C + n \log (2b_{res} + 2b_m)$ 43

3.6 Nonlinear least-squares regession (with 2bres fixed); $\log (Q/H) = \log C + n \log (2b_{res} + 2b_m)$ 44

A.1 Approximate normal stress increments and load cell voltage settings. 69

ABSTRACT

Five granite cores (10.0, 15.0, 19.3, 24.5, and 29.4 cm in diameter) containing natural fractures oriented normal to the core axis, were used to study the effect of sample size on the permeability of natural fractures. Each sample, taken from the same fractured plane, was subjected to three uniaxial compressive loading and unloading cycles with a maximum axial stress of 30 MPa. For each loading and unloading cycle, the flowrate through the fracture plane from a central borehole under constant (±2% of the pressure increment) injection pressures was measured at specified increments of effective normal stress.

Both fracture deformation and flowrate exhibited highly nonlinear variation with changes in normal stress. Both fracture deformation and flowrate hysteresis between loading and unloading cycles were observed for all samples, but this hysteresis decreased with successive loading cycles.

The results of this study suggest that a sample-size effect exists. Fracture deformation and flowrate data indicate that crushing of the fracture plane asperities occurs in the smaller samples because of a poorer initial distribution of contact points than in the larger samples, which deform more elastically. Steady-state flow tests also suggest a decrease in minimum fracture permeability at maximum normal stress with increasing sample size for four of the five samples. Regression analyses of the flowrate and fracture closure data suggest that deformable natural fractures deviate from the cubic relationship between fracture aperture and

flowrate and that this is especially true for low flowrates and small apertures, when the fracture sides are in intimate contact under high normal stress conditions.

In order to confirm the trends suggested in this study, it is necessary to quantify the scale and variation of fracture plane roughness and to determine, from additional laboratory studies, the degree of variation in the stress-permeability relationship between samples of the same size as well as between samples of different sizes.

1. INTRODUCTION

1.1 The Problem: Stress-Permeability Relationships and Sample Size

The flow of fluids in rock masses is important in many geotechnical and engineering geology problems. Rock slope design, mine drainage, and the effective exploration and development of oil, gas, groundwater, and geothermal resources must consider the hydraulic properties of rock masses. When a rock mass is fractured, the hydraulic properties of the fractures, as well as the intact rock blocks, must be investigated. In certain applications, such as the underground storage of radioactive waste, interconnected fractures form the dominant flow path, and detailed information on the ability of the fractures to conduct water and contaminants is essential.

The ability of a fractured medium to transport water and contaminants is controlled in part by the geometry of the fracture system and in part by the magnitude and orientation of the in-situ stress field (Gale, 1980a). The existing stress field can be changed by underground excavations, dewatering activities, and natural geological processes. These perturbations, depending on the initial state of stress, can significantly change the normal and shear stress acting across a fracture plane. Thus, it is important that we understand fully how fracture permeability varies as a function of stress.

Laboratory studies with both induced fractures (Gale, 1975; Iwai, 1976) and natural ones (Gale, 1980b), as well as a field study with natural fractures (Pratt et al., 1977) have shown that a rapid decrease in fracture permeability occurs with increase in normal stress. The fractures tested

varied in cross section from 0.02 m^2 to over 1.0 m^2. For our purposes, however, the most important finding of these studies was that, at the maximum normal stress applied, the minimum hydraulic conductivity of the fractures increased with increasing sample size, suggesting a sample-size effect (Witherspoon et al., 1979a).

Normal-stress fracture-permeability tests are usually conducted on core samples less than 0.15 m in diameter. If sample-size effects exist, current laboratory tests may be yielding stress-permeability relationships not representative of the in-situ fracture properties. Since the data summarized by Witherspoon et al. (1979a) were drawn from both natural and induced fractures in different crystalline rocks subject to different flow and boundary conditions, not all of them completely defined, the problem of a sample-size effect on the stress-permeability relationships of natural fractures remains to be isolated and resolved.

As part of a research program that investigated the effect of stress on fracture permeability in crystalline rocks, we report here on the results of a laboratory study to evaluate the effect of sample size on the normal-stress/permeability relationship of natural fractures. The report describes the test procedures, the experimental results, and our preliminary conclusions.

1.2 Previous Work

Published results on the effect of normal stress on the permeability of different sized natural and induced fractures are rare. Summaries of the few tests that have been undertaken are worth giving here.

Several investigators have reported on the variation of fracture permeability with normal stress from the results of both field and laboratory studies. Gale (1975; 1980b) and Iwai (1976) demonstrated that natural and induced fractures in granite are highly deformable and that changes in effective normal stress can produce changes in the effective low aperture or opening of fractures. Since fracture flux is a function of aperture cubed (Witherspoon et al., 1979b), small changes in fracture aperture will produce major changes in fracture flowrate.

Gale (1975) studied the effect of both fluid pressures and normal axial stress on fracture deformation, permeability, and pressure distribution, using induced fractures (wire sawed, sandblasted wire sawed, and tension) in a 0.95-m-diameter granite core. Radial divergent and radial convergent flow tests were conducted at normal stresses of 10 to 20 MPa. Fracture flux and fracture closure exhibited highly nonlinear behavior. Additional data from tests conducted on the same granite core are reported by Witherspoon et al. (1977).

Iwai (1976) investigated the effect of cyclic loading on the permeability of tension fractures in granite, marble, and basalt cores 0.15 m in diameter. Decreases in the initial and final fracture flowrates were observed with successive loading and unloading cycles. Hysteresis was also observed between loading and unloading.

In-situ field tests of the permeability of a natural fracture exposed at the surface in granite as a function of confining stress have been reported by Pratt et al. (1977). The permeability tests used two vertical boreholes drilled about 1 m apart along a vertical weathered fracture.

Stress across the fracture was controlled by flatjacks inserted in deep vertical slots cut parallel to the fracture on either side. The fracture probably extended beyond the depth of the flatjacks so that the flow field and boundary conditions of the tests were not well defined.

Several investigators have proposed empirical equations to describe the variation of fracture permeability as a function of normal stress. Jones (1975) tested artificial and natural fractures in small-diameter core samples subject to hydrostatic confining pressures up to 138 MPa. On the basis of his experimental results, he proposed an exponential relationship for the fracture permeability of carbonate rocks:

$$K = K_o \log (P_h/P)^3 \qquad (1)$$

where K_o is a constant and P_h is the effective healing pressure at which K = 0. This "effective healing pressure" is an extrapolated intercept, as Jones was unable to completely close the fractures tested.

Witherspoon et al. (1977) and Kranz et al. (1979) suggested a power-law relationship for fracture permeability of the form:

$$K_f = \beta\bar{\sigma}^{-\alpha} \qquad (2)$$

where K_f is the fracture hydraulic conductivity, $\bar{\sigma}$ is the effective normal stress, and β and α are empirically derived constants. Kranz et al. tested artificial fractures in small-diameter (3.5 cm) granite cores subjected to confining pressures up to 200 MPa. Split cylinders joined by surfaces of

controlled roughness, determined by surface grinding with different-sized cutting grits, and induced tension fractures were examined.

Nelson and Handin (1977) proposed a similar relationship for the fracture permeability of saw-cut fractures in small cores (3.7 cm diameter) of sandstone subject to maximum confining pressures of 69 MPa. Fracture permeability curves were fitted by regression analysis to a nonlinear power law of the form:

$$K = A + \beta\bar{\sigma}^{-\alpha} \tag{3}$$

where K is the fracture permeability; $\bar{\sigma}$ is the effective normal stress; and A, β, and α are empirically determined constants.

Gangi (1978) proposed a phenomenological model to account for the variation with pressure of fracture permeability. In his "bed of nails" model, a distribution of rods represented the asperities on the fracture face. With power-law distribution functions for the asperity heights, the functional dependence of fractured permeability was shown to be:

$$K = K_0[1 - (P/P_1)^m]^3 \tag{4}$$

where K_0 is the zero pressure permeability, P_1 is the effective modulus of the asperities, and m is a constant ($0 < m < 1$) that characterizes the distribution function of the asperities. Gangi's model was one of the first attempts to consider the physical mechanisms involved in fracture-permeability/stress phenomena. In his model, the composition and distribution of asperities on

the fracture plane determine the stress-permeability response of the fracture plane.

Kranz et al. (1979) have also shown that the stress-permeability relationship of artificial fractures is a function of the roughness of the fracture walls. In their study, the empirical constant α in Eq. (2) decreased with increasing surface roughness.

Iwai (1976) showed both numerically and experimentally that fracture permeability is a function of contact area. Increased contact area decreases the number of available flow paths and increases flow-path tortuosity, resulting in lower fracture permeability. Iwai found that, at low normal stress (0.26 MPa), the real area of contact of a tension fracture in a granite was less than 0.1% of the apparent total area and increased from 10 to 20% at 20 MPa normal stress. Iwai also suggested a linear variation in contact area with normal load.

Gale (1980b) has recently noted a difference in the stress-permeability relationships of induced tension fractures and natural fractures in granitic gneiss. Gale subjected cores of 0.15 m in diameter to cyclic loading and unloading. Lower minimum fracture permeabilities were observed with induced tension fractures than with natural fractures at the maximum normal stress applied in the tests. Larger net changes of fracture permeability with normal stress were also observed with the tension fractures.

Although several authors have investigated the stress-permeability relationship of fractures in small-diameter rock cores, there has been very

little effort to extend this work to flow in naturally fractured media. Witherspoon et al. (1979a), on the basis of data from Gale (1975), Witherspoon et al. (1977), Iwai (1976), and Pratt et al. (1977)--summarized in Fig. 1.1--have suggested that a scale effect exists for the stress-permeability relationships of fractures in granite. An increase in the minimum fracture hydraulic conductivity at maximum applied normal stress was noted with increasing sample size. However, as previously noted, the data summarized by Witherspoon et al. (1979a) were for both natural and induced fractures in different crystalline rocks subject to different flow and boundary conditions. The same authors have also proposed the conceptual model shown in Fig. 1.2 to account for the suggested influence of scale. With increasing sample size, the contact area expressed as a percent of the total fracture area reaches some average value for a given fracture. A sample in region B would possess the number and distribution of contact points (and thus the normal stress-permeability relationship) characteristic of the fracture plane in situ. Below the optimum sample size, in region A, there can be a variation in the percent contact area as well as its distribution over the fracture surface being tested. Witherspoon et al. propose a systematic increase in fracture permeability with increasing sample size.

A similar conceptual model developed by Hubbert (1956) and later by Bear (1972) for determining the properties of a porous medium may also be applicable to the sample-size problem in fracture permeability studies. The model (Fig. 1.3) is based on the concept of a representative elementary volume (REV). The REV is the size (u) or volume of a medium that must be

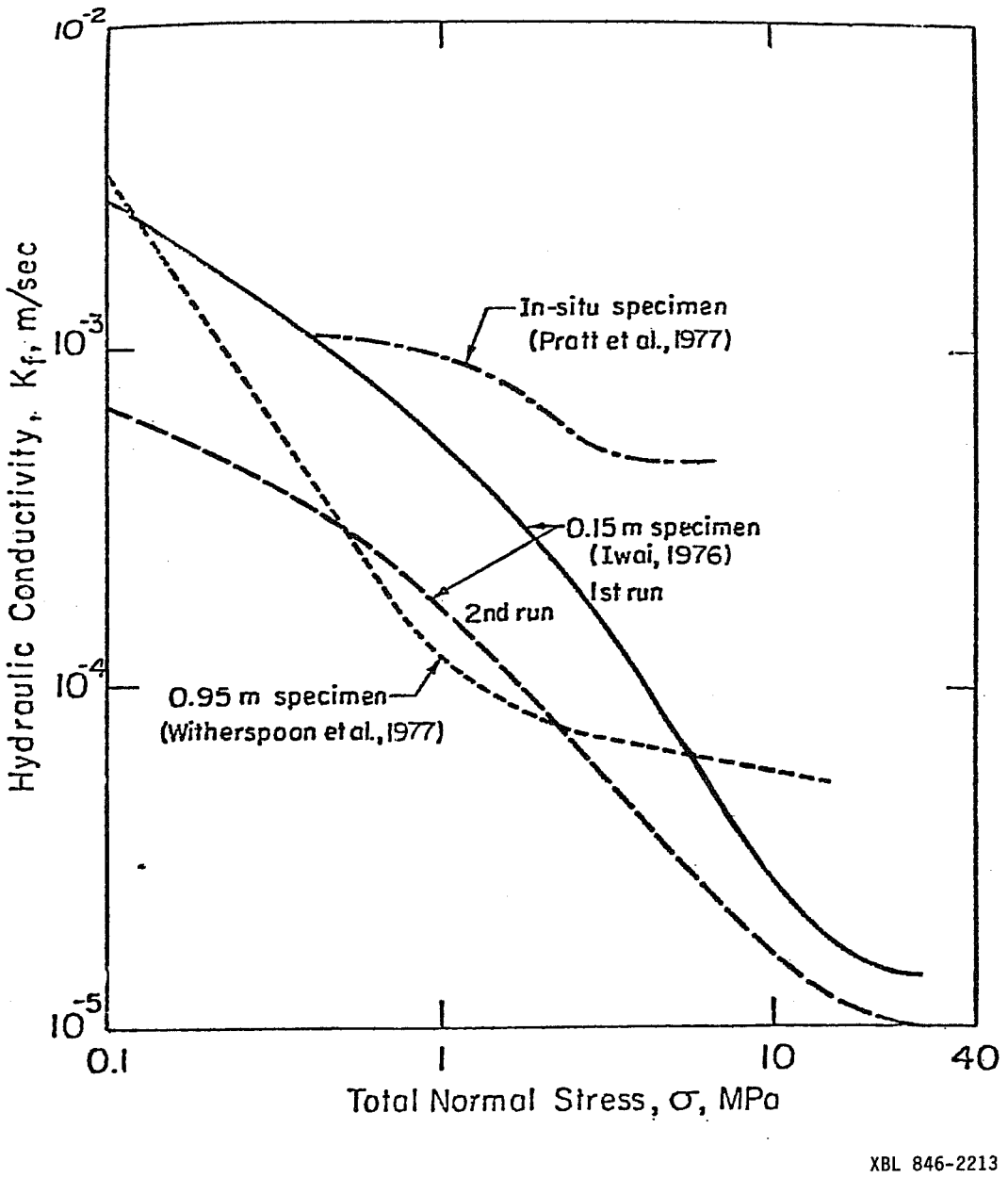

Fig. 1.1. Variation of hydraulic conductivity with normal stress across fracture in three rock specimens (after Witherspoon et al. 1979a).

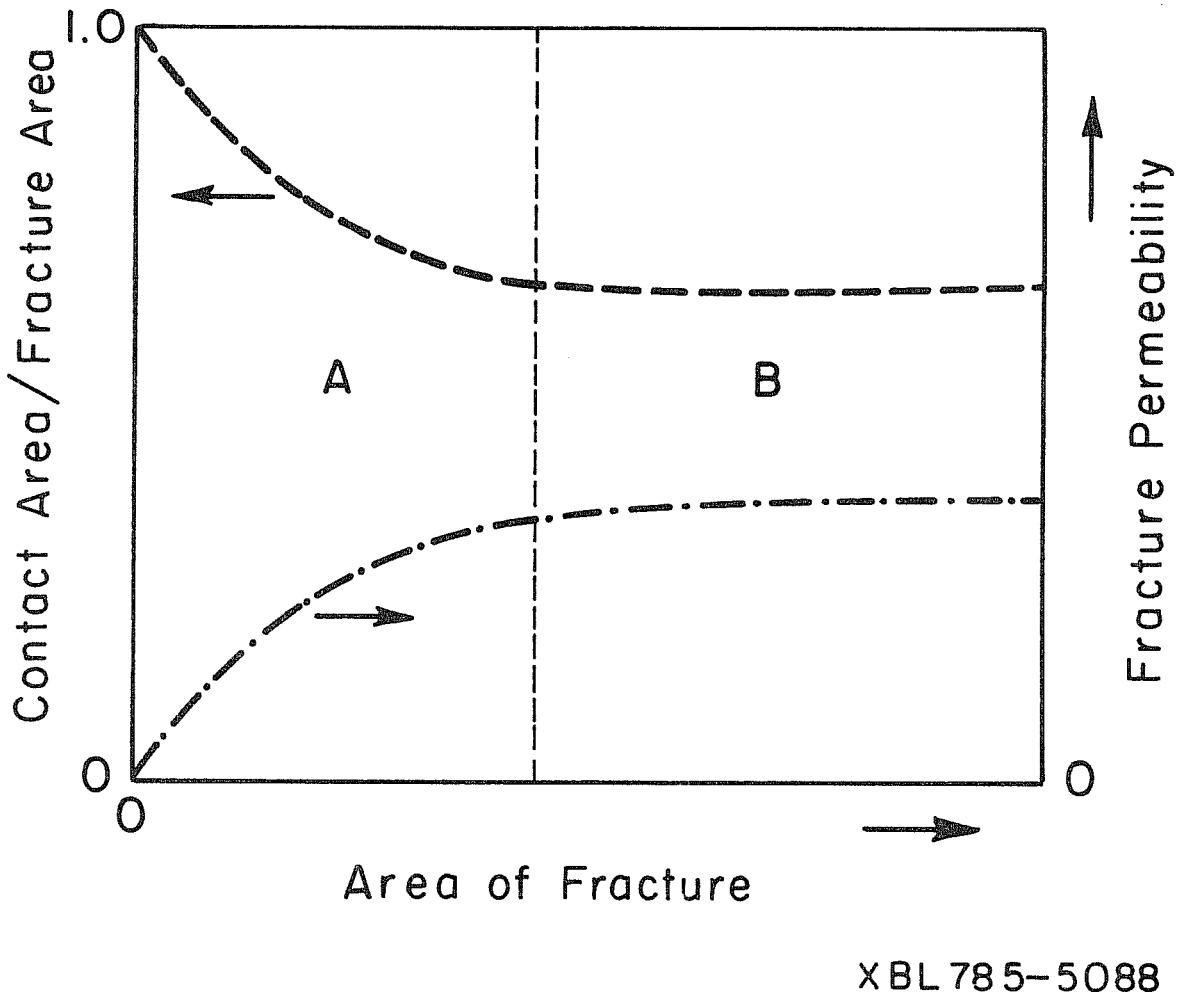

Fig. 1.2. Effect of contact area on fracture permeability, as proposed by Witherspoon et al. (1979a).

sampled in order to determine some representative property (n) of the medium. The REV is necessary because the macroscopically observed property (n) is a result of submacroscopic or microscopic processes. The characteristics of the stress-permeability relationship are a function of surface roughness and contact area. Samples from the same fracture plane with an area less than u_o in Fig. 1.3 are subject to extensive variability in permeability (K_n), reflecting the distribution of contact points in the fracture plane.

Similarly, in Bear's conceptual model, damped oscillating fracture permeability would be expected with increasing sample size for a sample fracture area less than but approaching u_o.

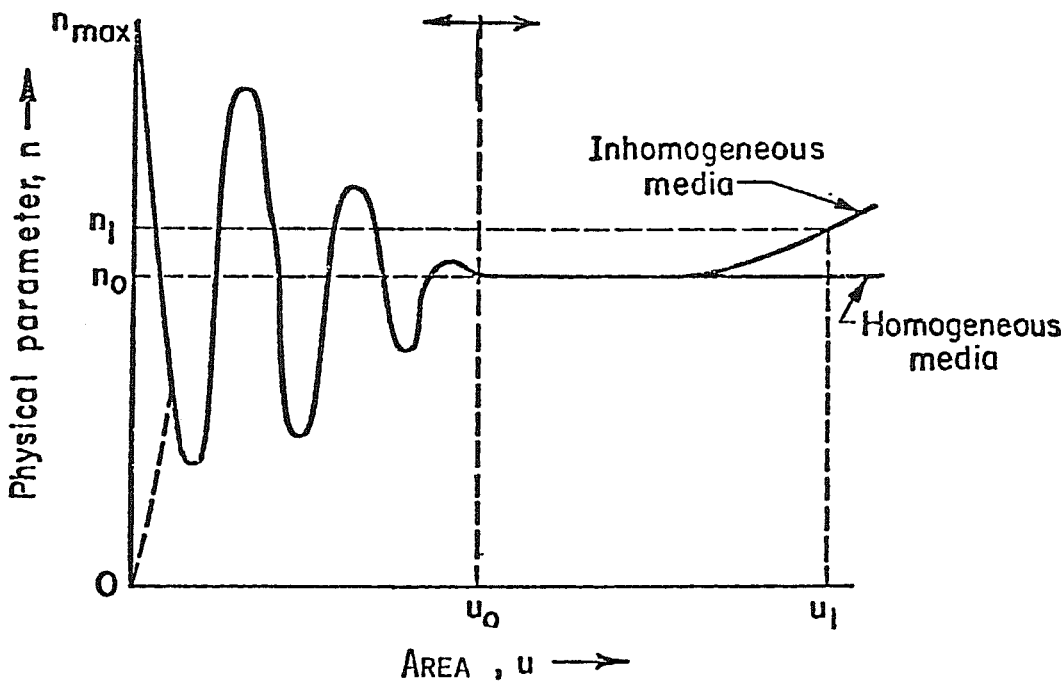

XBL 846-2214

Fig. 1.3. The "representative elementary volume" concept (after Hubbert, 1956).

2. SAMPLE COLLECTION, PREPARATION, AND TESTING PROCEDURES

Five cores were obtained from the Cold Spring Granite Company's "Charcoal Gray" granite quarry near St. Cloud, Minnesota (Fig. 2.1). Each core contained a single fracture normal to the core axis, with minor bifurcations (see maps, Appendix A.3). The trade name "Charcoal Gray" describes a gray augite hornblende granodiorite referred to by Morey (1978) as Reformatory granite. Reformatory granite is medium-grained, massive, and composed predominantly of sodic plagioclase (Table 2.1).

The five cores (10.0, 15.0, 19.3, 24.5, and 29.4 cm in diameter) were collected from the same fracture plane. These core samples, approximately 70 cm long, with natural fractures halfway down the core length, were collected using a rock-bolting, overcoring technique [Appendix A.1]. This technique consisted of drilling a center borehole and inserting a rock bolt to lock the two sides of the fracture together by exerting a compressive normal stress across the fracture plane.

The samples were prepared and instrumented [Appendix A.2] for testing in a uniaxial testing machine. End parallelism and length-to-diameter ratios of 2.1 to 1 were maintained for each sample. The dimensions of the samples are given in Table 2.2. Before testing, each sample was opened slightly to ensure that the flow path was continuous.

Figure 2.2 is a schematic of an instrumented sample placed within the loading frame and ready for testing. A 1.57-MN-capacity, closed-loop servo-controlled testing machine applied the axial loads. The applied load was measured with a 1.57-MN-capacity load cell built into the upper

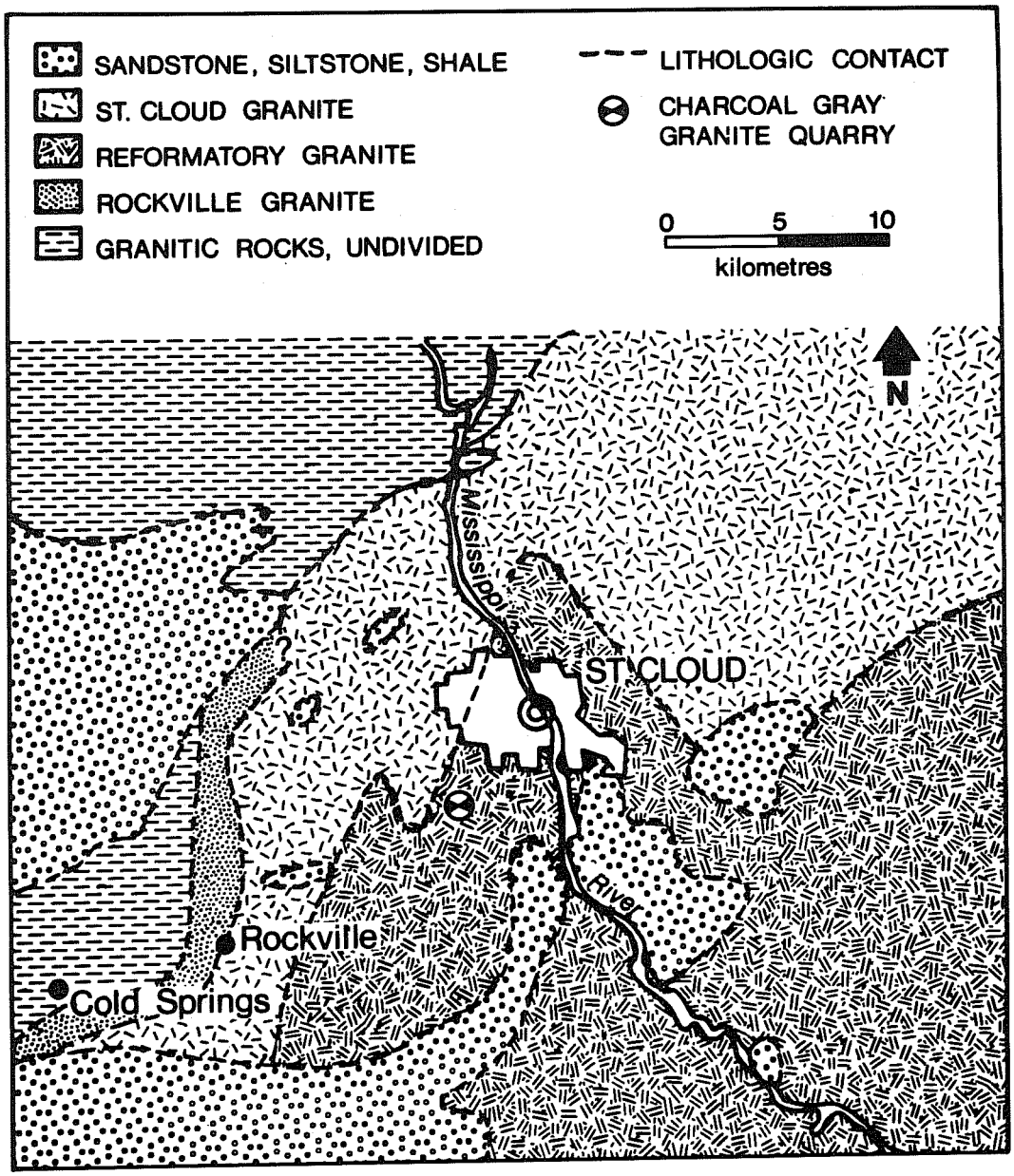

XBL 846-2215

Fig. 2.1. Generalized bedrock geology of the St. Cloud area (after Morey, 1978).

Table 2.1. Average nodal composition of Reformatory granite, St. Cloud, Minnesota (after Morey, 1978).

Mineral	Average Volume %
Sodic plagioclase	20-40
K-feldspar	25-45
Quartz	17-30
Hornblende	1-10
Biotite	1-8
Augite	1-4

Table 2.2 Dimensions of samples tested.

Sample No.	Diameter (cm)	Height (cm)	Height/Diameter Ratio	Area of Fracture Plane (cm^2)
1	10.0	21.7	2.17	76.7
2	15.0	31.6	2.11	174.4
3	19.3	41.6	2.15	290.7
4	24.5	52.4	2.14	463.0
5	29.4	63.0	2.14	671.6

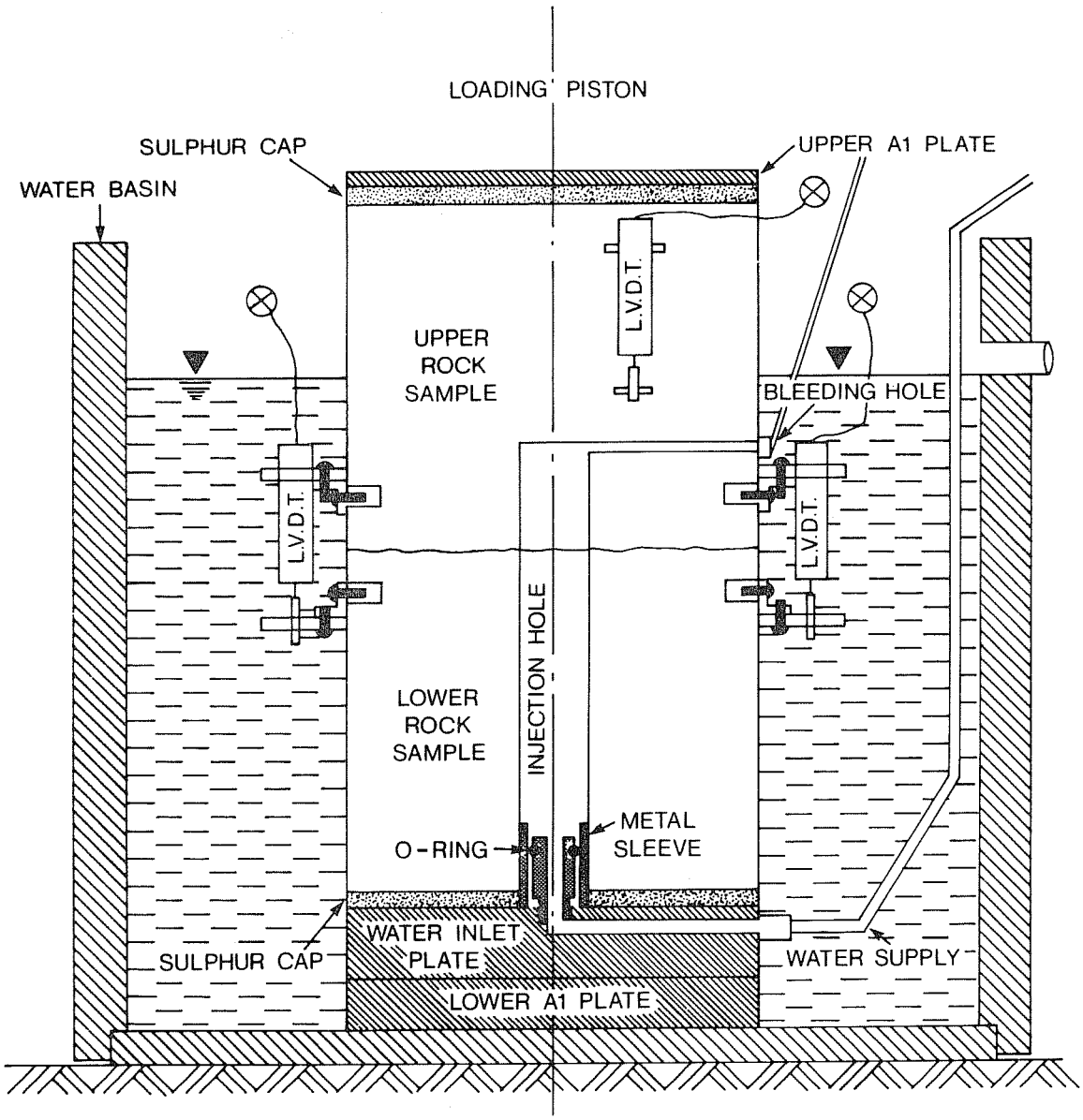

XBL 846-2217

Fig. 2.2. Schematic of instrumented sample placed within loading frame and ready for testing.

loading platen. The sample was placed in a plexiglass water tank with the water level above the fracture plane. Fracture and rock deformation across the plane were measured using three linear variable differential transformers (LVDTs) spaced 120° apart on the circumference of the fracture. The LVDTs are capable of recording deformations of less than 1 micrometer. Rock deformation and strains were measured with an LVDT and strain gauges affixed to the upper block of the fractured sample. One vertical string of strain gauges was applied to the outside of each sample to investigate the vertical stress distribution between the top of the sample and the fracture plane.

Figure 2.3 is a schematic of the laboratory test configuration. The testing equipment consisted of: (1) equipment to monitor fluid pressure and flow; (2) the sample and loading frame setup; and (3) the data acquisition system. Figure 2.3 also shows the arrangement of filters, LVDTs, pressure transducers, thermocouples, and valves. Details of the laboratory testing equipment and procedures are given in Appendix A.2.

Each sample was subjected to three cycles of incremental loading and unloading. The applied normal compressive stress levels ranged from 0.2 MPa to 30 MPa. The load capacity of the testing frame restricted the maximum normal stress for sample 5 to 23.6 MPa. At each stress level, steady-state radial flow tests from a central borehole were conducted. During each flow test, a permanent record of loads, water injection pressure, flowrate, displacement, and water temperature were recorded on punched paper tape and teletype printer. Strain-gauge readings were recorded manually.

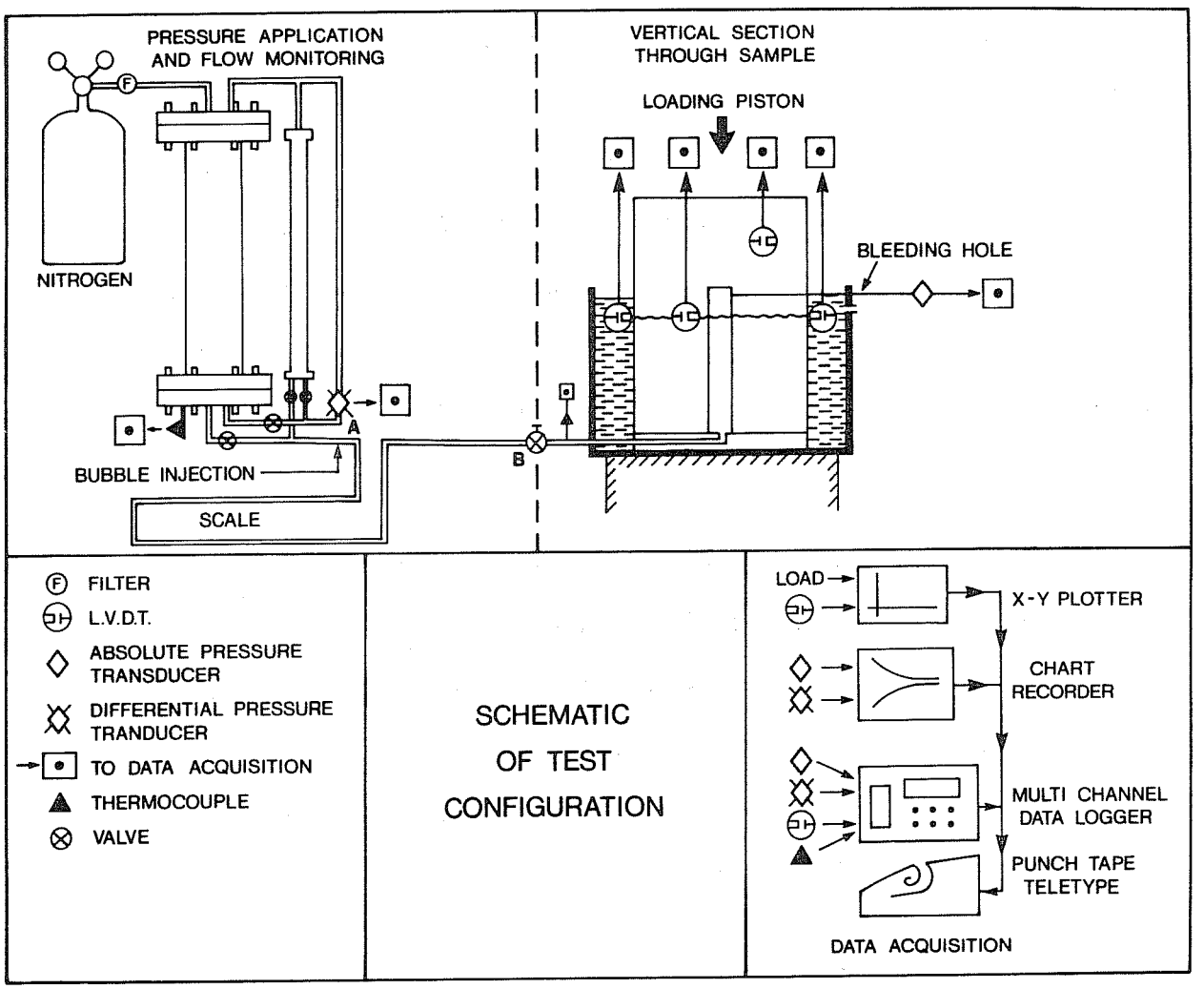

XBL 846-2245

Fig. 2.3. Schematic of laboratory test configuration.

A testing sequence at any given load increment was completed when steady readings of flowrate, fluid pressure, and applied load and displacement were achieved. A stable condition was assumed to exist if the load did not vary by more that ±0.2 kN and the fracture displacements by more than a micrometer. Stable flow rates were assumed to exist if they did not change by more than 5% over three consecutive readings (3 to 5 minutes apart) for changes in injection pressure of less than 5% for the same three readings. One full testing cycle (loading and unloading) required 8 to 16 hours to complete. Each sample was allowed to stabilize for a period of 8 to 12 hours between testing cycles until fracture displacements did not change by more than 1 micrometer over any three consecutive 5-minute readings.

3. EXPERIMENTAL RESULTS

3.1 Rock and Fracture Deformation Versus Normal Stress

Figures 3.1 and 3.2 show the relative fracture and rock deformation for the smallest and largest samples (nos. 1 and 5) for each of the three loading and unloading cycles. Fracture deformation was measured by three LVDTs mounted on anchor posts across the fracture plane; these posts were about 6.5 cm apart. Rock deformation was measured by an LVDT similarly mounted on posts about the same distance apart (See Fig. 2.2). Deformation and strain from the rock LVDT were used to subtract rock deformation from the measurements made by the fracture LVDTs. After this adjustment, the three measures of fracture deformation or closure were averaged. These averages are the fracture closures shown in Figs. 3.1 and 3.2. Similar plots for samples 2, 3, and 4 are given in Appendix B.2.

Two measures of vertical stress were used. One was based on the strain-gauge measurements taken at each stress increment during loading and unloading. From these measured vertical strains, vertical stress ($\sigma_{(m)}$) was computed by assuming linear elastic rock behavior and by using an average measurement of Young's modulus obtained from laboratory tests conducted by the Cold Spring Granite Co. (Appendix B.1). In the second approach, vertical stress ($\sigma_{(c)}$) was calculated by assuming a uniform distribution of the applied axial load over the area of the fracture plane. A comparison of these two measurements may indicate the degree to which the distribution of load over the plane was actually nonuniform.

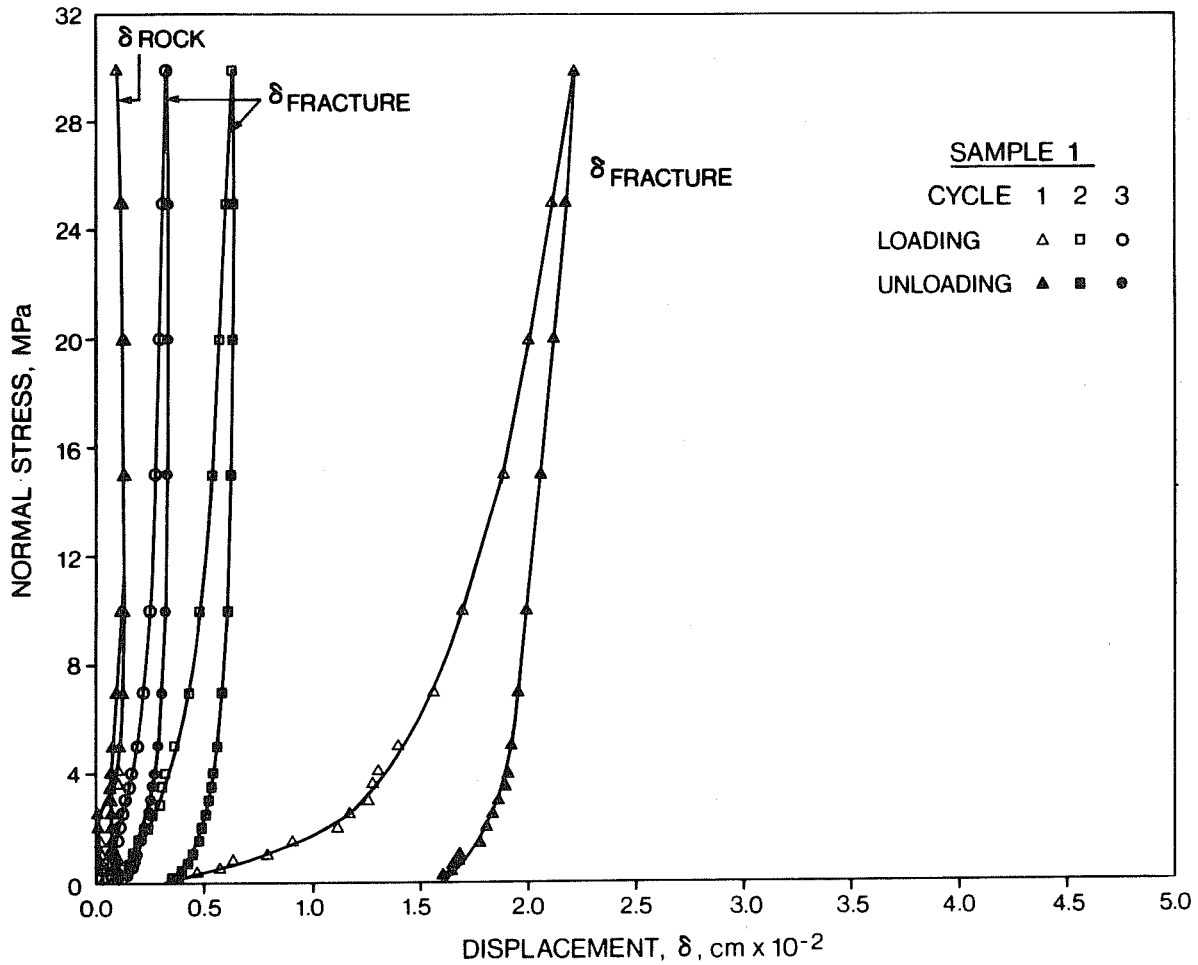

XBL 846-2219

Fig. 3.1. Fracture and rock displacement as a function of normal stress; sample 1, cycles 1, 2, and 3. Each symbol represents an increment of stress. Rock displacement is given for cycle 1 only.

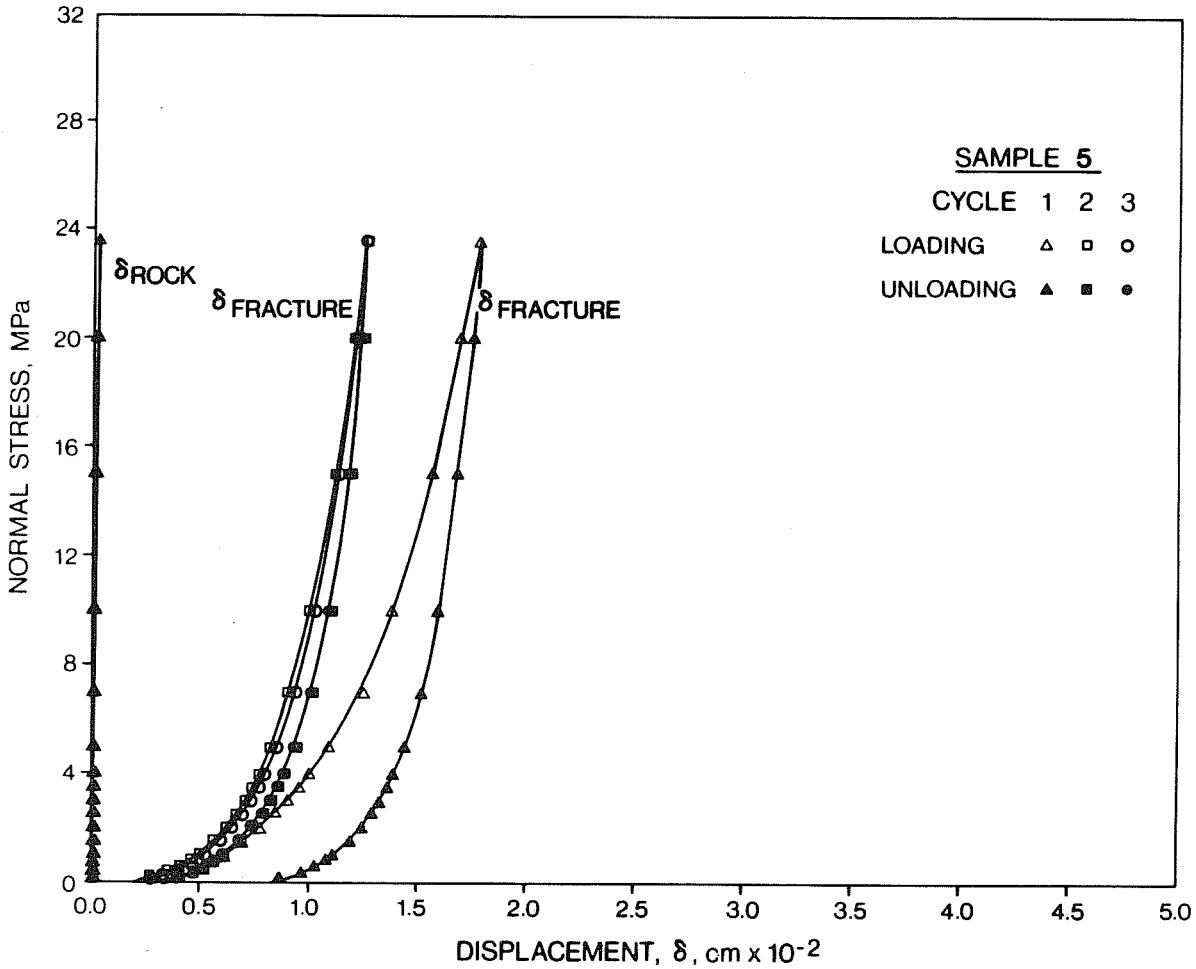

XBL 846-2220

Fig. 3.2. Fracture and rock displacement as a function of normal stress; sample 5, cycles 1, 2, and 3 (rock displacement for cycle 1 only).

Figure 3.3 shows a comparison of the measured ($\sigma_{(m)}$) and calculated ($\sigma_{(c)}$) vertical stress distribution above the fracture plane for all five samples during cycle 3 loading at a calculated vertical stress level of approximately 25 MPa. Measured and calculated stresses are compared as a ratio or stress concentration factor ($\sigma_{(m)}/\sigma_{(c)}$) versus dimensionless distance (D_N) from the fracture plane ($D_N = 0$) to the top of the sample ($D_N = 1.0$). These stress concentration profiles are similar at lower stresses to the results for the earlier loading and unloading cycles; this indicates that the distribution of load over the fracture plane did not substantially change during or between cycles.

Strain-gauge measurements were also compared with strains calculated from the rock LVDTs. In the smallest sample (no. 1), the LVDT and gauge-measured strains were similar. As sample size increased, however, the LVDT measurements declined relative to those of the strain gauges, to the point that, in the largest sample, the LVDT strains were an order of magnitude less than those of the gauges. As strain-gauge measurements for all samples are similar and close to those predicted from assumptions of linear elastic behavior, the rock LVDT measurements are probably in error, possibly because of temperature effects.

The rock LVDT measurements represent only 5% to 10% of the average fracture deformation of sample 1, decreasing to less than 1% of the average deformation for sample 5. Since initial fracture deformation is highly nonlinear, with most of the fracture closure occurring at normal stresses below 5 MPa, the probable error in LVDT-determined rock strains does not invalidate the fracture deformation measurements.

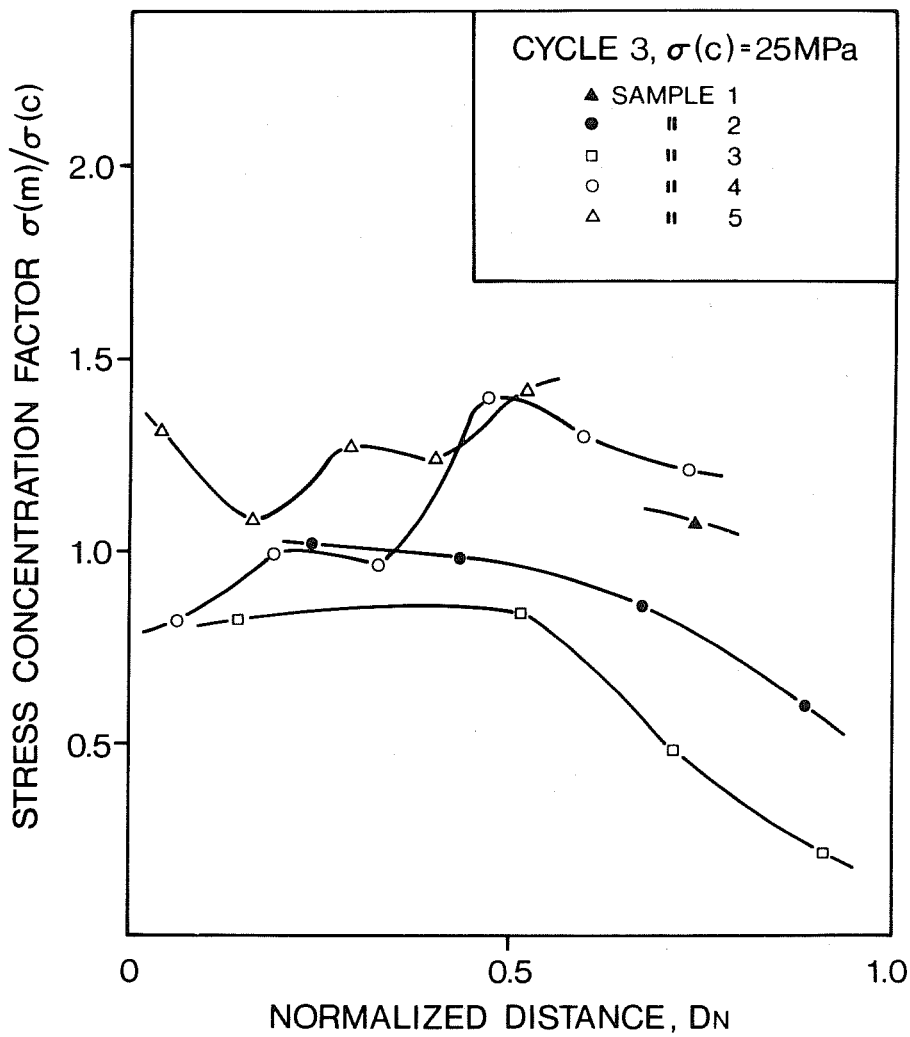

XBL 846-2218

Fig. 3.3. Vertical stress concentration profiles above fracture plane at applied normal stress of 25 MPa for all five samples.

The average fracture closure at maximum normal stress for each sample and loading cycle is summarized in Table 3.1.

3.2 Fracture Flowrate and Hydraulic Conductivity Versus Normal Stress

Semi-log plots of flowrate per unit head versus normal stress for each loading and unloading cycle for samples 1 and 5 are shown in Figs. 3.4 and 3.5. The flowrate per unit head for all samples is given in Table 3.2. Maximum flow at minimum normal stress and minimum flow at maximum normal stress are tabulated for each cycle and sample. Plots for samples 2, 3, and 4 are provided in Appendix C.

We used the parallel plate model for radial flow in a single fracture (Witherspoon et al. 1979b) to convert the data for flowrate per unit head to fracture hydraulic conductivities. Log-log plots of these conductivities versus normal stress are shown in Figs. 3.6 and 3.7 for samples 1 and 5 and for the other samples in Appendix C.

In general, fracture flowrate and hydraulic conductivity showed a nonlinear but smooth relationship with changes in normal stress. However, abrupt, nonstress-related changes in flowrate were observed during testing of sample 4, cycle 2, and sample 5, cycle 1. These are thought to be caused by clogging and clearing of the radial flow path within the fracture plane close to the central injection borehole. Redistribution of rock fragments crushed during initial loading cycles may alter the available flow aperture and effective diameter of the injection borehole.

Table 3.1. Average fracture closure at maximum normal stress ($2b_{avg.}$, cm x 10^{-2}).

Cycle	Sample				
	1	2	3	4	5
1	2.206	3.316	1.997	2.254	1.775
2	0.620	1.021	1.393	1.837	1.262
3	0.317	0.858	1.313	1.792	1.260

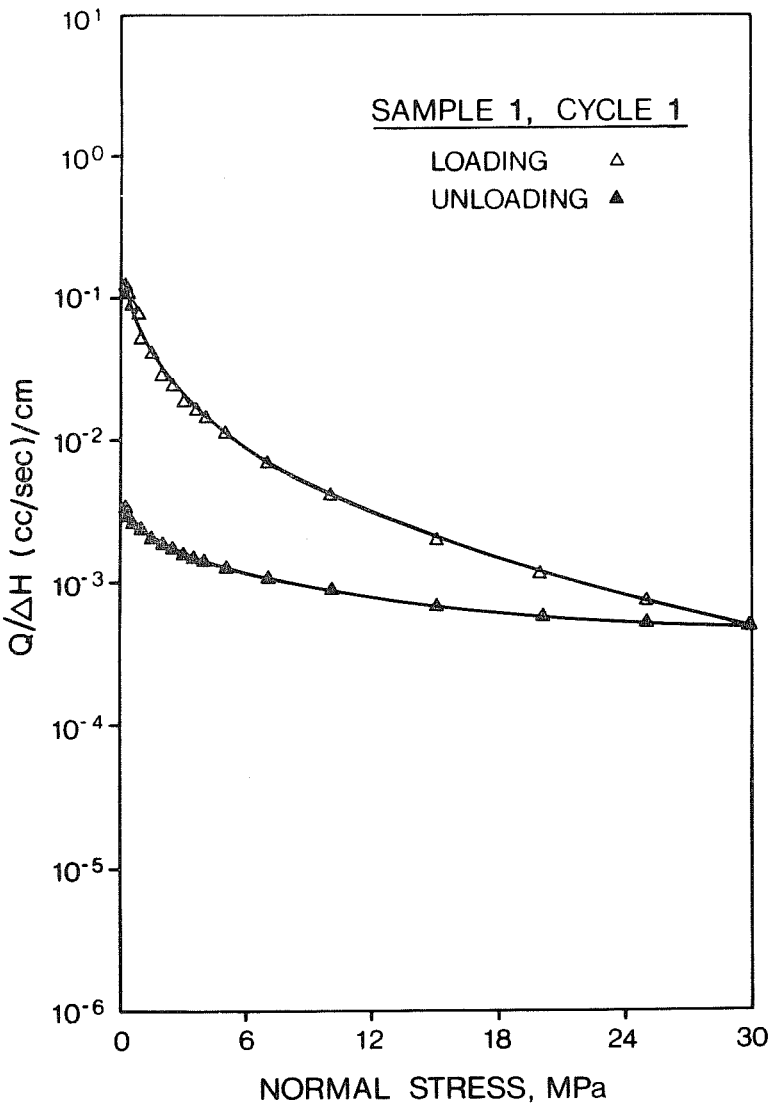

XBL 846-2244

Fig. 3.4. Fracture flowrate per unit head as a function of normal stress, sample 1: (a) cycle 1.

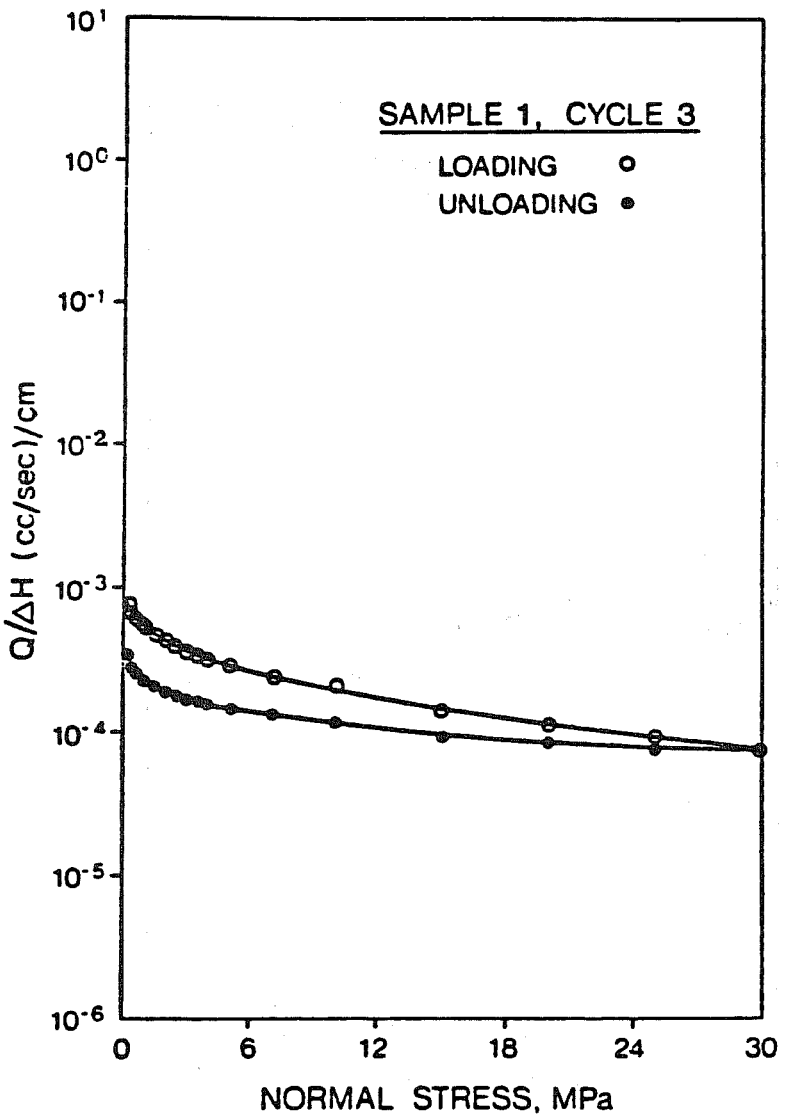

XBL 846-2242

Fig. 3.4(c). Cycle 3.

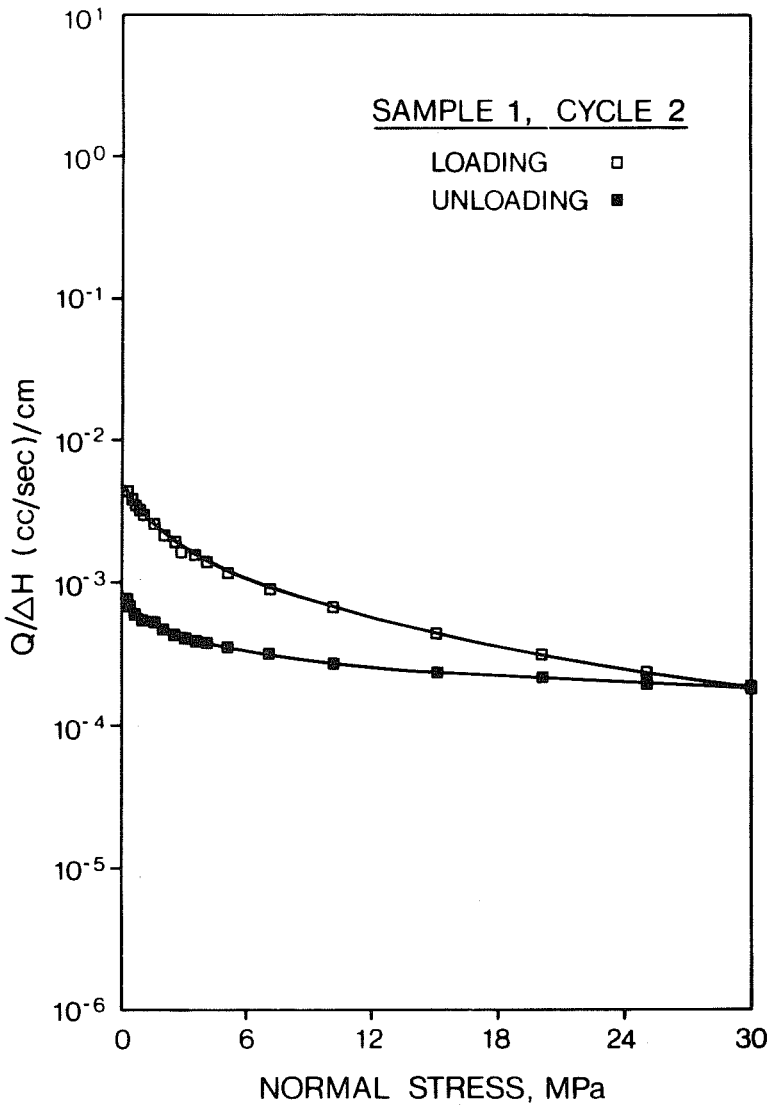

XBL 846-2243

Fig. 3.4(b). Cycle 2.

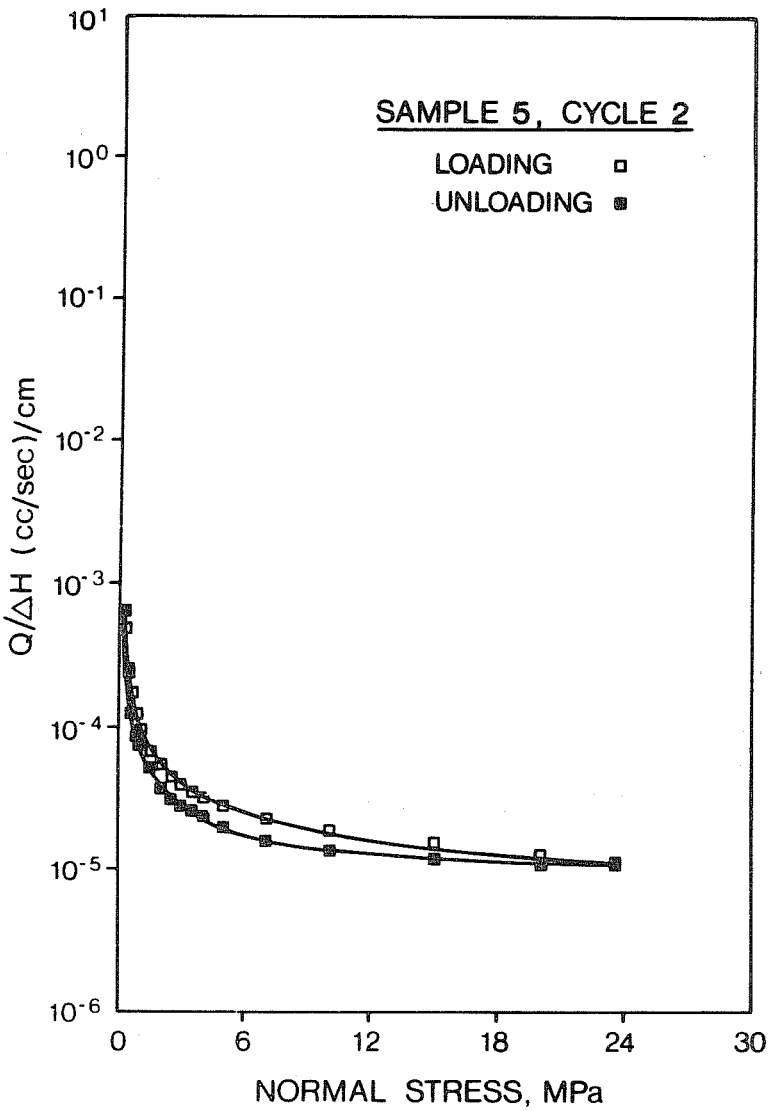

XBL 846-2240

Fig. 3.5(b). Cycle 2.

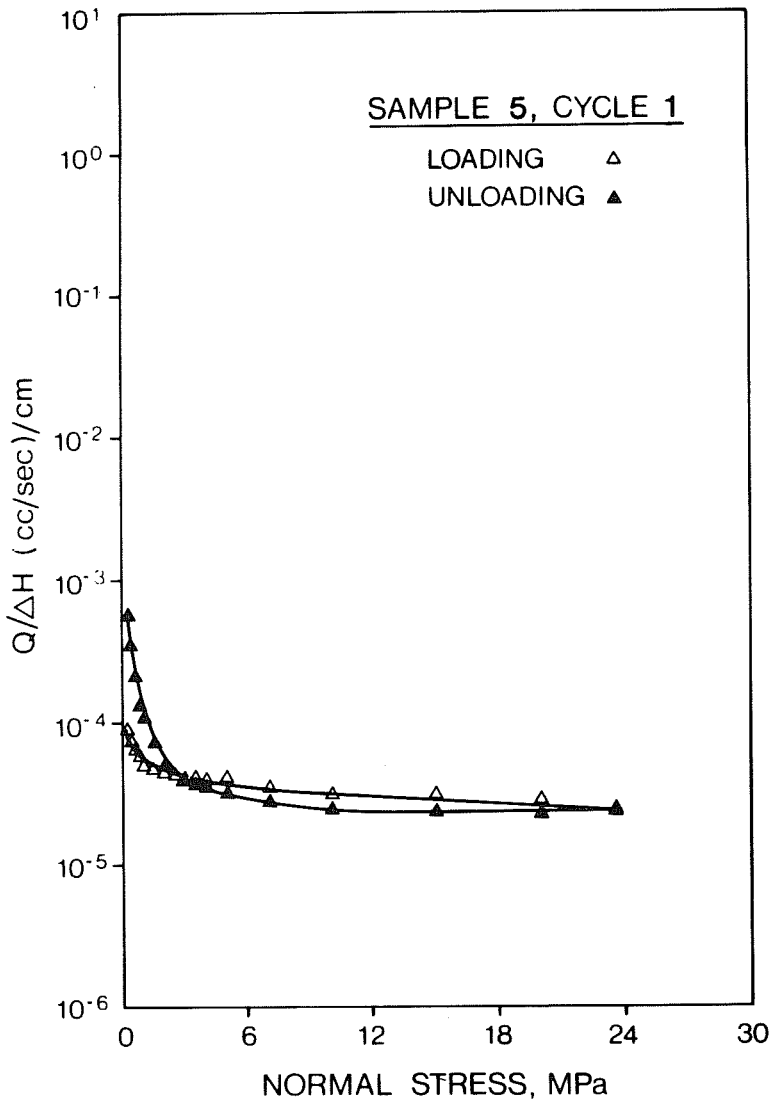

XBL 846-2241

Fig. 3.5. Fracture flowrate per unit head as a function of normal stress, sample 5: (a) cycle 1.

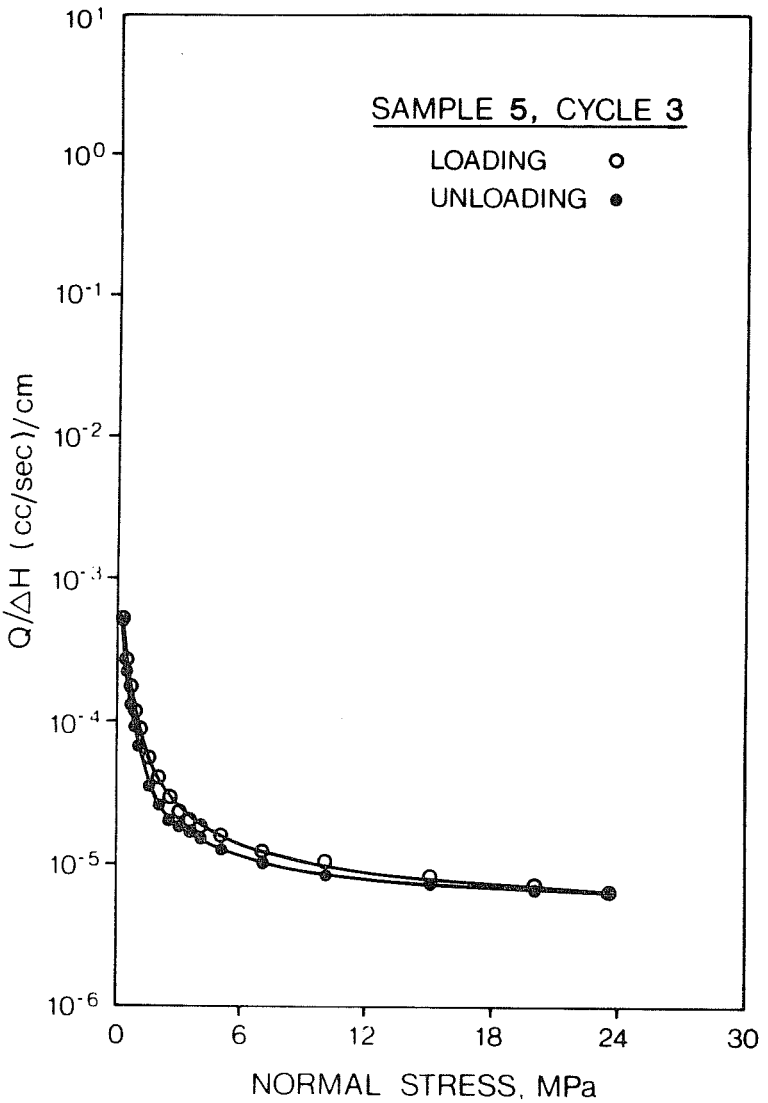

XBL 846-2239

Fig. 3.5(c). Cycle 3.

Table 3.2. Summary of flowrate per unit head, $Q/\Delta H$, (cc/sec)/cm x 10^4.

Cycle		Sample 1	2	3	4	5
1	max	1148.00	2483.00	568.90	1243.00	5.85
	min	4.85	7.20	2.98	4.86	0.24
2	max	43.56	38.04	21.60	39.20	6.15
	min	1.88	2.05	0.16	1.37	0.11
3	max	7.70	5.73	4.55	52.77	5.40
	min	0.75	0.99	0.05	1.97	0.06

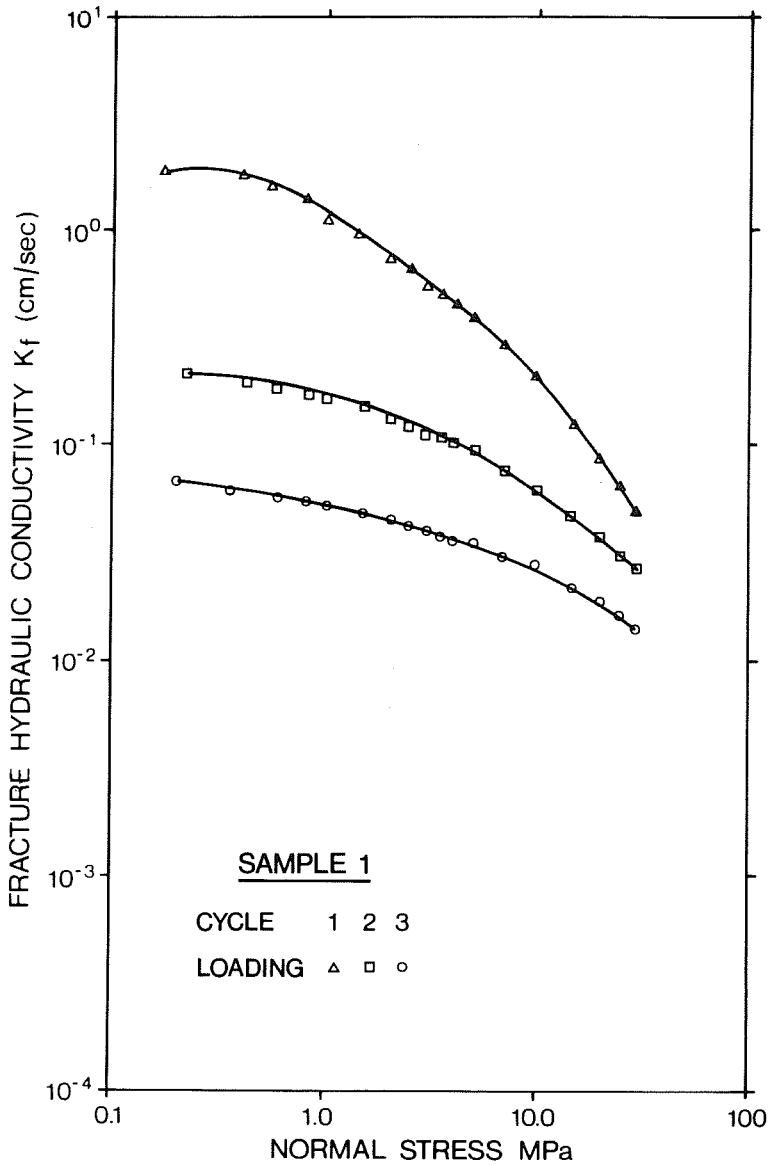

XBL 846-2238

Fig. 3.6. Fracture hydraulic conductivity as a function of normal stress, sample 1, loading cycles 1, 2, and 3.

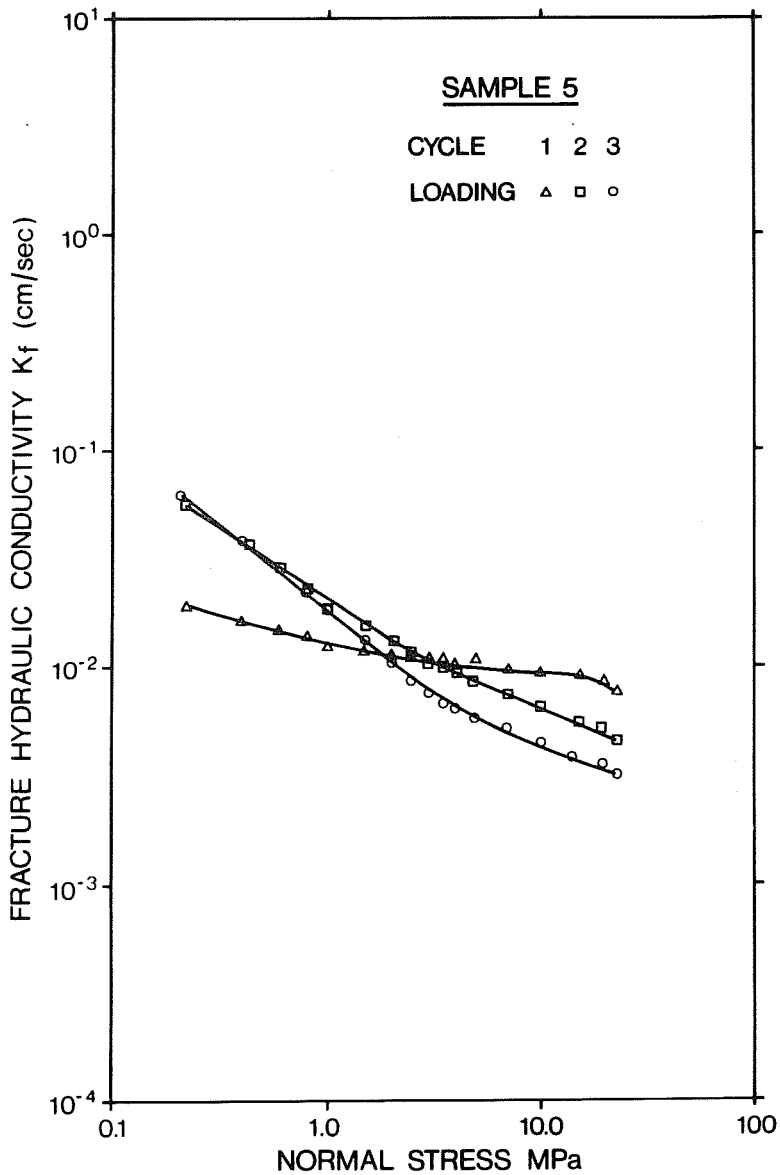

XBL 846-2237

Fig. 3.7. Fracture hydraulic conductivity as a function of normal stress, sample 5, loading cycles 1, 2, and 3.

3.3 Regression Analyses

To quantitatively evaluate the effect of sample size on the normal-stress/permeability relationship of the natural fractures tested, the fracture hydraulic conductivity and normal stress data were fitted to both linear and nonlinear power laws based on the models proposed by Witherspoon et al. (1977) and Handin (1977).

Fracture hydraulic conductivity (K_f) and total normal stress (σ) were fitted to the linear power law:

$$K_f = \beta\sigma^{-\alpha} \tag{5}$$

where β = the value of K_f at σ = 1.0 MPa and α = slope on a log K_f versus log σ diagram.

As indicated above, Eq. (5) may be linearized by log transformations, yielding:

$$\log K_f = \log \beta - \alpha \log \sigma \tag{6}$$

In this form, a linear least-squares regression analysis may be carried out to determine the slope α, intercept β, and correlation coefficient r. The resulting parameters are listed in Table 3.3.

Fracture hydraulic conductivity and total normal stress data were also fitted to a nonlinear power law of the form:

$$K_f = A + \beta\sigma^{-\alpha} \tag{7}$$

Table 3.3 Constants α and β derived from regression analyses for the empirical relation $K_f = \beta\sigma^{-\alpha}$.

Cycle		Sample 1	2	3	4	5
	β	1.15×10^{0}	1.46×10^{0}	5.70×10^{-1}	8.56×10^{-1}	1.49×10^{-2}
1	α	0.755	0.783	0.732	0.737	0.166
	r	0.970	0.994	0.989	0.997	0.984
	β	1.75×10^{-1}	1.62×10^{-1}	6.39×10^{-2}	8.75×10^{-2}	2.29×10^{-2}
2	α	0.440	0.425	0.612	0.446	0.522
	r	0.967	0.987	0.998	0.959	0.989
	β	5.62×10^{-2}	5.57×10^{-2}	1.68×10^{-2}	1.37×10^{-1}	2.04×10^{-2}
3	α	0.305	0.235	0.600	0.441	0.636
	r	0.996	0.983	0.960	0.997	0.984

Note: r = correlation coefficient, $\beta = K_f$ at 1.0 MPa in cm/sec,
α = slope in decades/decade.

where A, β, and α are regression-derived constants. A nonlinear least-squares regression analysis was used to estimate the parameters A, β, and α. Measures of the goodness of fit are indicated by the residual sum of the squares (Rss). The parameters A, β, α, and Rss for each cycle of each sample are listed in Table 3.4. In general, the fit of the nonlinear model improves with successive loading cycles and increasing sample size.

As an additional evaluation of the influence of sample size, the fracture deformation and flowrate data were analyzed to determine the validity of the cubic law for flow in deformable natural fractures. The cubic law is the relation between flowrate and aperture derived from solution of the Navier-Stokes equation for laminar flow between two parallel plates which are not in contact. As the walls of natural fractures are in contact, deviation from the cubic law may reflect the contribution of contact area to the change in fracture flowrate with changing normal stress.

In a simplified form, the cubic law may be written as:

$$Q/H = C(2b)^3 \tag{8}$$

where Q/H = flowrate per unit head through fracture,

2b = effective fracture aperture,

C = constant, which in the case of radial flow is given by

$$C = \frac{2\pi}{\ln(r_e/r_w)} \frac{\rho g}{12\mu} \tag{9}$$

Table 3.4. Constants A, α, β, and Rss (residual sum of squares) derived from regression analyses for the empirical relation $K_f = A + \beta\sigma^{-\alpha}$.

Cycle		Sample 1	2	3	4	5
	A	-1.263	-0.115	-0.125	-0.9599	0.0067
1	β	2.493	1.632	0.773	0.927	0.0079
	α	0.213	0.663	0.565	0.618	0.363
	Rss	0.258	0.409	0.217	0.041	0.0000028
	A	-0.112	-0.043	0.0065	0.0089	0.0038
2	β	0.295	0.214	0.0544	0.080	0.0183
	α	0.147	0.254	0.746	0.614	0.778
	Rss	0.0082	0.0053	0.00012	0.00078	0.0000023
	A	-0.012	-0.0052	0.0073	0.0122	0.0014
3	β	0.070	0.0619	0.0098	0.124	0.0191
	α	0.177	0.160	0.510	0.534	0.811
	Rss	0.00048	0.00028	0.0020	0.00017	0.0000097

Note: Rss = residual sum of the squares, A, β in cm/sec, α = slope in decades/decade.

The effective fracture aperture is not measured directly during the laboratory tests; only fracture closure measurements are recorded. To estimate the effective fracture aperture and thus check the validity of the cubic law, we follow the procedure suggested by Witherspoon et al. (1979b). First, we note that the effective flow aperture, 2b, has two components--an unknown residual aperture that exists at very high applied normal stress ($2b_{res}$) and a measured value determined from LVDT closure measurements ($2b_m$):

$$2b = 2b_{res} + 2b_m \tag{10}$$

The measured fracture aperture term ($2b_m$) is simply the difference between the maximum fracture closure ($2b_{Max}$) and the average LVDT fracture closure ($2b_{cl}$).

$$2b_m = 2b_{Max} - 2b_{cl} \tag{11}$$

With the exponent in Eq. (8) unknown, we may write:

$$Q/H = C\,(2b_{res} + 2b_m)^n \tag{12}$$

With fracture flowrate and LVDT fracture closure data, separate regression analyses were carried out for the loading and unloading parts of each test cycle for all samples to determine the values of the unknown parameters that would best fit the data. Two models were run for all the data. These models were:

(1) a log transformation of the nonlinear model with both residual aperture ($2b_{res}$) and exponent n treated as unknown;

(2) a log transformation of the nonlinear model with residual aperture ($2b_{res}$) treated as known by assuming the cubic law is valid at maximum applied normal stress, and with exponent n as unknown.

In both models, a nonlinear least-squares regression routine was used to estimate the parameters. Log transformations were selected to reduce potential weighting problems with the residual as the flowrate per unit head data ranged over several orders of magnitude. With log transformations, Eq. 12 may be rewritten:

$$\log (Q/H) = \log C + n \log (2b_{res} + 2b_m) \qquad (13)$$

The best-fit parameters n and $2b_{res}$ as well as the residual sum of the squares for the above model are shown in Table 3.5. The calculated residual aperture ($2b_{cal}$) that assumes the validity of the cubic law at maximum normal stress is also shown. The calculated residual aperture is not close to the regression-derived residual aperture for all data sets. In all cases, the exponent n is greater than 3.0, generally increasing with successive loading cycles and increasing sample size.

The exponent n was also determined by assuming that the cubic law is valid at maximum normal stress. The results of these model fits are evident in Table 3.6. Similar trends in exponent n and residual sum of the squares (Rss) are observed with this model. In all cases, assuming that the cubic law is valid at maximum applied normal stress (or at any one stress state) decreases the exponent n but also increases the residual (Rss).

Table 3.5. Nonlinear least-squares regression - log transformation, $\log(Q/H) = \log C + n\log(2b_{res} + 2b_m)$.

Cycle		Sample 1	2	3	4	5
1	n	3.37	3.43	3.75	3.57	4.82
	$2b_{res}$[a]	41.1	48.0	66.6	56.8	85.4
	$2b_{cal}$[a]	26.0	31.7	24.5	26.9	10.3
	Rss	0.74	6.11	1.59	1.29	9.54
2	n	3.40	3.83	4.12	4.29	4.69
	$2b_{res}$[a]	41.1	70.6	50.4	95.4	92.5
	$2b_{cal}$[a]	18.9	20.8	9.3	17.7	7.9
	Rss	0.56	1.98	2.47	3.56	1.08
3	n	3.52	3.86	4.48	3.95	4.56
	$2b_{res}$[a]	38.4	45.6	61.9	79.9	70.2
	$2b_{cal}$[a]	13.8	16.4	6.4	20.0	6.7
	Rss	0.079	3.43	2.24	0.28	1.58

[a] In micrometers.

Table 3.6. Nonlinear least-squares regression (with $2b_{res}$ fixed); $\log(Q/H) = \log C + n\log(2b_{res} + 2b_m)$.

Cycle		Sample 1	2	3	4	5
	n	3.23	3.28	3.36	3.30	3.85
1	$2b_{res}$[a]	26.0	31.7	24.5	26.9	10.3
	Rss	1.21	6.66	4.45	2.80	34.7
	n	3.10	3.30	3.56	3.53	3.74
2	$2b_{res}$[a]	18.9	20.8	9.3	17.7	7.9
	Rss	1.71	4.90	10.62	10.6	17.6
	n	3.11	3.37	3.68	3.37	3.75
3	$2b_{res}$[a]	13.8	16.4	6.4	20.0	6.7
	Rss	1.63	7.61	17.7	3.98	18.2

[a] In micrometers.

4. DISCUSSION

It has been suggested (Iwai, 1976; Witherspoon et al., 1979a) that the number and distribution of contact points within a fracture plane determine the stress/fracture-deformation relationship and thus the stress/fracture-permeability relationship. The number and distribution of contact points within a fracture plane are determined by the surface roughness or asperity of the fracture walls. Asperities in contact affect permeability by increasing flow tortuosity and restricting fracture closure. A conceptual model based on the number and distribution of contact points within a fracture plane provides a useful point of reference for the interpretation of stress-deformation and stress-permeability relationships. Such a conceptual model is adopted in this paper to interpret the observed effects of both cyclic loading and sample size.

The most notable feature of both the fracture deformation and fracture flowrate curves during loading and unloading is the highly nonlinear behavior with pronounced hysteresis. Trends in nonlinearity and hysteresis with both sets of data for successive loading cycles and varying sample size are similar. This reflects the close relationship between fracture deformation and fracture flowrate. Nonlinear behavior is compatible with the mechanics of fracture deformation. As stress is applied to the fracture plane, the fracture closes, rapidly increasing the number of contact points; this increase redistributes load, increases flow tortuosity, and decreases the closure rate. Hysteresis (the difference between loading and unloading paths) for both fracture deformation and fracture flowrate may be the result of improved seating of the fracture due to crushing of contact points or fracture asperities during loading.

Permanent fracture deformation and both deformation and flowrate hysteresis were observed in each test cycle for all samples. The permanent deformation and hysteresis also decreased with successive loading cycles (see Figs. 3.1, 3.2, 3.4, and 3.5). An approximate measure of the permanent fracture deformation imparted with successive loading cycles for each sample is evident in the change in average fracture closure at maximum normal stress (Table 3.1). The change in average fracture closure is greater between the first and second cycles than between the second and third cycles, indicating that most of the irrecoverable fracture deformation occurred during the first loading cycle. A larger number of contact points and a more even distribution of them in the fracture plane probably occurs with successive loading cycles. As the number of contact points increases, and as their distribution becomes more uniform, both permanent fracture deformation and deformation and flowrate hysteresis decrease.

The amount of permanent fracture deformation and hysteresis that occurs is probably linked to the initial (unloaded) distribution of asperity heights within the fracture plane. Fractures with only a few tall asperities unevenly distributed over the plane would exhibit pronounced hysteresis and major changes in flowrate and deformation as the load-carrying asperities permanently deform under increasing normal stress. With successive test cycles, the mean height of the asperities would be reduced. As this process continues, the fracture becomes stiffer at a lower normal stress. This should produce a higher rate of fracture closure during the initial stages of loading, and only limited additional fracture closure and flowrate reduction under higher normal stress. Samples 1 and 2, the smallest fracture

samples, appear to behave in this manner. Both exhibit the most dramatic decrease in average fracture closure at maximum applied normal stress with successive loading cycles. This suggests that significant changes in the mean asperity height and surface roughness of the fracture plane occur with successive loading cycles.

Fractures with a greater number of asperities and a more uniform distribution of their heights should show less permanent fracture deformation and less pronounced deformation and flowrate hysteresis. With a greater number and more uniform distribution of contact points, the load per contact is lower, and thus so are the contact-point stresses. Under these circumstances, asperities are more likely to deform elastically, resulting in less fracture wall damage and greater uniformity of stress and deformation over the sample area. This would be expected to result in less change in the stress-permeability relationships with repeated loading cycles. Sample 5, the largest, demonstrates deformation and flowrate behavior similar to this model. Changes in average fracture closure at maximum normal stress with successive test cycles are significantly less for sample 5 than for samples 1 and 2. As is evident in Fig. 3.5, flowrate hysteresis is also significantly reduced over repeated loading and unloading cycles.

Thus the smallest sample comes closest to the predictions of one model, while the largest comes closest to the other. The remaining samples fall somewhere in between. Sample 3 exhibited permanent deformation and hysteresis behavior that was intermediate but closer to the sample 5 model. Sample 4 also exhibited intermediate behavior (closer in this case

to samples 1 and 2), but its fracture is thought to have had significantly different properties for two reasons: (1) the fracture yielded anomalously high flowrates, and (2) it was difficult to refit during pre-test preparations.

Kranz et al. (1979) have suggested that the stress-permeability relationship for artificial fractures is a function of the surface roughness. These workers tested various controlled-roughness surfaces at constant confining stress and various field or pore pressures. Their results suggest that the empirical constant α will increase with decreases in surface roughness when the stress acting normal to the fracture plane has been constant. In the present study, however, α decreased with successive cycles for four of the five samples. Sample 5 is the exception. Its flowrates at low stress in cycle 1 were less during loading than unloading; in this case, flushing of the radial flowpath during unloading may have occurred.

The empirical constant α in this study is a measure of the net change in fracture hydraulic conductivity over the loading normal stress range of 0.2 to 30 MPa. The term α is therefore a measure of the response of the fracture asperities to applied load. Major changes in α would reflect significant changes in the asperity height distribution and surface roughness of the fracture walls. Samples 1 and 2 exhibit the largest reduction of α with successive test cycles. Sample 5 shows a slight increase in α between cycles 2 and 3 that may be attributed to final flushing of the fracture surface during cycle 2 loading. Sample 3 shows reductions in α that are less than those of samples 1 and 2, suggesting a more uniform

distribution of contact points. The α values for the linear power law determined in this study decrease with successive loading cycles for samples 1, 2, and 3. Samples 4 and 5 are inconsistent with this trend, reflecting changes in the hydraulic properties of the fracture that, as previously discussed, are unrelated to the stress-permeability relationship; in all cases, the correlation coefficients for the linear power law relation are greater than 0.95.

The results of attempts to fit the deformation and flowrate data to the cubic law may be also interpreted in light of the contact-point distribution model. Both regression analyses show that the cubic law does not appear to be valid for flow in deformable natural fractures where the fracture walls are in contact. This conclusion is not unrealistic when one considers that the cubic law was derived for flow between two smooth-walled parallel plates not in contact. That the residual fracture aperture was not close to the value calculated from assumptions of the validity of the cubic law, combined with the values of the exponent n being greater than 3.0 in all cases, indicates that the cubic law is not applicable to flow in deformable natural fractures where varying contact area can contribute significantly to changes in fracture flowrate.

It is important that the regression-derived exponents are all greater than 3.0. This indicates that factors other than fracture deformation contribute to the change in fracture flowrate with changing stress. The variation with stress in the number and distribution of contact points within the fracture plane may be the important factor in this reduction.

Asperities in contact increase flowpath tortuosity and reduce the number of available paths. Increasing contact area would be expected to increase the value of the regression-derived exponent n above 3.0. Only where there is no contact between the fracture planes would the exponent n be expected to equal 3.0. In general, n increases with successive loading cycles and increasing sample size. The most notable exceptions are sample 5, cycle 1, and sample 4, cycle 2. These cycles experienced non-stress-related changes in flowrate. The fracture samples most likely to behave as a smooth parallel plate are those which possess a limited number and a poor distribution of contact points. With increasing sample size and successive loading cycles, the parallel-plate analogy becomes the least adequate means to describe the stress-permeability relationships of deformable natural fractures.

The hydraulic-conductivity/normal-stress fracture data for loading cycle 3 of all samples are plotted in Fig. 4.1 to show the effect of sample size on the stress-permeability relationship of natural fractures. The anomalous position of the sample 4 data can be seen. The other samples possess similar initial conductivites at the minimum normal stress (approximately 0.2 MPa). If sample 4 is set aside as anomalous, then we observe, with increasing sample size, a decrease in minimum fracture conductivity and an increase in the net change in conductivity with normal stress.

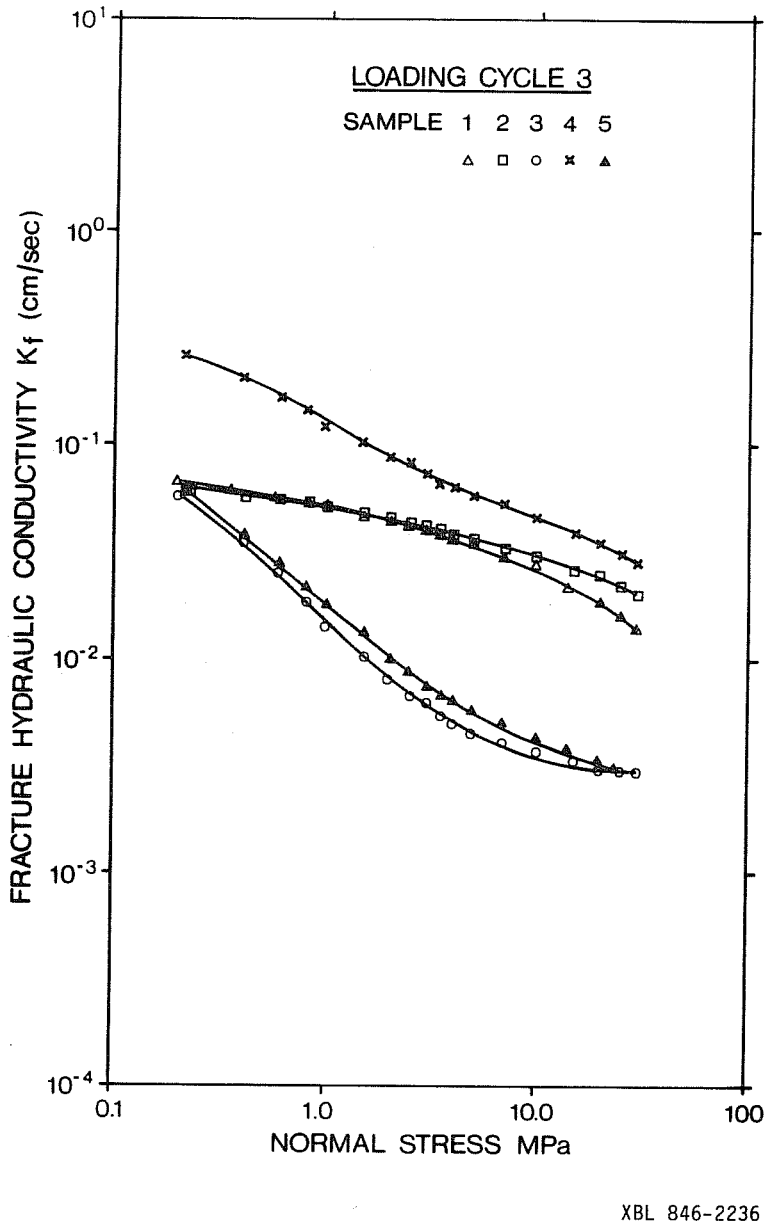

Fig. 4.1. Fracture hydraulic conductivity as a function of normal stress, samples 1 to 5, loading cycle 3.

The data in Fig. 4.1 for samples 1 and 5 have been superimposed in Fig. 4.2 on the previously published fracture hydraulic conductivity/normal-stress plot given by Witherspoon et al. (1979a). The sample-size results of this study appear to be the reverse of those suggested by Witherspoon et al. (1979a), for both minimum fracture hydraulic conductivity and net change in conductivity as a function of stress. That is, the smallest sample in our series showed the smallest rate of change in hydraulic conductivity as a function of stress, instead of the largest sample as predicted by Witherspoon et al., and the hydraulic conductivities at maximum stress were largest for the smallest sample.

Several explanations are available to explain this difference. The data presented by Witherspoon et al. were collected from tests on both natural and induced fractures. Recent work by Gale (1980b) has shown that the stress permeability characteristics of natural and induced fractures in the same rock type can be quite different, and, therefore, it may not be valid to compare the two fracture types. Also, as reported by Witherspoon et al., the boundary conditions for the field data, representing the largest samples that they reported, were not well defined, and the fractures tested were from different granites. Thus, to pursue the question of scale effects, it is necessary to compare samples from the same fracture as well as to conduct tests on similar fractures in situ under controlled boundary conditions.

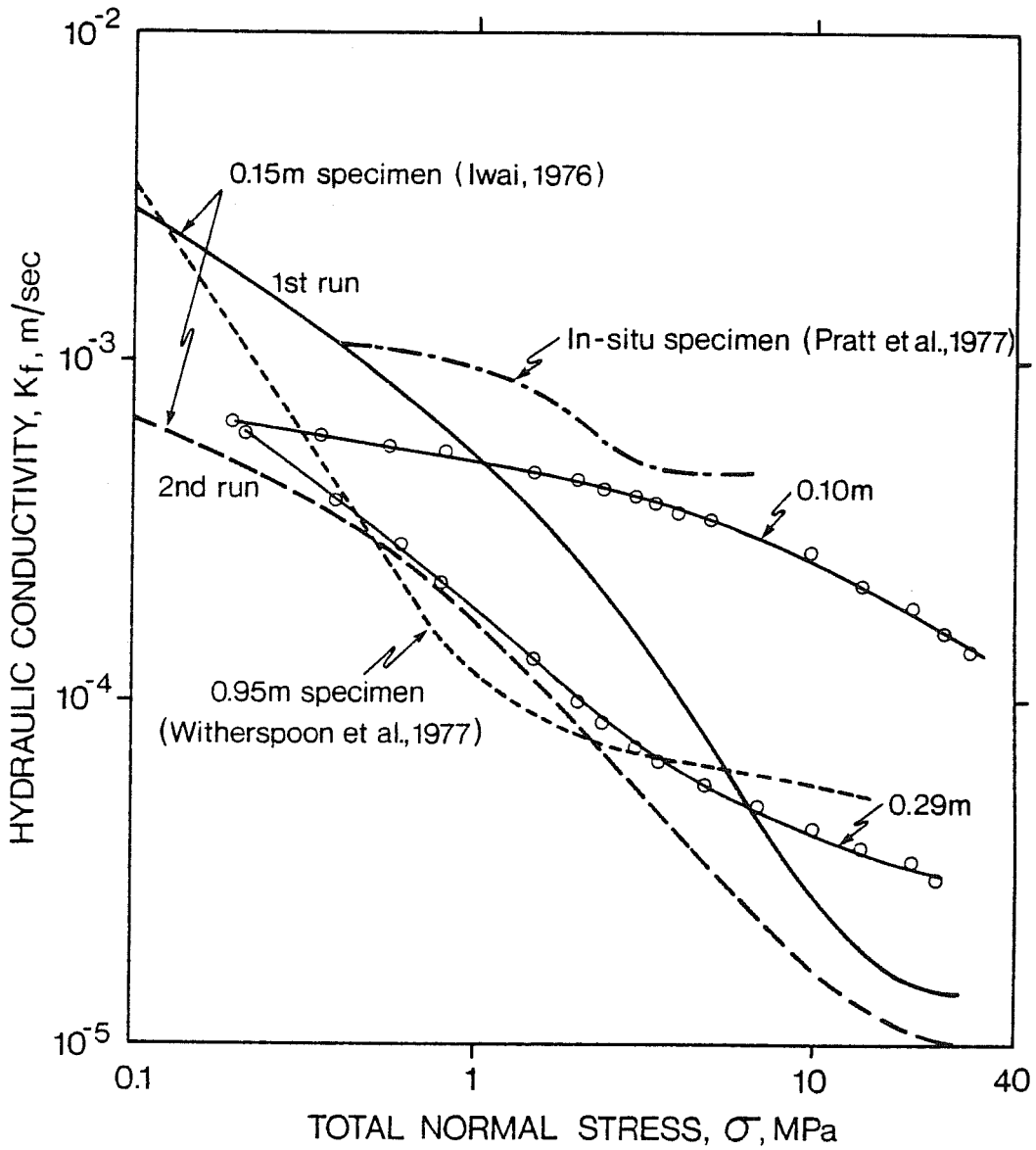

XBL 846-2216

Fig. 4.2. Comparison of the variation of fracture hydraulic conductivity with normal stress, samples 1 and 5, with published data; after Witherspoon et al. (1979a).

5. CONCLUSIONS AND RECOMMENDATIONS

Analysis of the data obtained from this experiment has not been completed, hence the conclusions presented here can only be considered tentative. Despite the scatter in the data, there does appear to be a size effect. In addition, our initial analysis suggests that the cubic law is not valid for flow in deformable natural fractures where the fracture walls are in contact. The actual factors that determine the size effect and the variation in the flowrate/fracture-aperture relationship are not immediately obvious. Certainly a major one is the scale and nature of fracture-plane roughness and the associated properties of contact-point distribution and asperity.

Thus, in order to evaluate the application of conceptual models of contact area to the observed relations between fracture deformation, fracture flowrate, and stress, the number and distribution of contact points, as a function of stress, should be determined for the samples tested in this study. If we can identify the scale and variation of fracture-plane roughness, we may be able to define the sample sizes necessary to adequately represent a natural fracture plane. Also, with a detailed knowledge of fracture-plane roughness, we may be able to apply the appropriate theories of contact stress (Landau and Lifshitz, 1959) to the interpretation of the laboratory data.

It is essential that we determine the nature of the variation in test results between samples of the same size as well as between samples of different sizes. Thus, we are currently undertaking a study of five

additional samples from the same fracture plane. In addition, the largest sample will, after initial testing, be successively cored and tested to produce decreasing sample sizes of the same piece of the fracture plane.

ACKNOWLEDGMENTS

This study was part of a broad research program funded under Subcontract No. 4500410 from the Lawrence Berkeley Laboratory, University of California, to the senior author at the University of Waterloo. The contract was administered by the Waterloo Research Institute and referenced under Account No. 809-17-02. The work was supported by the Assistant Secretary for Nuclear Energy, Office of Civilian Work Management, U. S. Department of Energy under Contract No. DE-AC03-76SF00098. Funding for this project was administered by the Office of Crystalline Repository Development at Battelle Memorial Institute.

The authors would like to acknowledge the assistance provided by M. Deverill, B. Schmitke, D. Bearinger, G. Jones, and D. Cameron during sample collection and testing. Special thanks are extended to Joe Peters and the staff of the Cold Spring Granite Company for their cooperation and assistance during sample collection.

The drafting and photographic efforts of Maureen Marziaz and Peter Fisher are gratefully acknowleged. Thanks are extended to J. Love and E. Stern for typing the manuscript.

REFERENCES

Bear, J., 1972. Dynamics of Fluids in Porous Media. American Elsevier Publishing Company, New York.

Gale, J. E., 1975. A Numerical, Field and Laboratory Study of Flow in Rocks with Deformable Fractures, Ph.D. Thesis, University of California, Berkeley, 255 pp.

Gale, J. E., 1980a. "Assessing the Permeability Characteristics of Fractured Rock," in Recent Trends in Hydrogeology, Special Publication of the Geological Society of America, in press.

Gale, J. E., 1980b. "Effects of Stress on Fracture Permeability - Considerations for Nuclear Waste Storage in Granitic Rock," paper presented at 13th Canadian Rock Mechanics Symposium, Toronto, May 28-29.

Gangi, A. F., 1978. "Variation of Whole and Fractured Porous Rock Permeability with Confining Pressure," Int. J. Rock Mech. Min. Sci. and Geomech. Abstr., Vol. 15, pp. 249-257.

Hubbert, M. K., 1956, "Darcy's Law and the Field Equations of the Flow of Underground Fluids," AIME Jour. Petrol. Tech., October, pp. 222-245.

Iwai, K., 1976. Fundamental Studies of Fluid Flow Through a Single Fracture, Ph.D. Thesis, University of California, Berkeley, 208 pp.

Jones, F. O., 1975. "A Laboratory Study of the Effects of Confining Pressure on Fracture Flow and Storage Capacity in Carbonate Rocks," J. Pet. Tech., January, pp. 21-27.

Kranz, R. L., Frankel, A. D., Engelder, T., and Scholz, C. H., 1979. "The Permeability of Whole and Jointed Barrier Granite," Int. J. Rock Mech. Min. Sci. and Geomech. Abstr., Vol. 16, pp. 225-235.

Landau, L. D. and Lifshitz, E. M., 1959. Theory of Elasticity. Pergamon Press, N.Y., pp. 39.

Morey, G. B., 1978. Lower and Middle Precambrian Stratigraphic Nomenclature for East Central Minnesota, Minnesota Geological Survey, Report of Investigations No. 21.

Nelson, R. A. and Handin, J. W., 1977. "Experimental Study of Fracture Permeability in Porous Rock," Amer. Assoc. Pet. Geol. Bull., Vol. 61, No. 2, pp. 227-236.

Pratt, H. R., Swolfs, H. S., Brace, W. F., Black, A. D., and Handin, J. W., 1977. "Elastic and Transport Properties of in situ Jointed Granite," Int. J. Rock Mech. Min. Sci. and Geomech. Abstr., Vol. 14, pp. 35-45.

Witherspoon, P. A., Amick, C. H., and Gale, J. E., 1977. Stress-Flow Behavior of a Fault Zone with Fluid Injection and Withdrawal, Report No. 77-1, Department of Materials Science and Mineral Engineering, University of California, Berkeley.

Witherspoon, P. A., Amick, C. J., Gale, J. E., and Iwai, K., 1979a. "Observations of a Potential Size Effect in Experimental Determination of the Hydraulic Properties of Fractures," Water Resources Res., Vol. 15, No. 5, pp. 1142-1146.

Witherspoon, P. A., Wang, J. S. Y., Iwai, K., and Gale, J. E., 1979b. Validity of Cubic Law for Fluid flow in a Deformable Rock Fracture. Lawrence Berkeley Laboratory Report LBL-9557, SAC-23.

APPENDIX A: SAMPLE COLLECTION, TESTING, AND MAPPING

A.1 Collection and Preparation

Collection of the fractured core samples at the "Charcoal Gray" granite quarry consisted of several steps: (1) selecting an appropriate fracture plane; (2) drilling a narrow borehole (1.6 cm diameter in the 10.0-, 15.0-, and 19.3-cm-diameter cores, and 3.2 cm diameter in the 24.5- and 29.4-cm-diameter cores) 5 to 15 cm below the fracture plane; (3) installing a rock bolt in this hole, bolting the rock blocks above and below the fracture plane together; and (4) overcoring the hole with an appropriately sized diamond-core barrel. The sampled rectangular block was about 70 cm thick and 70 cm long, with the fracture plane in the center and perpendicular to the axis. The cores, held together by the rock bolt, were then crated and transported to the laboratory to be prepared for testing.

At the laboratory, three pairs of holes approximately 0.6 cm diameter and 2.5 cm deep were drilled, one hole on either side of the fracture plane. Each pair was spaced 120° from the others around the sample circumference. A similar pair of holes was drilled above but close to the fracture plane. Aluminum-threaded plugs were epoxyed into all the holes with 3 M structural adhesive 2216. Each pair of plugs was separated by approximately 6.5 cm to accommodate displacement-measuring instrumentation.

Aluminum plates were attached across the fracture plane of the two smallest cores. These plates held the two blocks firmly together and kept the fracture closed. The heavier samples required a stronger tensioning system. Three sets of holes (1.3 cm diameter by 2.6 cm deep) were

drilled above and below the fracture plane approximately 30 cm apart, and threaded steel anchor posts were epoxyed into the holes. A system of angle-iron and 0.95-cm-diameter threaded rods thus held the two blocks firmly together. These anchor posts also served as hoisting lugs.

Once the samples were firmly held together from the outside, the center rock bolt was removed and the sample ends prepared for testing. The ends of the three smaller cores were cut off with a diamond saw so that the fracture was centered on the core sample and the length-to-diameter ratio of the core was about 2.1 to 1. The ends were then ground flat to ensure end parallelism for testing.

The two larger cores required additional treatment. Sulfur caps were placed on the ends of the 24.5-cm-diameter sample to ensure end parallelism. The 29.4-cm-diameter sample had to be lengthened to attain a length-to-diameter ratio of 2.1 to 1. A series of 0.64-cm-diameter holes was drilled into the top of the sample and a steel reinforcing mesh epoxyed into the holes. An early high-strength portland cement was poured on the mesh to increase the length. The concrete surface was ground flat and a sulfur cap was applied to the bottom of the sample. A cylinder of the concrete mix was tested and found to have a yield strength of 45 MPa.

To protect the sample ends from potential chipping during the instrumentation and testing setup, steel straps were applied by means of gear clamps around the circumference of both the 24.5- and 29.4-cm-diameter samples, near

near the ends. These straps also provided additional confining pressure for the concrete and sulfur caps.

To bleed air pockets from the fracture and center hole during the initial setup for testing, as well as to provide a means of measuring fluid pressure during permeability tests, a hole (0.64 cm diameter for 10.0-and 15.0-cm-diameter samples and 1.3 cm diameter for 19.3-, 24.5- and 29.4-cm-diameter samples) was drilled through the surface to the top of the center hole (see Fig. 2.2). A swaglock fitting was epoxyed into this hole to serve as the pressure port.

The history of opening and closing of the sample fractures during preparation may be important in the interpretation of the test results. Following is a brief summary of this history for each sample.

Sample 1 To remove the center hole rock bolt, the upper and lower blocks were separated; this was done easily and completely, and the sample was carefully reset.

Sample 2 The upper block was tapped with a rubber mallet to open the fracture, which was sealed at one point on the side of the sample. The sample was carefully reset. The sample was never completely separated.

Sample 3 The fracture was opened easily by outscrewing the 0.95-cm threaded rods against the anchor posts. The upper and lower blocks were completely separated in order to epoxy the center hole. The sample was carefully reset.

Sample 4 Same as sample 3 except that considerable difficulty was encountered in attempting to reset the fracture.

Sample 5 The fracture was opened easily by outscrewing the threaded rods about 0.25 cm. The sample was carefully reset.

The upper and lower blocks were separated to varying extents in all five samples, indicating that the fractures tested were not sealed and represented continuous breaks.

A.2 Instrumentation and Testing Procedures

To investigate stress distribution between the top of sample and the fracture plane, as well as to provide data on rock deformation to check LVDT deformation measurements, strain gauges were applied to the outside of the core samples. Beam SR-4 strain gauges were epoxyed to each sample to measure vertical strains. One vertical string of gauges was applied to each sample. An additional gauge, located 180° from the string, was applied to all samples except no. 1 (the 10.0-cm-diameter sample). All gauges were rubber-and epoxy-coated to allow submersible operation. To monitor strain fluctuations that might be due to temperature transients, two strain gauges were applied to two cores of Stripa granite that were placed close to the testing frame. These cores were not loaded and the gauges were monitored during loading and unloading of the test samples. Hence, any changes in the output for these gauges reflected a response to changes in environmental conditions. In all cases, strains were measured with a 1/4 Wheatstone bridge, 3-wire, external-dummy gauge system.

Figure 2.2 is a schematic of an instrumented sample placed within the loading frame and ready for testing. A brass sleeve was machined and epoxyed into the center hole at the base of the sample. A water inlet plate with an O-ring seal attached was fitted to the base of the sample. The O-ring seal between the brass sleeve and the nipple of the base plate provided a watertight connection for the water supply during injection testing. Once the baseplate was attached, the sample was placed in a Plexiglas tank. The aluminum plates or angle iron and threaded rod holding the sample together were removed once the tank was placed within the loading frame. Three linear variable differential transformers (LVDTs) were mounted 120° apart in the bracket holes drilled on either side of the fracture plane, and a fourth LVDT was similarly mounted above the plane. Before mounting the LVDTs, the separation between the mounting pins was measured with a vernier caliper.

The three LVDTs mounted across the fracture measured fracture and rock deformation. Both strain gauges and the LVDT mounted above the fracture measured intact rock deformation. From both sets of deformation data, the amount of displacement due to fracture deformation alone was derived.

Finally, an absolute pressure transducer (0 - 500 psia) was attached to the pressure port to measure center hole injection pressure during permeability tests.

The laboratory testing configuration consisted of three basic components: (1) the fluid pressure application and flow monitoring equipment, (2) the sample and loading frame setup, and (3) the data acquisition system.

Compressed nitrogen was applied to water in three positive displacement tanks providing a constant fluid pressure for the injection tests. The flowrate was calculated by measuring the change in water level in a tank over a given time period. A differential pressure transducer measured the change in water level. By varying the internal diameter of the flow tank, flowrates could be accurately measured over several orders of magnitude. The bubble injection method indicated in Fig. 2.3 was replaced with a small-diameter flow tank. Figure 2.3 shows the arrangement of filters, LVDTs, pressure transducers, thermocouples, and valves.

A 1.78-MN Material Testing Services (MTS) closed-loop-servo-controlled testing unit applied the axial loads. The applied load was measured with a 1.57-MN capacity load cell built into the upper loading platen. This platen is spherically seated, allowing a small range of tilt in the platen. Maximum load capacity of the frame is 1.57 MN. All samples were tested under load control feedback conditions. Normal stresses were determined by dividing the applied load by the area of the sample at the fracture plane.

The central component of the data acquisition system was a Fluke 2240 A datalogger. Interfaced with the datalogger was a teletype and paper-tape punch to provide data both in a numerical form during testing and in a computer-compatible format for later computer-assisted data reduction and analysis. A strip-chart recorder monitored both center-hole pressure and the differential pressure of the flow transducer during injection tests. An X-Y-Y plotter also monitored the rock deformation LVDT and one fracture deformation LVDT as a function of applied load.

Load, pressure, flowrate, displacement, and temperature, as well as transducer power supplies, were recorded on punched paper tape and teletype. Strain gauge measurements were recorded manually.

After the sample was placed in the MTS frame and instrumented, testing consisted of the following steps:

1. Raising the level of water in the Plexiglas reservoir just above the fracture.

2. Flushing the flow lines, pressure lines, and the sample with carbon dioxide, followed by deionized water.

3. Allowing the sample to stabilize for a period of 12 to 24 hours to determine if the instruments were functioning correctly and to provide appropriate background values for the LVDTs, pressure transducers, strain gauges, and thermocouples.

4. Increasing the load in the increments shown in Table A.1 up to 30 MPa and then decreasing until no load remained on the sample.

At each loading increment, measurements of flowrate, fluid pressure, applied load, displacement, strain, and temperature were made. About 10 to 45 minutes was required to obtain stable readings at any one load increment. Once stable readings were obtained, the testing sequence was completed for that increment. One full cycle required about 8 to 16 hours to complete. Each sample was subjected to three loading and unloading cycles. The samples

Table A.1. Approximate normal-stress increments and load cell voltage settings.

Normal-Stress Increments		Load-Cell Voltage Settings				
MPa	psi	Sample 1 @ 20% [a]	Sample 2 @ 50%	Sample 3 @ 50%	Sample 4 @ 100%	Sample 5 @ 100%
0.2	29.01	0.043	0.039	0.065	0.052	0.075
0.4	58.01	0.086	0.078	0.131	0.104	0.151
0.6	87.03	0.129	0.117	0.196	0.156	0.226
0.8	116.03	0.172	0.157	0.261	0.208	0.302
1.0	145.04	0.215	0.196	0.327	0.260	0.377
1.5	217.56	0.323	0.294	0.490	0.390	0.566
2.0	290.08	0.431	0.392	0.653	0.520	0.754
2.5	362.60	0.538	0.490	0.187	0.650	0.943
3.0	435.11	0.646	0.588	0.980	0.780	1.132
3.5	507.63	0.754	0.686	1.144	0.911	1.321
4.0	580.15	0.861	0.784	1.307	1.041	1.509
5.0	725.19	1.077	0.980	1.634	1.301	1.887
7.0	1015.27	1.508	1.373	2.387	1.821	2.641
10.0	1450.38	2.154	1.961	3.268	2.602	3.774
15.0	2175.57	3.231	2.941	4.901	3.903	5.661
20.0	2900.76	4.308	3.992	6.535	5.204	7.548
25.0	3625.95	5.384	4.902	8.169	6.505	8.900[b]
30.0	4351.14	6.461	5.883	9.803	7.806	

[a] Load capacity settings.
[b] Maximum normal stress - 23.6 MPa.

were allowed to stabilize for a period of about 8 to 12 hours between cycles. After loading was completed at each increment, nitrogen was passed through the sample and the test lines to determine if the flow circuit was leaking at any of the connections.

A.3 Surface Maps

The location of the conducting fracture, ancillary cracks and tight seams as well as instrument position, were mapped by wrapping Mylar around the core and tracing. The resulting maps are shown in Figs. A.1 to A.5.

Samples 1 and 5 do not have significant ancillary cracks or tight seams. Sample 2 has some braided fracturing immediately below the fracture plane as well as a moderately dipping poorly expressed tight seam in the upper block. Samples 3 and 4 both possess minor cracks in the upper block. Although the cracks in samples 3 and 4 appear hydraulically tight, the central boreholes in both samples were epoxyed in the vicinity of the cracks. Aside from these minor cracks and seams, both the upper and lower blocks are massive and homogeneous.

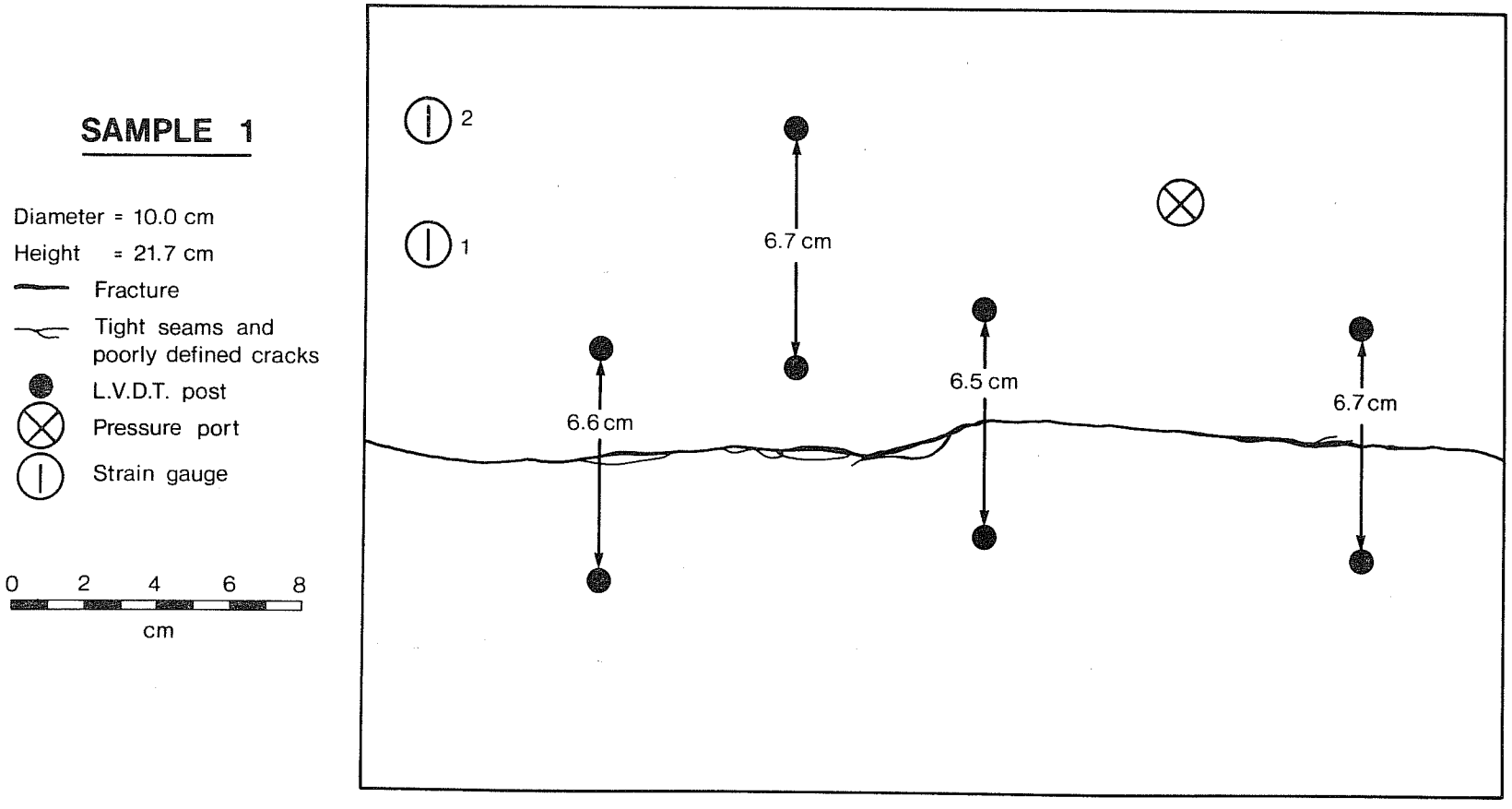

XBL 846-2208

Fig. A.1. Surface map of sample 1.

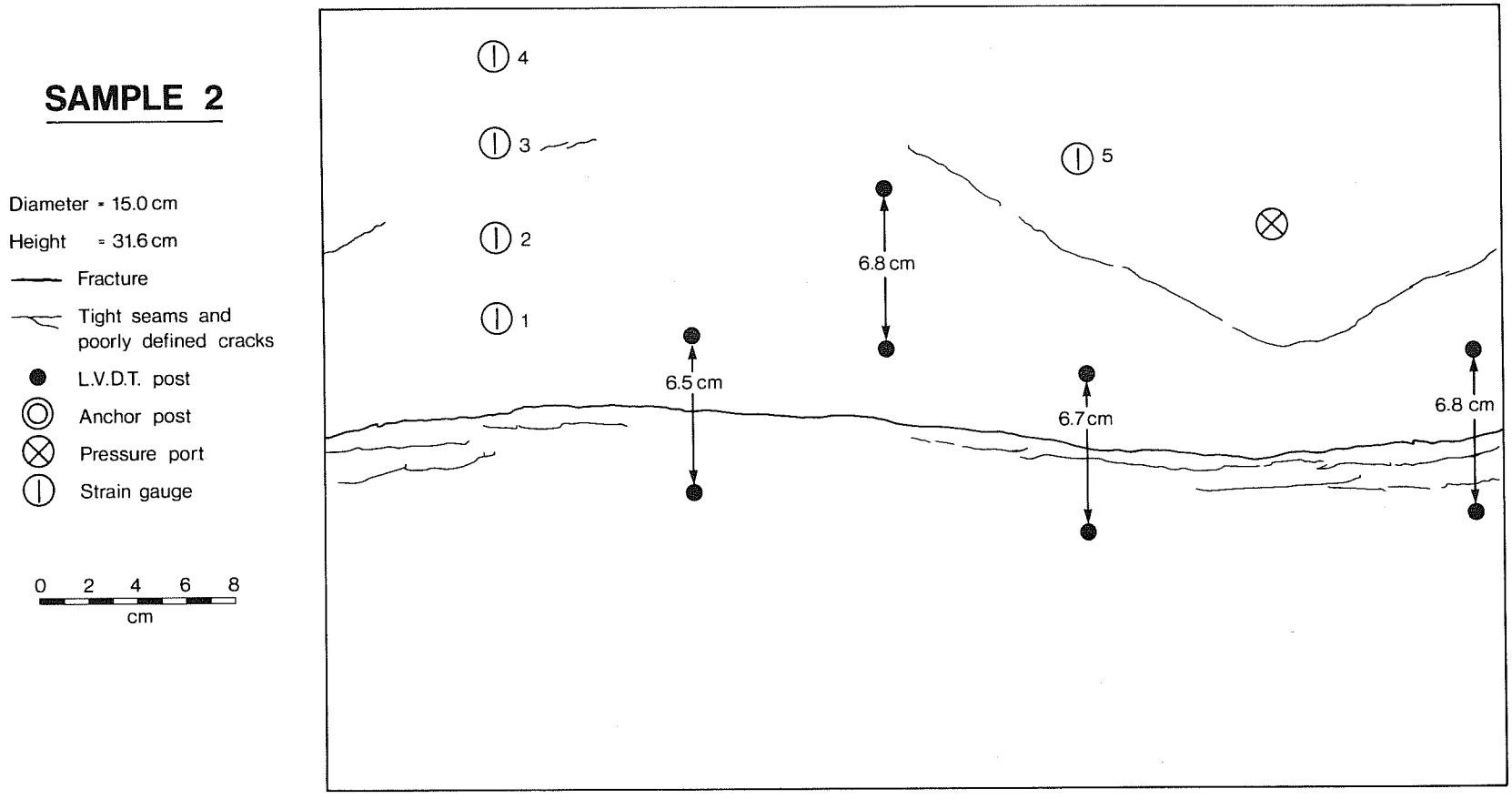

XBL 846-2209

Fig. A.2. Surface map of sample 2.

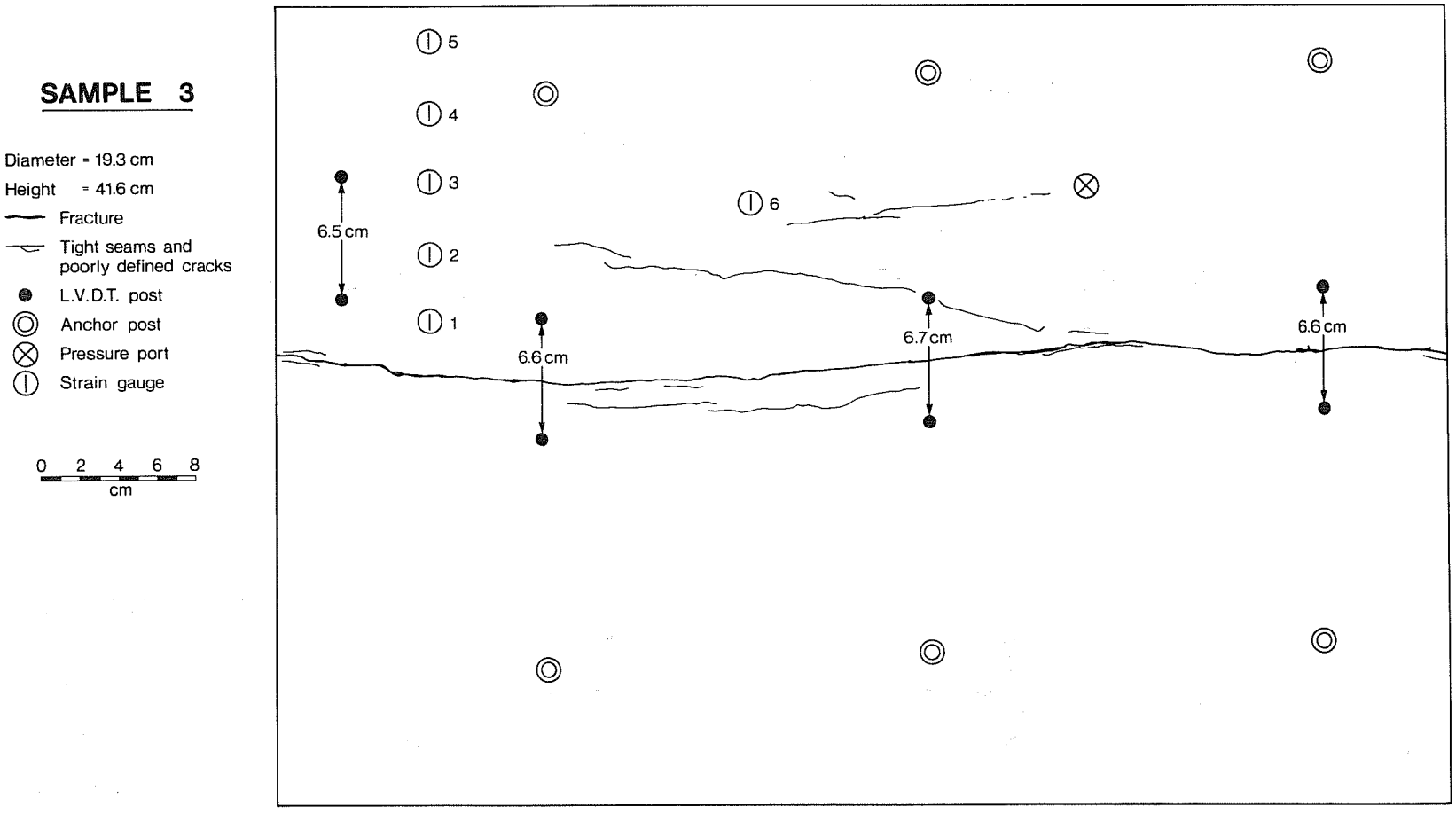

XBL 846-2210

Fig. A.3. Surface map of sample 3.

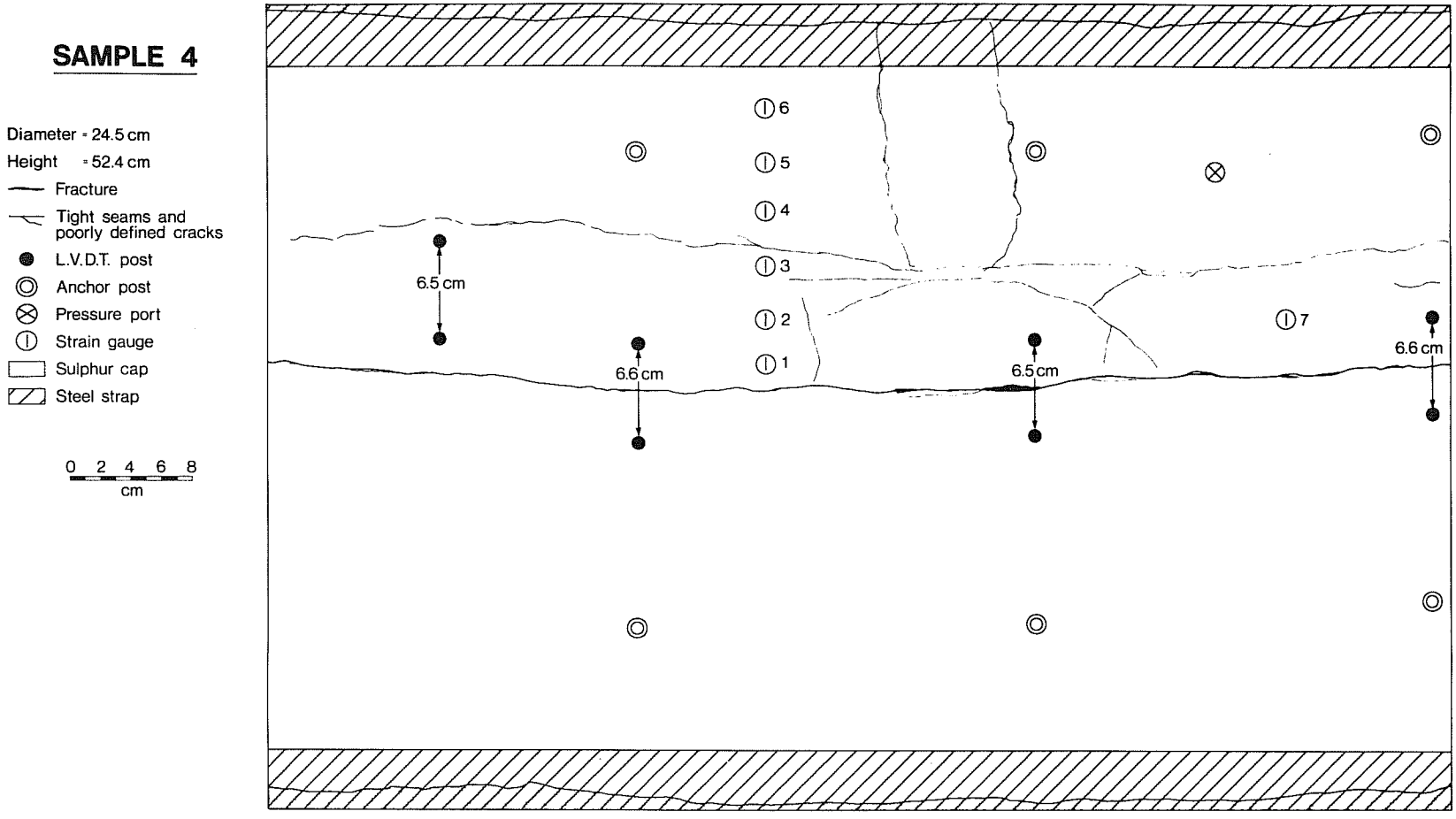

XBL 846-2211

Fig. A.4. Surface map of sample 4.

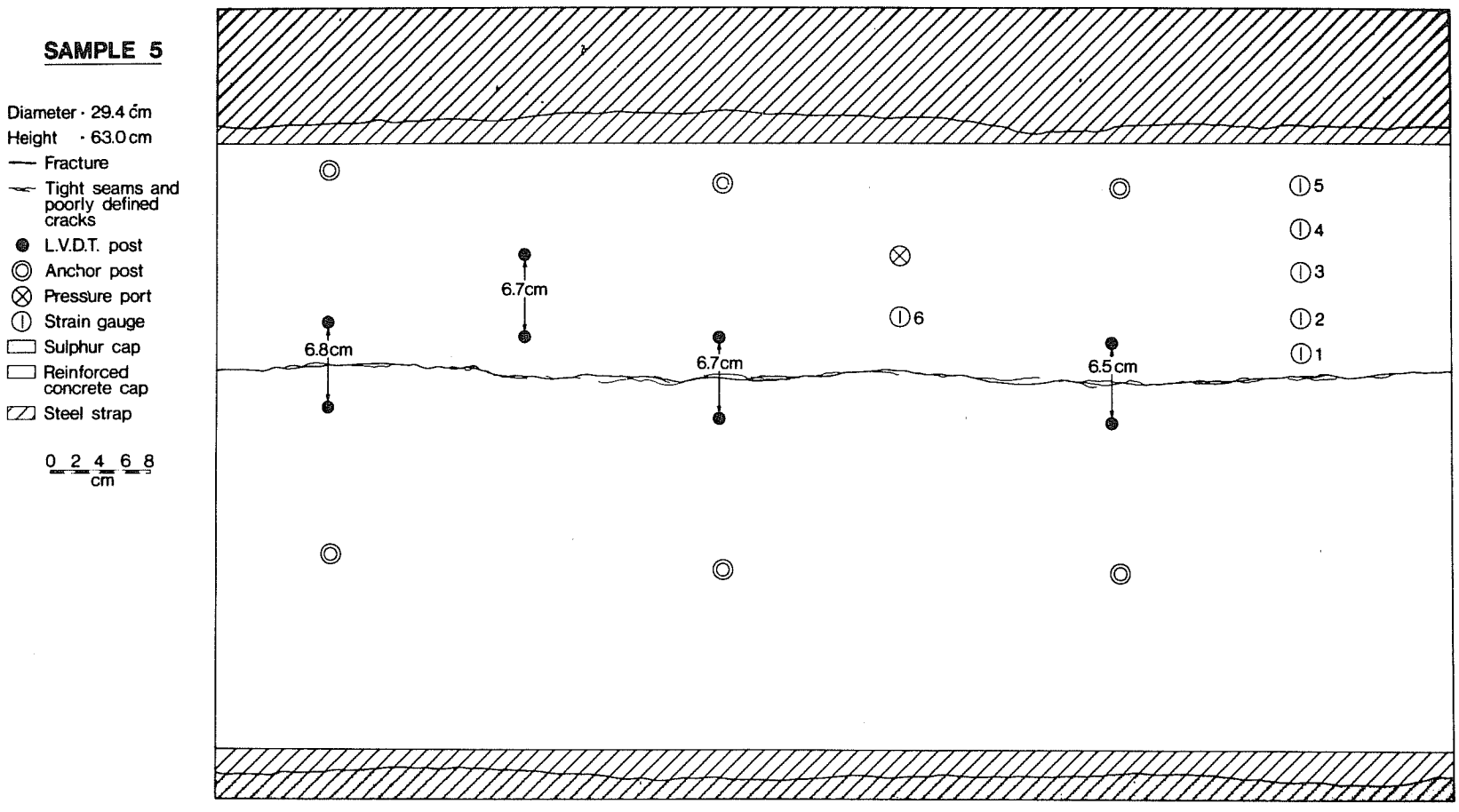

XBL 846-2212

Fig. A.5. Surface map of sample 5.

APPENDIX B: REFORMATORY GRANITE AND CORE DEFORMATION DATA

(Material property tests on Reformatory granite courtesy Cold Spring Granite Company)

REPORT OF: TEST OF GRANITE CORES

PROJECT: MATERIAL CHECK - CHARCOAL GRAY

DATE: July 12, 1978

REPORTED TO: Cold Spring Granite Co.
202 South Third Ave.
Cold Spring, MN 56320
Attn: Joe Peters

FURNISHED BY:
COPIES TO:

LABORATORY NO. 6-18454

INTRODUCTION

Six granite cores approximately 2" long x 1" in diameter were received on June 7, 1978. It was requested that we determine the Modulus of Elasticity of this granite in compression.

In preparation for the Young's Modulus Test, the sides of three six cylinders were lightly sanded to enable attachment of the strain gauges. Two gauges were attached on opposite sides at the middle of each cylinder. Of the three remaining cylinders, two were used to determine the ultimate stress of the granite and the other was used as a temperature compensator.

TEST PROCEDURE

Modulus of Elasticity	Essentially in accordance with ASTM:C469, "Standarad Method of Test for Static Modulus of Elasticity of Concrete in Compression."
Method of Strain Measurement	Strain Gauges, CEA-06-500UW-120

TEST RESULTS

Type of Granite	Charcoal Gray		
Cylinder Number	1	2	3
Diameter, in.	0.975	0.969	0.995
Length of Specimen, in.	2.024	2.016	2.028
Date Tested	6-21-78	6-21-78	6-21-78
Modulus of Elasticity (Average	10.94×10^6, psi		

REMARKS

This work was authorized by your Purchase Order Number 3449.

REPORT OF: TEST OF GRANITE CORES

PROJECT: MATERIAL CHECK

DATE: March 20, 1973

REPORTED TO: Cold Spring Granite Co.
202 South Third Ave.
Cold Spring, MN 56320
Attn: Joe Peters

FURNISHED BY:
COPIES TO:

LABORATORY NO. 8-631A

IDENTIFICATION Charcoal Gray; West of St. Cloud, Minnesota

BULK DENSITY (ASTM:C97-47)

Type of Specimens	2" x 2" x 2" cubes		
Sample Number	1	2	3
Bulk Specific Gravity	2.72	2.72	2.72
Bulk Density (pcf)	170.9	170.9	170.9
Average Bulk Density (pcf)		170.9	

ABSORPTION (ASTM:C97-47)

Type of Specimens	2" x 2" x 2" cubes		
Sample Number	1	2	3
Absorption (%)	0.12	0.13	0.12
Average Absorption (%)		0.12	

COMPRESSION STRENGTH (ASTM:C170-50)

Type of Specimens	2" x 2" x 2" cubes		
Condition at Test	Oven dry		
Sample Number	1	2	3
Compressive strength (psi)	28,100	33,400	33,500
Average Compressive Strength (psi)		21,670	

MODULUS OF RUPTURE (ASTM:C99-52)

Type of Specimens	Approximate 4" x 2 1/4" x 8"prisms		
Condition at Test	Oven dry		
Span Length	7 inches		
Sample Number	1	2	3
Modulus of Rupture (psi)	2025	2010	1980
Average Modulus of Rupture (psi)		2005	

REMARKS

The above specimens were submitted to the laboratory and received here on February 21, 1973.

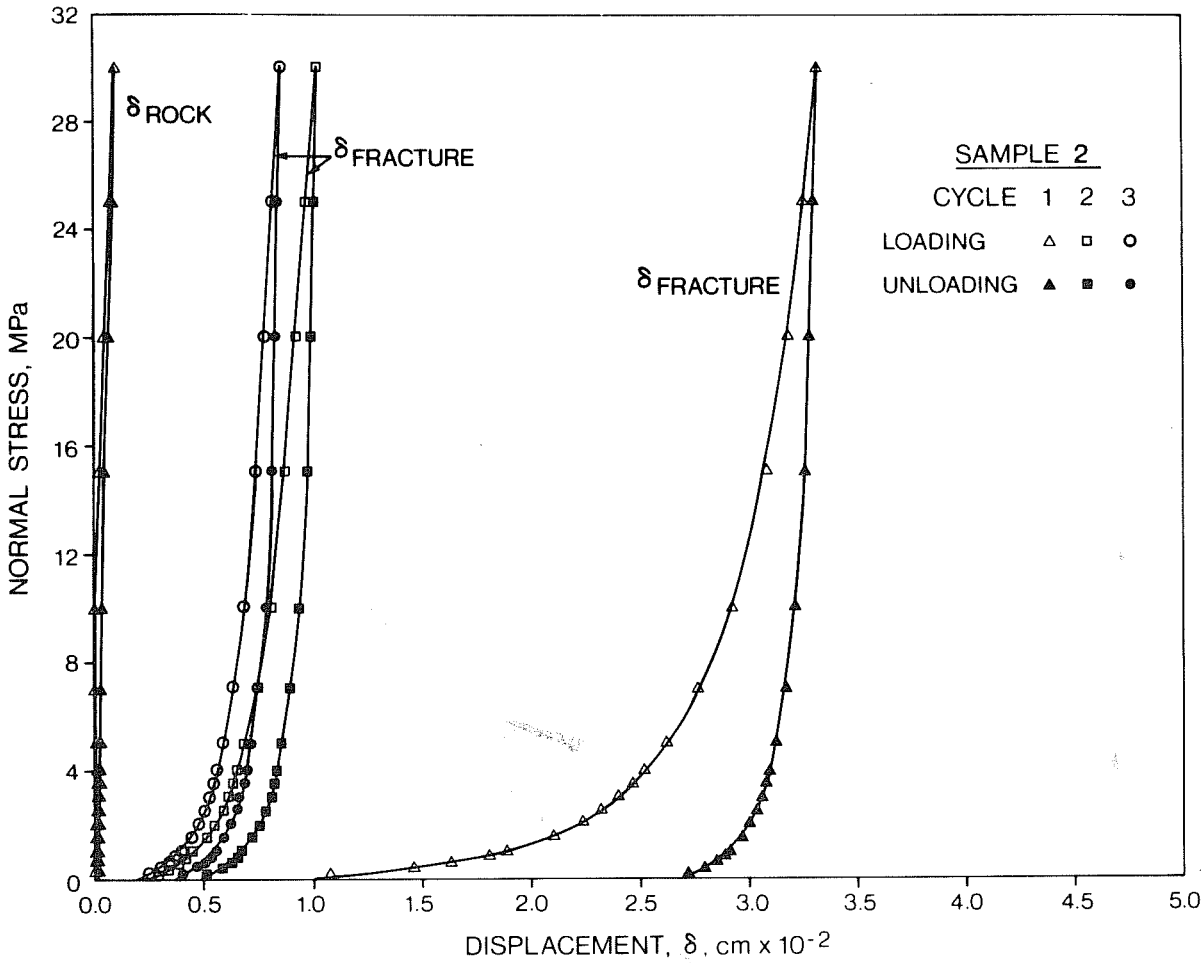

XBL 846-2221

Fig. B.1. Fracture and rock displacement as a function of normal stress, sample 2, cycles 1, 2, and 3.

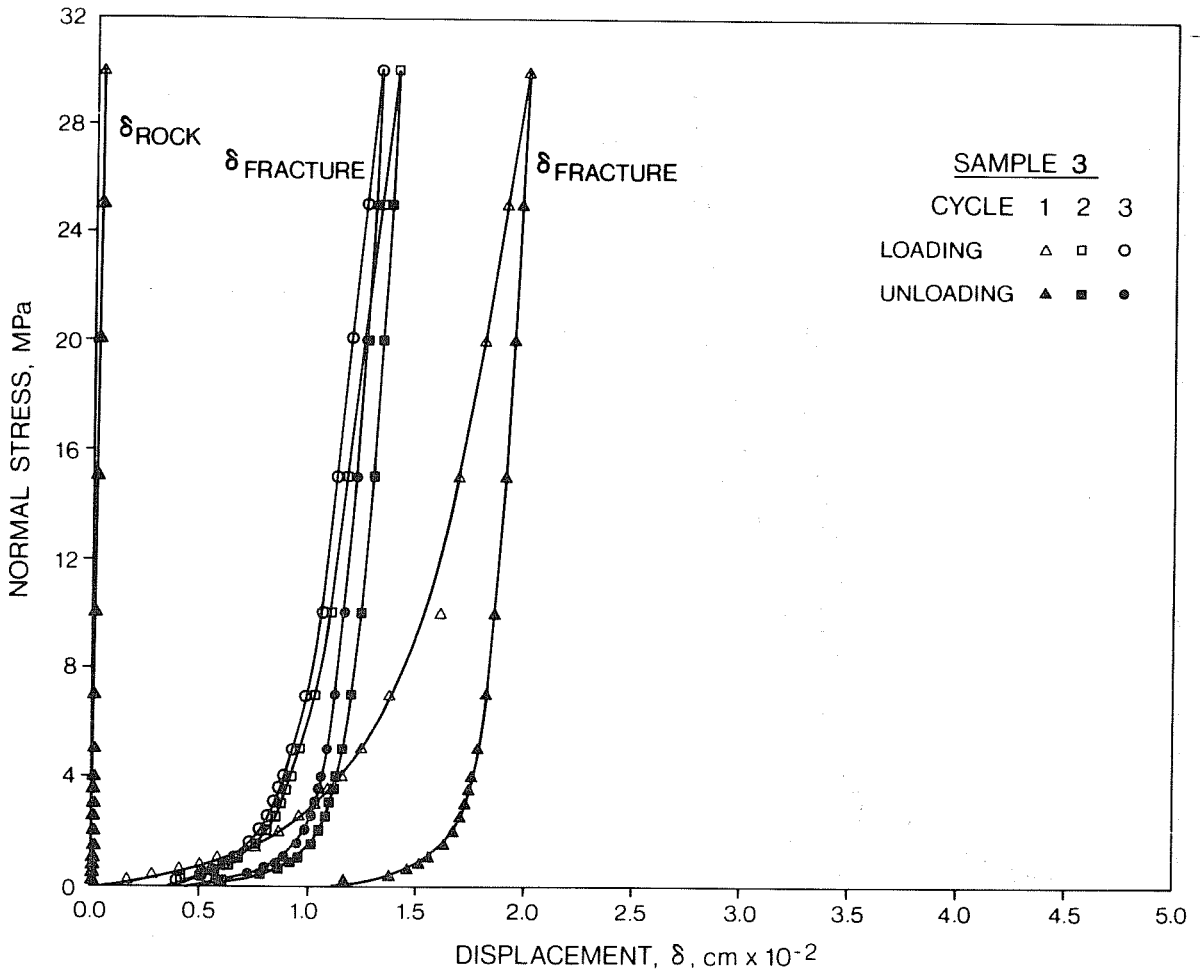

XBL 846-2222

Fig. B.2. Fracture and rock displacement as a function of normal stress, sample 3, cycles 1, 2, and 3.

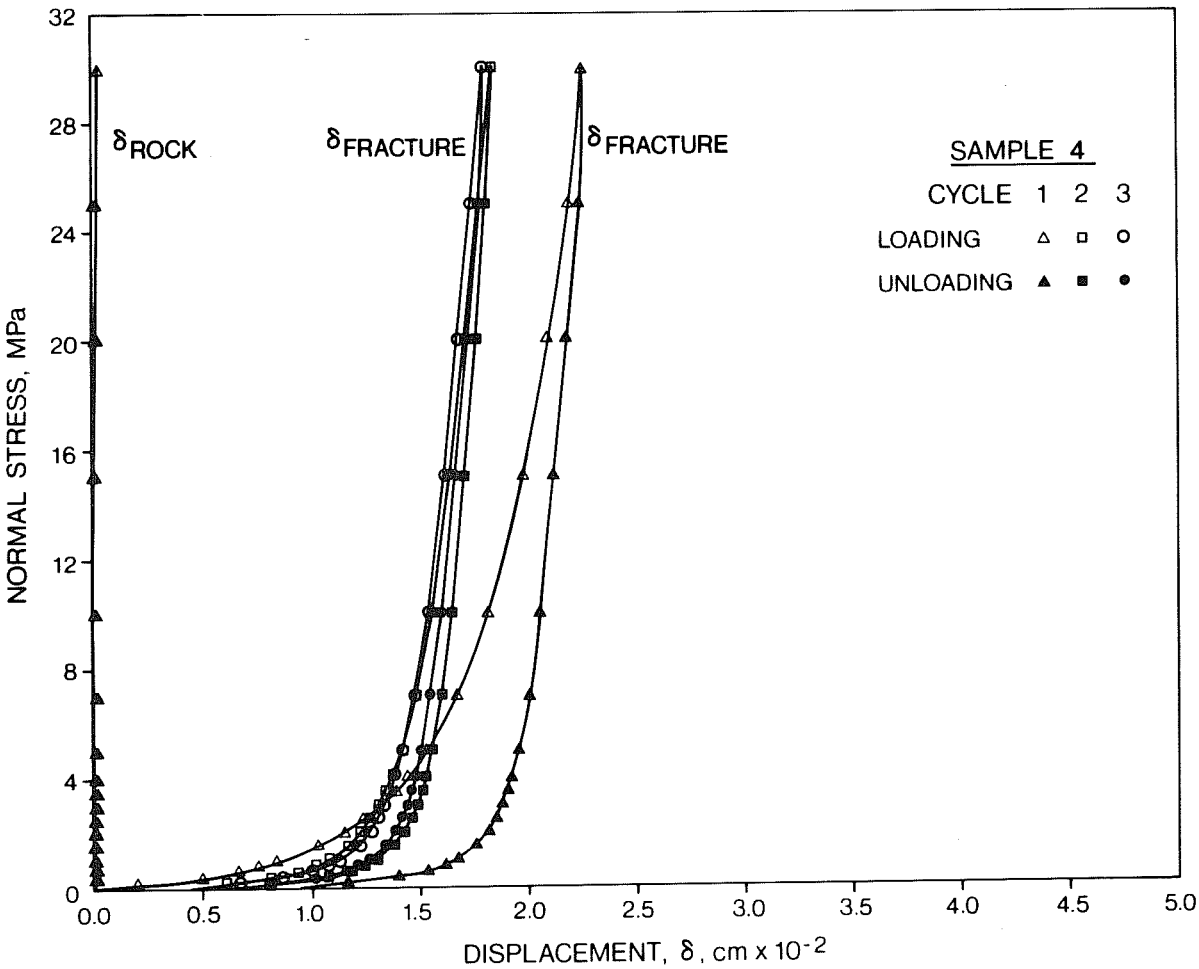

XBL 846-2223

Fig. B.3. Fracture and rock displacement as a function of normal stress, sample 4, cycles 1, 2, and 3.

APPENDIX C: PLOTS OF FRACTURE FLOWRATE PER UNIT HEAD AND OF HYDRAULIC CONDUCTIVITY VERSUS NORMAL STRESS FOR SAMPLES 2-4

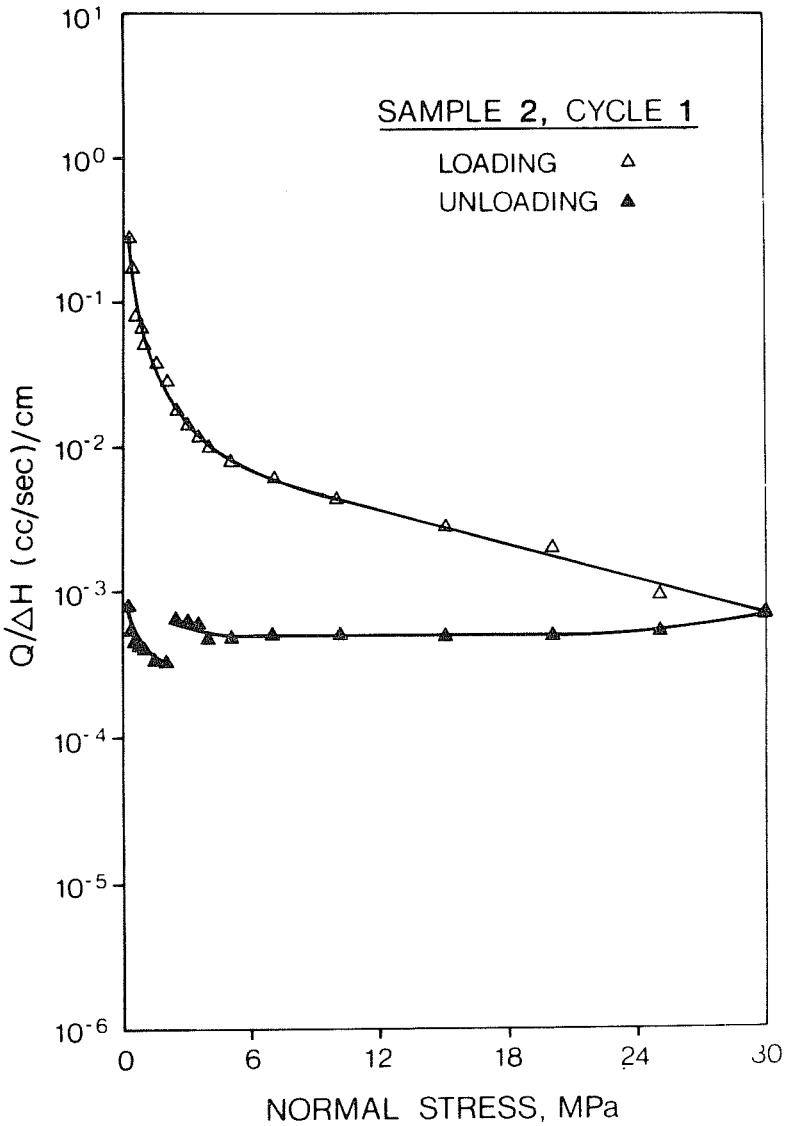

XBL 846-2235

Fig. C.1. Fracture flowrate per unit head as a function of normal stress, sample 2, cycle 1.

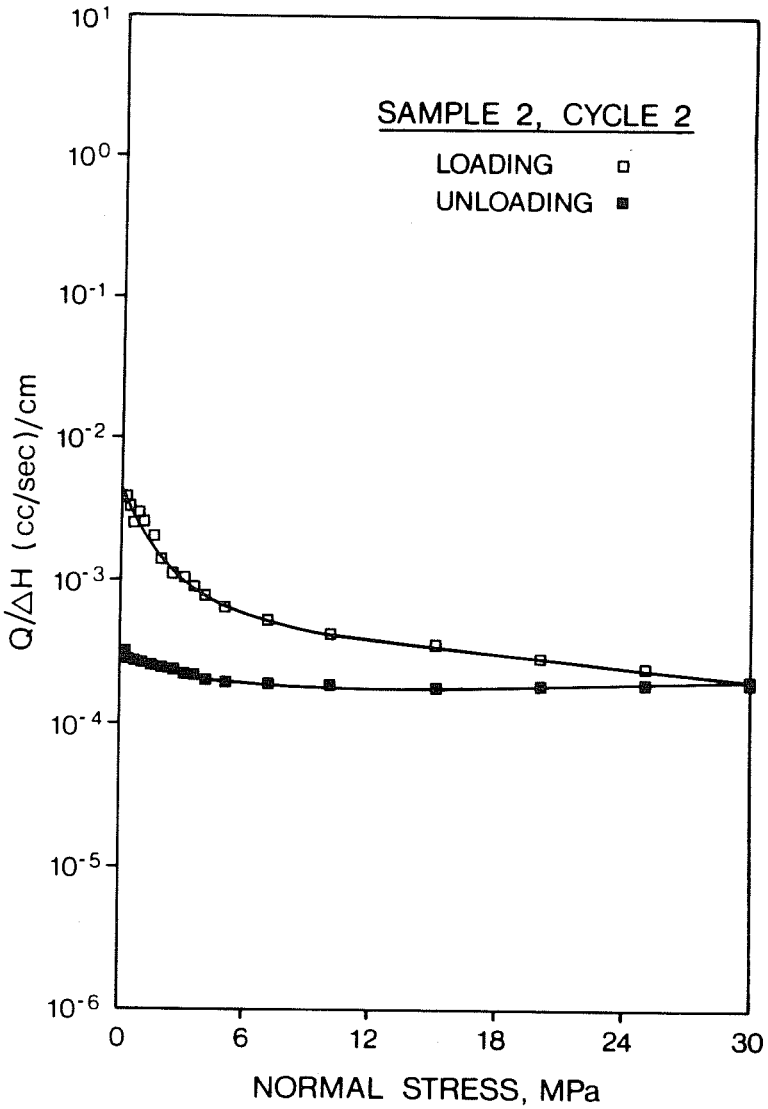

XBL 846-2234

Fig. C.2. Fracture flowrate per unit head as a function of normal stress, sample 2, cycle 2.

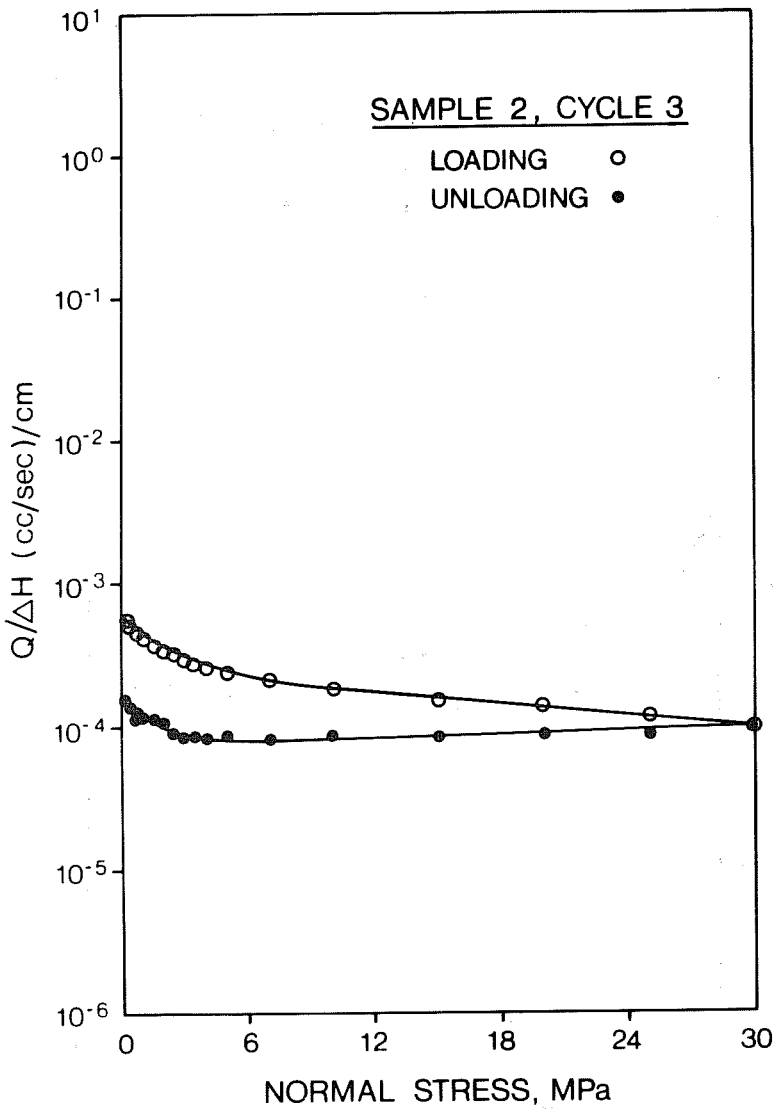

XBL 846-2233

Fig. C.3. Fracture flowrate per unit head as a function of normal stress, sample 2, cycle 3.

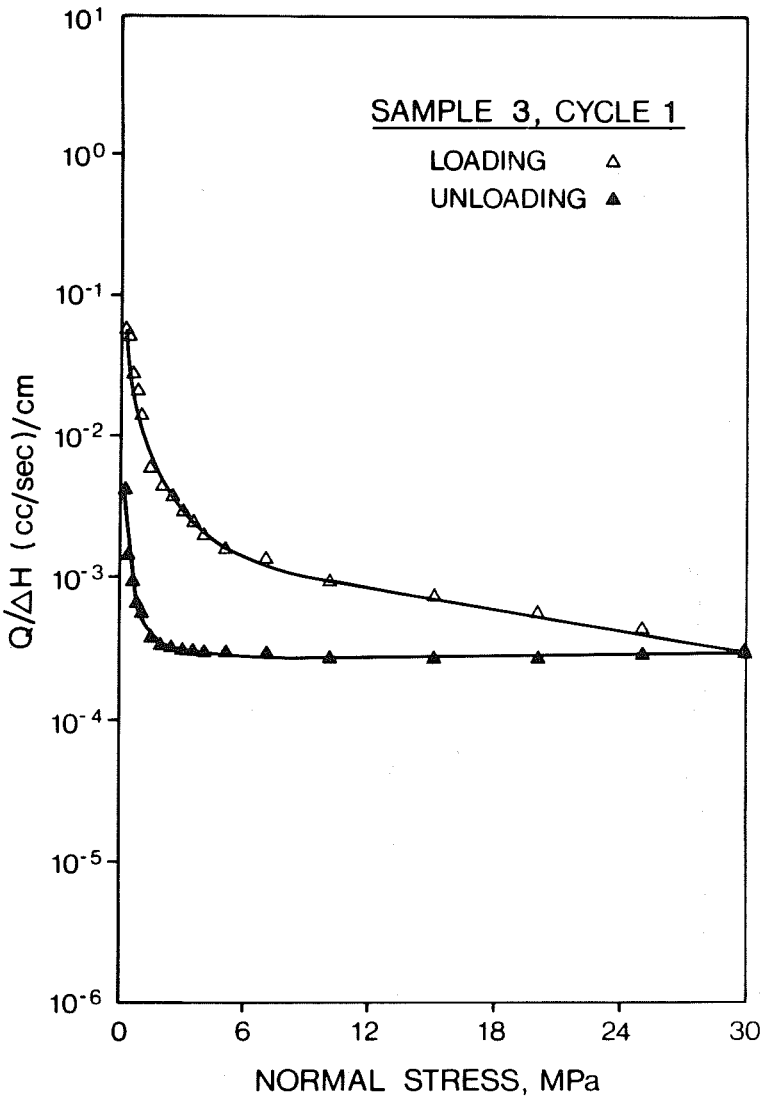

XBL 846-2232

Fig. C.4. Fracture flowrate per unit head as a function of normal stress, sample 3, cycle 1.

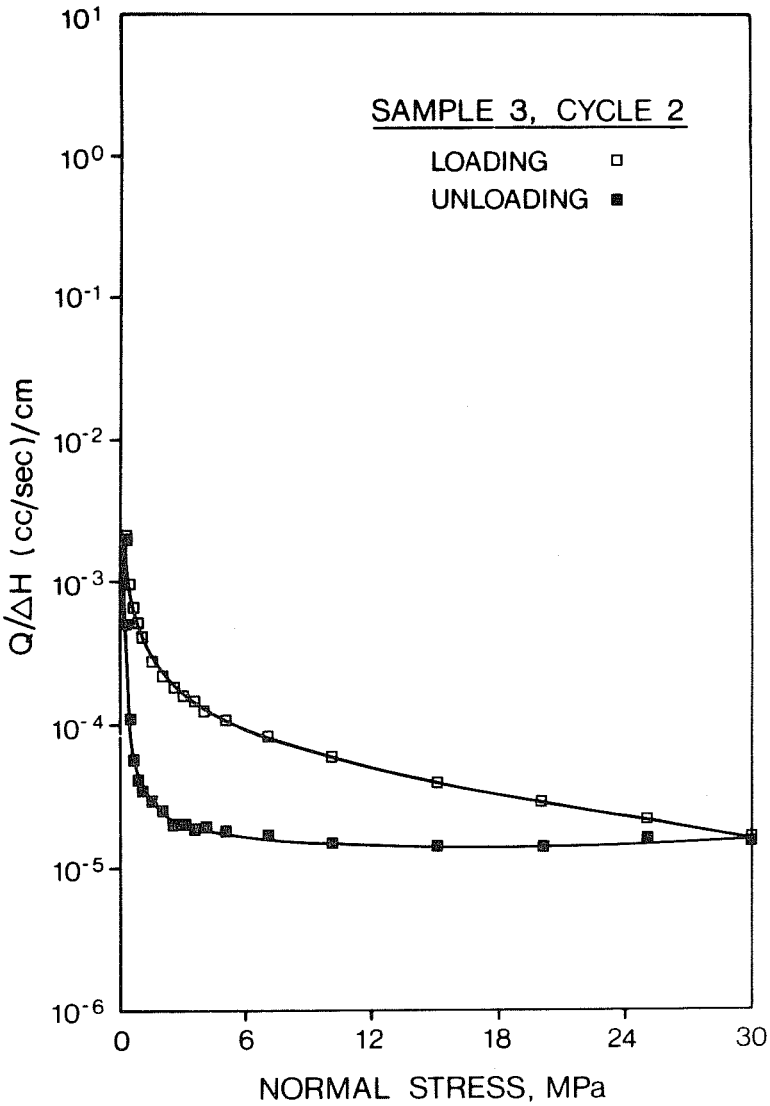

XBL 846-2231

Fig. C.5. Fracture flowrate per unit head as a function of normal stress, sample 3, cycle 2.

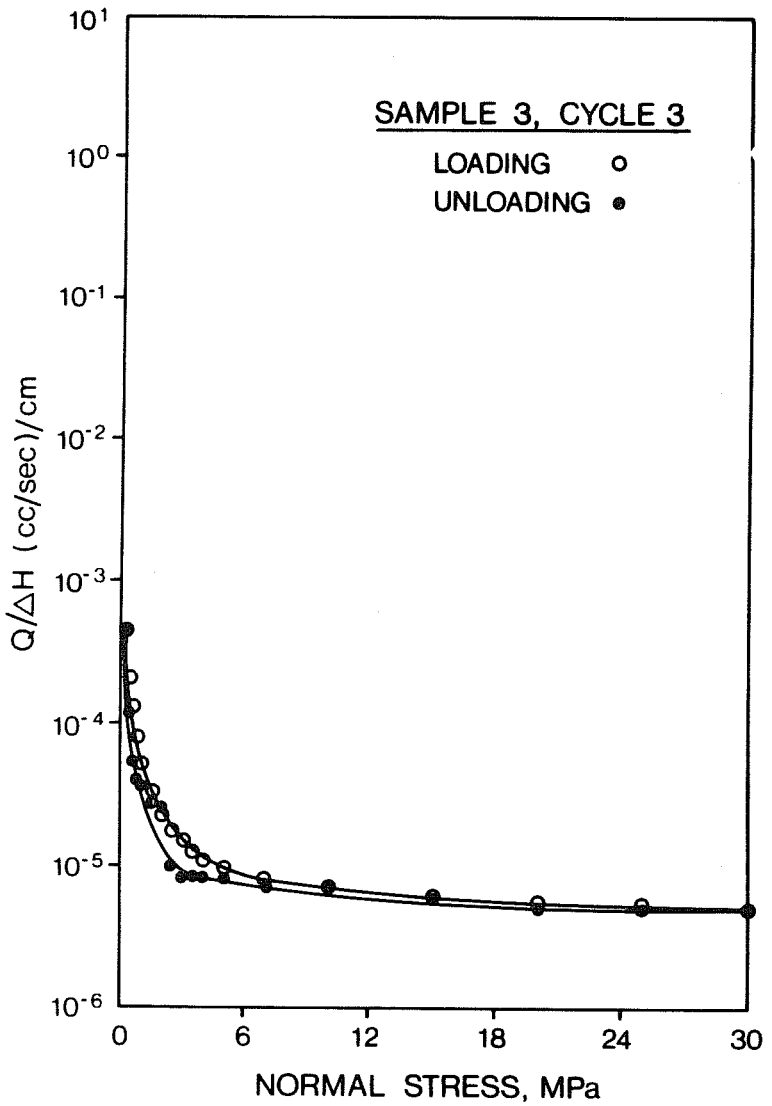

XBL 846-2230

Fig. C.6. Fracture flowrate per unit head as a function of normal stress, sample 3, cycle 3.

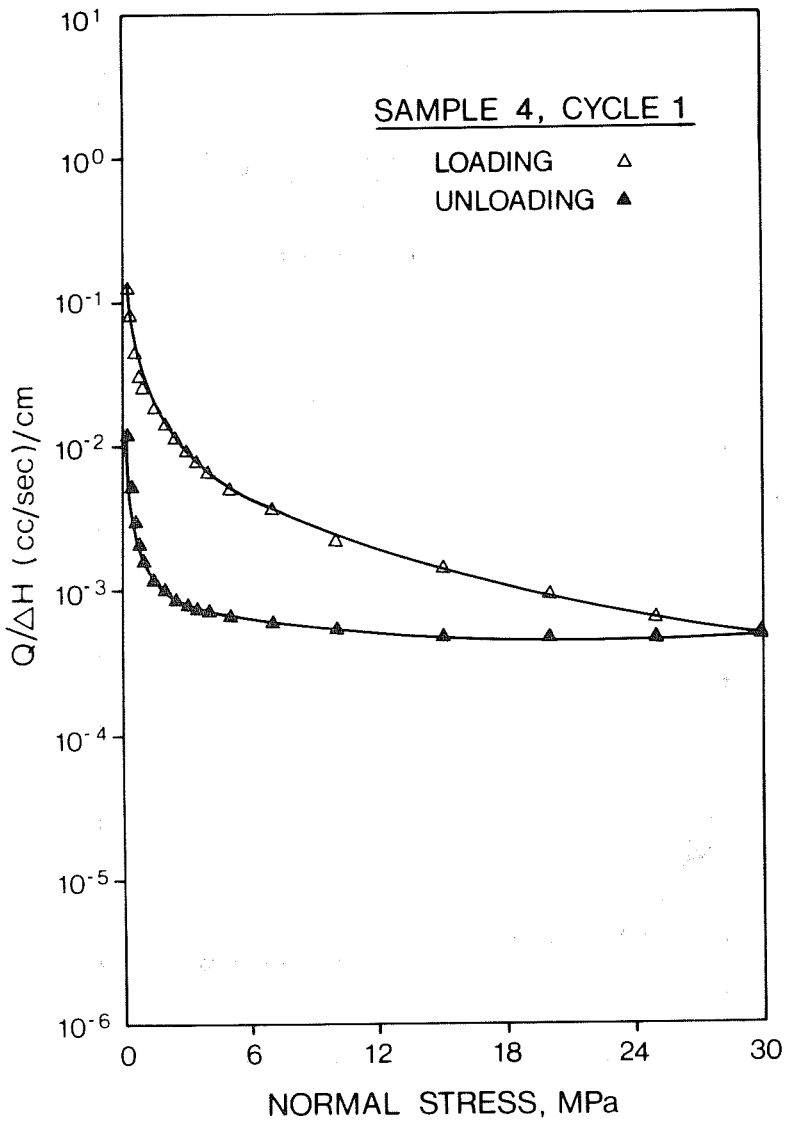

XBL 846-2229

Fig. C.7. Fracture flowrate per unit head as a function of normal stress, sample 4, cycle 1.

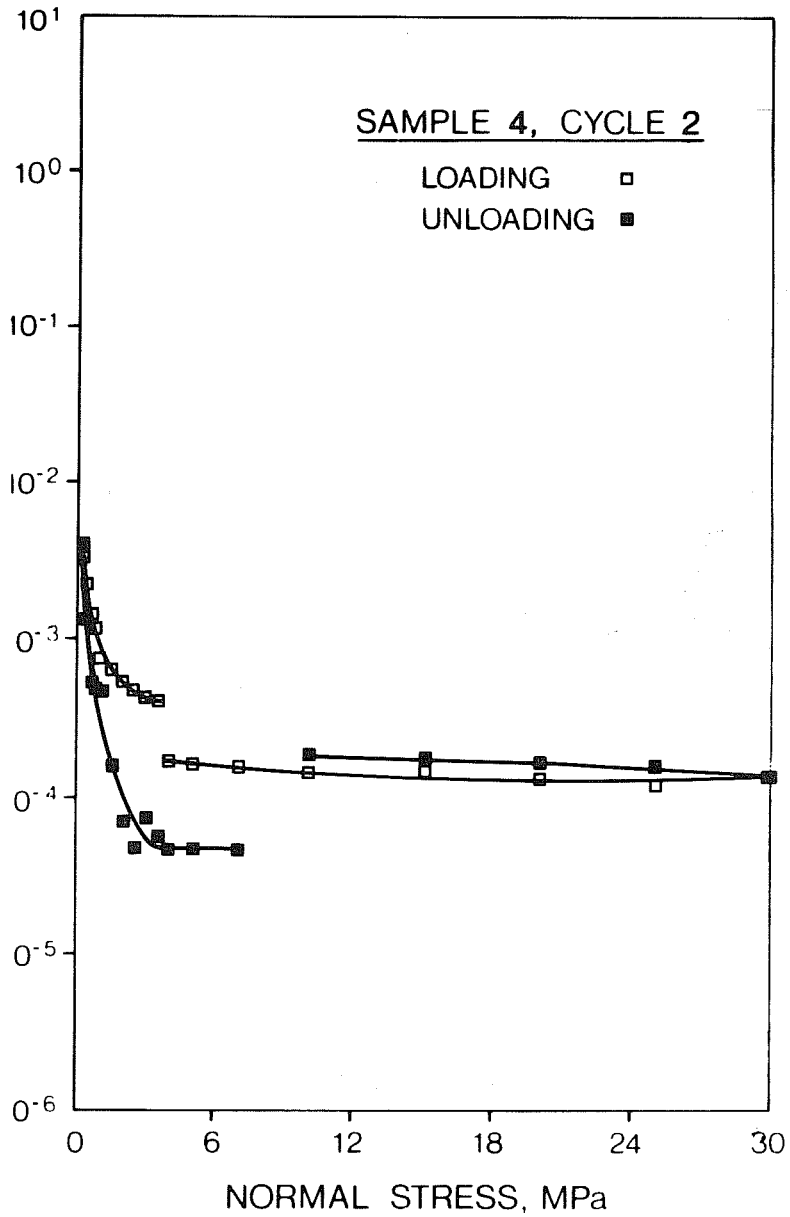

XBL 846-2228

Fig. C.8. Fracture flowrate per unit head as a function of normal stress, sample 4, cycle 2.

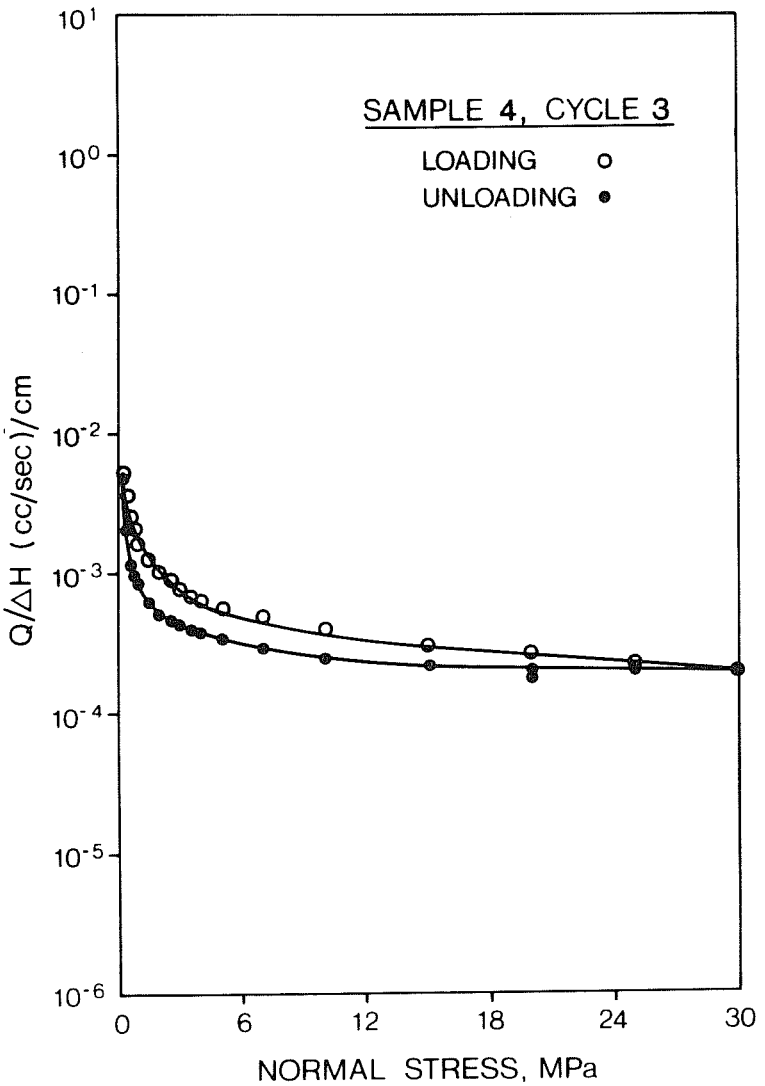

XBL 846-2227

Fig. C.9. Fracture flowrate per unit head as a function of normal stress, sample 4, cycle 3.

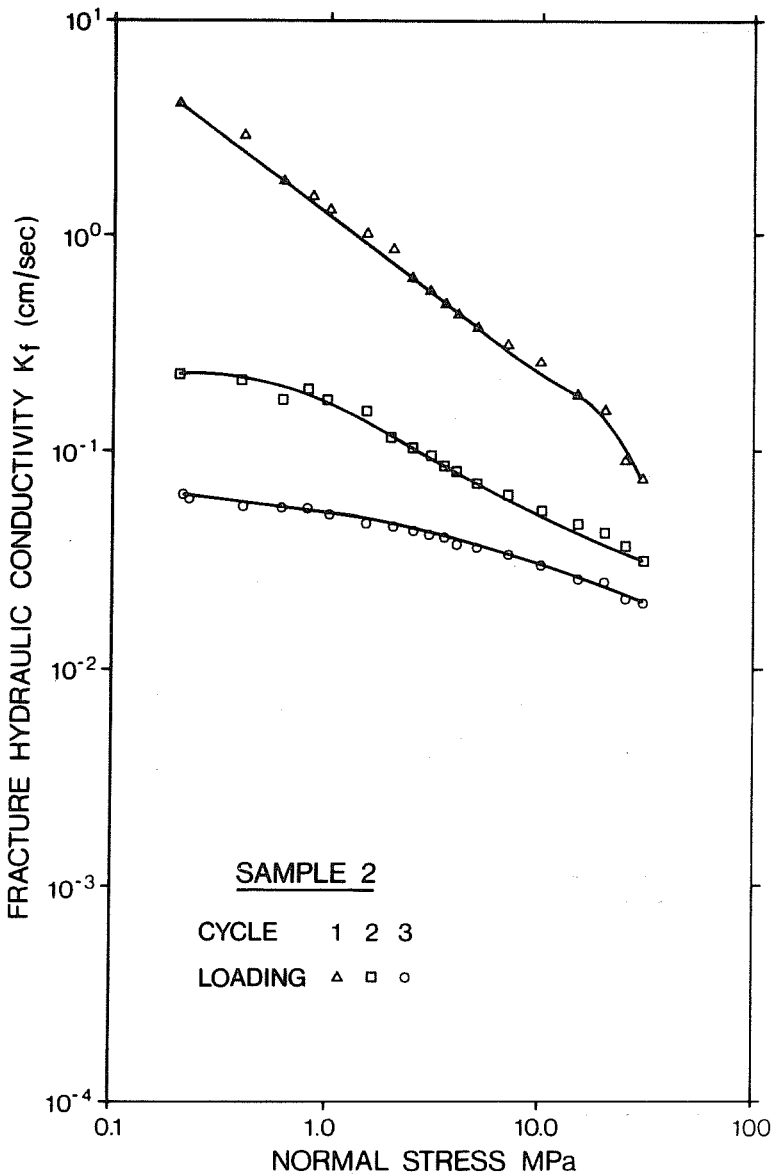

XBL 846-2226

Fig. C.10. Fracture hydraulic conductivity as a function of normal stress, sample 2, loading cycles 1, 2, and 3.

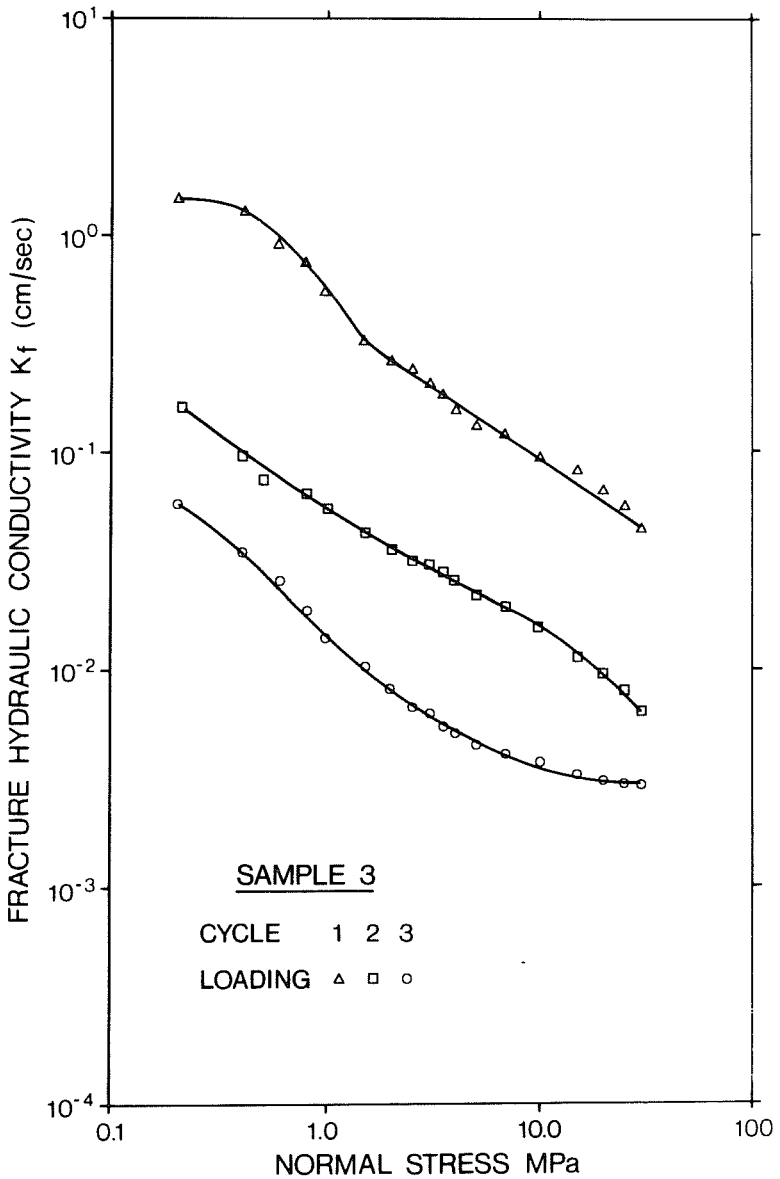

XBL 846-2225

Fig. C.11. Fracture hydraulic conductivity as a function of normal stress, sample 3, loading cycles 1, 2, and 3.

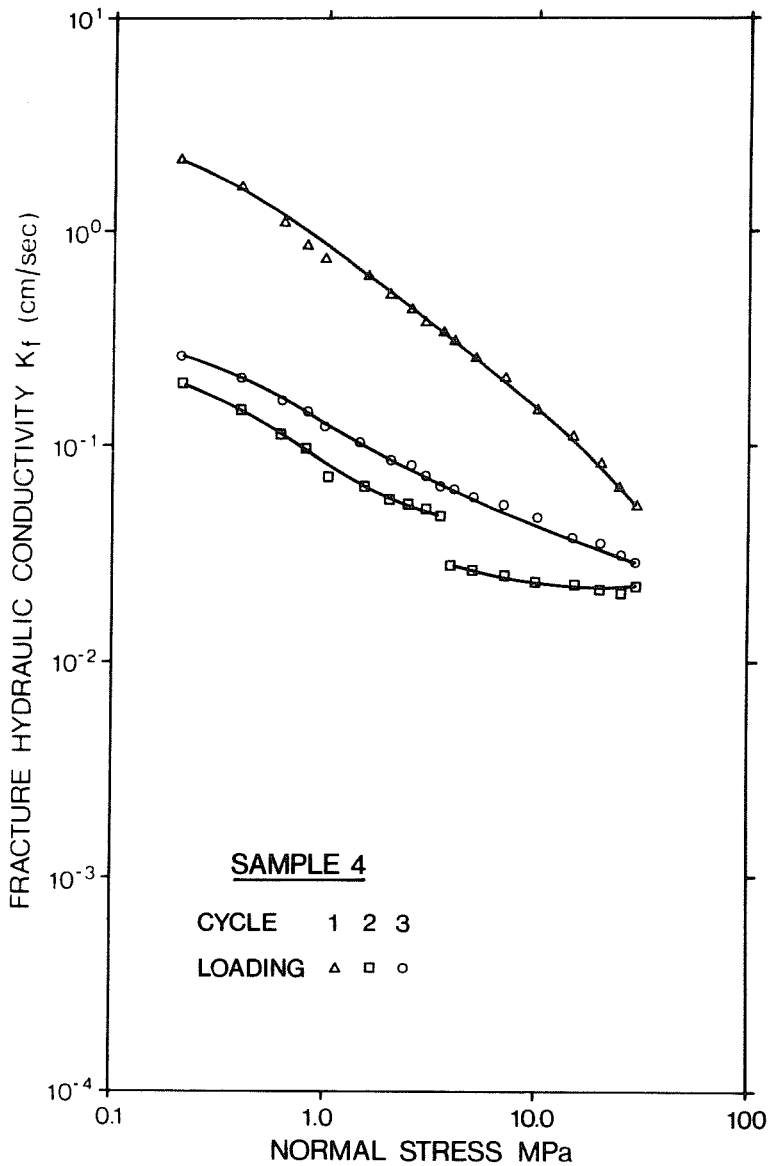

XBL 846-2224

Fig. C.12. Fracture hydraulic conductivity as a function of normal stress, sample 4, loading cycles 1, 2, and 3.

APPENDIX D: STRESS-PERMEABILITY DATA

SIGMA = Average normal stress in MPa.

Q = Flow rate in cm^3/sec.

DH = Differential head in cm.

Q/DH = Normalized flow rate.

mean D2D = Average fracture deformations, determined by averaging the three fracture LVDT's in cm.

DL-Rock = Deformation of rock, over given span, in cm.

SAMPLE 1 CYCLE 1

STRESS PERMEABILITY DATA SUMMARY

SIGMA (MPA)	Q (CC/SEC)	DH (CM)	Q/DH (CC/SEC-CM)	MEAN D2B (CM)	DL-ROCK (CM)
0.1717	0.2031E 02	171.52	0.1184E 00	0.3318E-02	0.3543E-03
0.4037	0.1758E 02	168.46	0.1044E 00	0.4637E-02	0.3250E-03
0.5522	0.1667E 02	191.94	0.8685E-01	0.5667E-02	0.2680E-03
0.8353	0.1576E 02	209.29	0.7530E-01	0.6312E-02	0.2304E-03
1.0116	0.1503E 02	302.20	0.4974E-01	0.7897E-02	0.2279E-03
1.4942	0.1321E 02	339.98	0.3886E-01	0.9072E-02	0.1388E-03
2.0186	0.9107E 01	339.98	0.2679E-01	0.1113E-01	0.3238E-03
2.5152	0.7924E 01	341.00	0.2324E-01	0.1171E-01	0.3115E-04
2.9792	0.6284E 01	353.25	0.1779E-01	0.1256E-01	0.5316E-03
3.6196	0.5647E 01	368.56	0.1532E-01	0.1276E-01	0.9344E-03
4.1022	0.5191E 01	376.73	0.1378E-01	0.1305E-01	0.9711E-03
4.9932	0.4189E 01	391.02	0.1071E-01	0.1396E-01	0.1019E-02
6.9654	0.2687E 01	410.42	0.6547E-02	0.1559E-01	0.1176E-02
9.9817	0.1594E 01	402.25	0.3963E-02	0.1695E-01	0.1262E-02
15.0027	0.7650E 00	402.25	0.1902E-02	0.1880E-01	0.1263E-02
19.9820	0.4561E 00	402.25	0.1134E-02	0.2000E-01	0.1196E-02
25.0262	0.2985E 00	406.34	0.7346E-03	0.2105E-01	0.1086E-02
29.9590	0.1907E 00	393.07	0.4852E-03	0.2206E-01	0.8992E-02
25.0076	0.2032E 00	398.17	0.5103E-03	0.2165E-01	0.1068E-02
20.0284	0.2280E 00	400.21	0.5697E-03	0.2116E-01	0.1189E-02
14.9888	0.2653E 00	397.15	0.6680E-03	0.2053E-01	0.1209E-02
10.0003	0.3275E 00	382.86	0.8554E-03	0.1988E-01	0.1079E-02
6.9886	0.4229E 00	408.38	0.1036E-02	0.1949E-01	0.8943E-03
4.9978	0.4975E 00	408.38	0.1218E-02	0.1919E-01	0.7537E-03
3.9815	0.5473E 00	403.28	0.1357E-02	0.1901E-01	0.6704E-03
3.4804	0.5804E 00	398.17	0.1458E-02	0.1889E-01	0.6260E-03
3.0070	0.6219E 00	404.30	0.1538E-02	0.1858E-01	0.6411E-03
2.4919	0.6758E 00	403.28	0.1676E-02	0.1833E-01	0.5924E-03
2.0233	0.7463E 00	410.42	0.1818E-02	0.1803E-01	0.6522E-03
1.4478	0.8085E 00	409.40	0.1975E-02	0.1771E-01	0.7111E-03
1.0070	0.8789E 00	402.25	0.2185E-02	0.1677E-01	0.8181E-03
0.8353	0.9784E 00	409.40	0.2390E-02	0.1675E-01	0.1040E-02
0.6079	0.1016E 01	404.30	0.2513E-02	0.1648E-01	0.9887E-03
0.3620	0.1184E 01	415.30	0.2849E-02	0.1638E-01	0.7848E-03
0.2413	0.1366E 01	422.67	0.3232E-02	0.1600E-01	0.7006E-03

SAMPLE 1 CYCLE 2

STRESS PERMEABILITY DATA SUMMARY

SIGMA (MPA)	Q (CC/SEC)	DH (CM)	Q/DH (CC/SEC-CM)	MEAN D2B (CM)	DL-ROCK (CM)
0.2274	0.1730E 01	397.15	0.4356E-02	0.1194E-02	0.1277E-02
0.4362	0.1457E 01	387.96	0.3756E-02	0.1378E-02	0.1721E-03
0.5986	0.1360E 01	397.15	0.3424E-02	0.1485E-02	0.1798E-03
0.8353	0.1219E 01	383.88	0.3175E-02	0.1495E-02	0.1964E-03
1.0255	0.1078E 01	364.48	0.2958E-02	0.1600E-02	0.2066E-03
1.5128	0.9080E 00	354.27	0.2563E-02	0.1943E-02	0.2356E-03
2.0047	0.7711E 00	362.44	0.2128E-02	0.2272E-02	0.2452E-03
2.4780	0.6882E 00	358.35	0.1920E-02	0.2513E-02	0.2347E-03
2.8261	0.5680E 00	345.08	0.1646E-02	0.2903E-02	0.2189E-03
3.5129	0.5182E 00	333.85	0.1552E-02	0.2982E-02	0.2134E-03
4.0048	0.4768E 00	341.00	0.1398E-02	0.5655E-02	0.1903E-03
5.0071	0.3939E 00	339.98	0.1159E-02	0.3524E-02	0.1301E-03
7.0304	0.3027E 00	337.93	0.8957E-02	0.4168E-02	0.3115E-04
10.0142	0.2322E 00	341.00	0.6809E-03	0.4701E-02	0.1308E-03
14.9749	0.1534E 00	345.08	0.4445E-03	0.5290E-02	0.3944E-03
20.0052	0.1119E 00	352.23	0.3177E-03	0.5696E-02	0.6972E-03
25.0169	0.8084E-01	341.00	0.2371E-03	0.5979E-02	0.1028E-02
30.0008	0.6426E-01	342.02	0.1879E-03	0.6204E-02	0.1371E-02
25.0076	0.6841E-01	349.16	0.1959E-03	0.6280E-02	0.1064E-02
20.0052	0.7463E-01	343.04	0.2176E-03	0.6271E-02	0.7605E-03
14.9934	0.7877E-01	334.87	0.2352E-03	0.6224E-02	0.4764E-03
9.9910	0.9121E-01	332.83	0.2740E-03	0.5993E-02	0.2757E-03
7.0211	0.1036E 00	329.77	0.3142E-03	0.5793E-02	0.1921E-03
4.9978	0.1161E 00	329.77	0.3521E-03	0.5540E-02	0.1604E-03
4.0187	0.1244E 00	328.75	0.3784E-03	0.5373E-02	0.0178E-03
3.5082	0.1285E 00	324.66	0.3958E-03	0.5285E-02	0.1755E-03
2.9885	0.1285E 00	318.54	0.4034E-03	0.5166E-02	0.1668E-03
2.4873	0.1451E 00	335.89	0.4320E-03	0.5030E-02	0.1792E-03
1.9954	0.1534E 00	331.81	0.4623E-03	0.4883E-02	0.1847E-03
1.5221	0.1617E 00	310.37	0.5210E-03	0.4719E-02	0.1900E-03
1.0023	0.1824E 00	335.89	0.5430E-03	0.4455E-02	0.2057E-03
0.8028	0.1907E 00	336.91	0.5660E-03	0.4340E-02	0.2128E-03
0.6079	0.2031E 00	331.81	0.6121E-03	0.4175E-02	0.2310E-03
0.3805	0.2197E 00	332.83	0.6601E-03	0.4003E-02	0.2433E-03
0.1856	0.2570E 00	334.87	0.7675E-03	0.3682E-02	0.2630E-03

SAMPLE 1 CYCLE 3

STRESS PERMEABILITY DATA SUMMARY

SIGMA (MPA)	Q (CC/SEC)	DH (CM)	Q/DH (CC/SEC-CM)	MEAN D2B (CM)	DL-ROCK (CM)
0.1949	0.3027E 00	393.07	0.7701E-03	0.1628E-03	0.1311E-03
0.3666	0.2653E 00	406.34	0.6529E-03	0.4493E-03	0.1431E-03
0.5847	0.2405E 00	404.30	0.5949E-03	0.5559E-03	0.1557E-03
0.8260	0.2197E 00	394.09	0.5575E-03	0.6703E-03	0.1267E-03
1.0627	0.2073E 00	395.11	0.5247E-03	0.6897E-03	0.1348E-03
1.5221	0.1824E 00	398.17	0.4581E-03	0.8455E-03	0.1277E-03
2.0279	0.1700E 00	398.17	0.4270E-03	0.1040E-02	0.1274E-03
2.4827	0.1534E 00	399.19	0.3843E-03	0.1164E-02	0.1089E-03
3.0070	0.1410E 00	401.23	0.3514E-03	0.1293E-02	0.8665E-04
3.4572	0.1327E 00	399.19	0.3324E-03	0.1447E-02	0.7648E-04
3.9583	0.1244E 00	400.21	0.3108E-03	0.1598E-02	0.5736E-04
5.0117	0.1161E 00	407.36	0.2850E-03	0.1880E-02	0.1079E-04
6.9779	0.8706E-01	367.54	0.2369E-03	0.2111E-02	0.1271E-03
9.9910	0.7463E-01	365.50	0.2042E-03	0.2430E-02	0.2976E-03
14.9842	0.5597E-01	399.19	0.1402E-03	0.2741E-02	0.6109E-03
20.0098	0.4560E-01	406.34	0.1122E-03	0.2905E-02	0.9729E-03
24.9752	0.3731E-01	406.34	0.9182E-04	0.3028E-02	0.1332E-02
29.9498	0.3040E-01	407.36	0.7463E-04	0.3169E-02	0.1705E-02
24.9844	0.2902E-01	400.21	0.7251E-04	0.3265E-02	0.1383E-02
19.9681	0.3455E-01	411.44	0.8397E-04	0.3288E-02	0.1070E-02
14.9888	0.3731E-01	406.34	0.9182E-04	0.3261E-02	0.7626E-02
9.9539	0.4768E-01	417.57	0.1142E-04	0.3131E-02	0.4848E-03
6.9561	0.5390E-01	412.46	0.1307E-03	0.2950E-02	0.3605E-03
5.0396	0.6012E-01	414.51	0.1450E-03	0.2784E-02	0.2920E-03
3.9444	0.6426E-01	409.40	0.1570E-03	0.2646E-02	0.2704E-03
3.5082	0.6633E-01	408.38	0.1624E-03	0.2570E-02	0.2609E-03
2.9374	0.6841E-01	407.36	0.1679E-03	0.2473E-02	0.2347E-03
2.5569	0.7256E-01	418.59	0.1733E-03	0.2361E-02	0.2304E-03
1.9861	0.7877E-01	425.74	0.1850E-03	0.2207E-02	0.2199E-03
1.4478	0.9950E-01	500.27	0.1989E-03	0.2047E-02	0.2149E-03
0.9559	0.1119E 00	510.47	0.2192E-03	0.1817E-02	0.2152E-03
0.7703	0.1202E 00	511.50	0.2350E-03	0.1757E-02	0.2122E-03
0.5754	0.1285E 00	510.47	0.2517E-03	0.1682E-02	0.2239E-03
0.4223	0.1368E 00	507.41	0.2696E-03	0.1562E-02	0.2291E-03
0.1995	0.1700E 00	500.27	0.3398E-03	0.1119E-02	0.2436E-03

SAMPLE 2 CYCLE 1

STRESS PERMEABILITY DATA SUMMARY

SIGMA (MPA)	Q (CC/SEC)	DH (CM)	Q/DH (CC/SEC-CM)	MEAN D2B (CM)	DL-ROCK (CM)
0.2091	0.2322E 02	81.68	0.2843E 00	0.1075E-01	0.5397E-04
0.4591	0.2313E 02	133.74	0.1729E 00	0.1460E-01	0.7370E-04
0.6121	0.1403E 02	175.60	0.7990E-01	0.1627E-01	0.6414E-04
0.8467	0.9472E 01	142.93	0.6627E-01	0.1807E-01	0.6969E-04
1.0099	0.7832E 01	152.12	0.5149E-01	0.1886E-01	0.8480E-04
1.5302	0.5920E 01	155.18	0.3815E-01	0.2100E-01	0.1132E-03
2.0760	0.4645E 01	161.31	0.2880E-01	0.2233E-01	0.9776E-04
2.4993	0.4645E 01	261.36	0.1777E-01	0.2323E-01	0.1345E-03
3.0196	0.3597E 01	256.26	0.1404E-01	0.2397E-01	0.1557E-03
3.5144	0.3005E 01	256.26	0.1173E-01	0.2464E-01	0.1391E-03
4.0091	0.2550E 01	256.26	0.9951E-02	0.2518E-01	0.1403E-03
5.0140	0.2095E 01	259.32	0.8079E-02	0.2620E-01	0.1150E-03
6.9931	0.1639E 01	266.47	0.6151E-02	0.2764E-01	0.1058E-03
9.9974	0.1700E 01	385.92	0.4405E-02	0.2925E-01	0.2405E-04
15.0522	0.1609E 01	564.59	0.2850E-02	0.3083E-01	0.1850E-03
20.0253	0.1161E 01	572.75	0.2027E-02	0.3185E-01	0.4505E-03
25.0291	0.5224E 00	548.25	0.9528E-03	0.3259E-01	0.7595E-03
30.0482	0.4063E 00	564.59	0.7196E-03	0.3316E-01	0.1062E-02
25.0393	0.2902E 00	550.29	0.5274E-03	0.3303E-01	0.8604E-03
20.0202	0.2736E 00	549.27	0.4981E-03	0.3284E-01	0.6516E-03
15.0063	0.2736E 00	562.54	0.4864E-03	0.3260E-01	0.4564E-03
10.0229	0.2031E 00	392.04	0.5181E-03	0.3215E-03	0.3093E-03
6.9880	0.1949E 00	384.90	0.5064E-03	0.3167E-01	0.2353E-03
5.0038	0.1907E 00	398.17	0.4789E-03	0.3120E-01	0.1952E-03
3.9683	0.1866E 00	394.09	0.4735E-03	0.3092E-01	0.1841E-03
3.4991	0.2612E 00	442.07	0.5909E-03	0.3076E-01	0.1693E-03
2.9890	0.2778E 00	435.95	0.6372E-03	0.3056E-01	0.1637E-03
2.4993	0.2819E 00	437.99	0.6436E-03	0.3036E-01	0.1653E-03
1.9995	0.1493E 00	455.34	0.3279E-03	0.3002E-01	0.1591E-03
1.5047	0.1596E 00	467.59	0.3413E-03	0.2965E-01	0.1452E-03
0.9793	0.1824E 00	452.28	0.4033E-03	0.2910E-01	0.1295E-03
0.8008	0.1845E 00	439.01	0.4203E-03	0.2888E-01	0.1206E-03
0.5917	0.1949E 00	448.20	0.4349E-03	0.2847E-01	0.1147E-03
0.3877	0.2322E 00	418.59	0.5547E-03	0.2789E-01	0.1443E-03
0.1887	0.3607E 00	449.22	0.8030E-03	0.2711E-01	0.1542E-03

SAMPLE 2 CYCLE 2

STRESS PERMEABILITY DATA SUMMARY

SIGMA (MPA)	Q (CC/SEC)	DH (CM)	Q/DH (CC/SEC-CM)	MEAN D2B (CM)	DL-ROCK (CM)
0.2091	0.1895E 01	498.22	0.3804E-02	0.2693E-02	0.4040E-04
0.3928	0.1584E 01	473.72	0.3344E-02	0.3335E-02	0.6044E-04
0.6121	0.1173E 01	460.45	0.2548E-02	0.3852E-02	0.7000E-04
0.8161	0.1285E 01	428.80	0.2997E-02	0.4215E-02	0.5797E-04
0.9997	0.1124E 01	446.16	0.2519E-02	0.4437E-02	0.6013E-04
1.5404	0.1252E 01	611.55	0.2047E-02	0.5055E-02	0.7216E-04
1.9077	0.8743E 00	624.82	0.1399E-02	0.5480E-02	0.4101E-04
2.5350	0.7104E 00	629.93	0.1128E-02	0.5864E-02	0.1665E-04
3.0247	0.5224E 00	494.14	0.1057E-02	0.6101E-02	0.1419E-04
3.5195	0.4623E 00	505.37	0.9148E-03	0.6359E-02	0.1141E-04
4.0040	0.4042E 00	506.39	0.7982E-03	0.6542E-02	0.1295E-04
5.0140	0.3317E 00	502.31	0.6604E-03	0.6902E-02	0.3577E-04
7.0084	0.2736E 00	508.43	0.5381E-03	0.7458E-02	0.8665E-04
10.0025	0.2260E 00	515.58	0.4383E-03	0.8068E-02	0.1789E-03
15.0114	0.1866E 00	509.45	0.3663E-03	0.8775E-02	0.3997E-03
20.0202	0.1534E 00	513.54	0.2987E-03	0.9324E-02	0.6812E-03
25.0291	0.1285E 00	502.31	0.2558E-03	0.9791E-02	0.9794E-03
30.0482	0.1036E 00	504.35	0.2054E-03	0.1021E-01	0.1284E-02
25.0087	0.9550E-01	503.33	0.1977E-03	0.1012E-01	0.1040E-02
20.0202	0.9743E-01	506.39	0.1924E-03	0.9988E-02	0.7947E-03
15.0114	0.9328E-01	504.35	0.1850E-03	0.9809E-02	0.5446E-03
9.9923	0.9743E-01	506.39	0.1924E-03	0.9353E-02	0.2985E-03
7.0135	0.9950E-01	505.37	0.1969E-03	0.8919E-02	0.1785E-03
5.0140	0.9950E-01	501.29	0.1985E-03	0.8563E-02	0.1033E-03
3.9938	0.1057E 00	505.37	0.2092E-03	0.8327E-02	0.6044E-04
3.4889	0.1140E 00	511.50	0.2229E-03	0.8232E-02	0.3670E-04
2.9941	0.1182E 00	513.54	0.2302E-03	0.8087E-02	0.1819E-04
2.5146	0.1265E 00	516.60	0.2449E-03	0.7838E-02	0.2467E-05
1.9842	0.1265E 00	512.52	0.2468E-03	0.7531E-02	0.1912E-04
1.5098	0.1327E 00	514.56	0.2579E-03	0.7207E-02	0.3546E-04
0.9742	0.1389E 00	507.41	0.2737E-03	0.6697E-02	0.5921E-04
0.7957	0.1389E 00	493.12	0.2817E-03	0.6557E-02	0.5242E-04
0.6172	0.1410E 00	496.18	0.2842E-03	0.6269E-02	0.3361E-04
0.4030	0.1451E 00	504.35	0.2877E-03	0.5839E-02	0.3515E-04
0.1938	0.1638E 00	509.45	0.3215E-03	0.5101E-02	0.4286E-04

SAMPLE 2 CYCLE 3

STRESS PERMEABILITY DATA SUMMARY

SIGMA (MPA)	Q (CC/SEC)	DH (CM)	Q/DH (CC/SEC-CM)	MEAN D2B (CM)	DL-ROCK (CM)
0.2244	0.3097E 00	540.08	0.5734E-03	0.2439E-02	0.1203E-04
0.2295	0.2778E 00	533.96	0.5203E-03	0.2451E-02	0.1634E-04
0.4234	0.2570E 00	537.02	0.4786E-03	0.3056E-02	0.1604E-04
0.6121	0.2529E 00	533.96	0.4736E-03	0.3387E-02	0.2220E-04
0.8059	0.2322E 00	510.47	0.4549E-03	0.3695E-02	0.2621E-04
1.0099	0.2135E 00	508.43	0.4199E-03	0.3945E-02	0.3053E-04
1.5302	0.1886E 00	505.37	0.3732E-03	0.4421E-02	0.3577E-04
2.0097	0.1721E 00	501.29	0.3433E-03	0.4741E-02	0.4718E-04
2.5044	0.1803E 00	553.35	0.3258E-03	0.5011E-02	0.5859E-04
2.9941	0.1658E 00	554.38	0.2991E-03	0.5224E-02	0.6877E-04
3.5093	0.1534E 00	548.25	0.2798E-03	0.5413E-02	0.8419E-04
4.0091	0.1451E 00	555.40	0.2613E-03	0.5579E-02	0.9775E-04
5.0191	0.1327E 00	551.31	0.2407E-03	0.5876E-02	0.1308E-03
7.0339	0.1202E 00	551.31	0.2180E-03	0.6338E-02	0.1998E-03
10.0433	0.1161E 00	622.78	0.1864E-03	0.6852E-02	0.3127E-03
15.0420	0.9536E 01	621.76	0.1534E-03	0.7444E-02	0.5551E-03
20.0457	0.8845E-01	635.03	0.1393E-03	0.7865E-02	0.8530E-02
25.0648	0.7463E-01	628.91	0.1187E-03	0.8232E-02	0.1159E-02
30.0584	0.6012E-01	608.49	0.9880E-04	0.8577E-02	0.1465E-02
25.0036	0.5252E-01	615.63	0.8531E-04	0.8480E-02	0.1229E-02
20.0202	0.5390E-01	611.55	0.8814E-04	0.8368E-02	0.9843E-03
14.9961	0.5113E-01	609.51	0.8389E-04	0.8215E-02	0.7278E-03
9.9923	0.5390E-01	614.61	0.8770E-04	0.7840E-02	0.4724E-03
7.0288	0.5113E-01	620.74	0.8237E-04	0.7436E-02	0.3423E-03
4.9987	0.5390E-01	614.61	0.8770E-04	0.7065E-02	0.2507E-03
3.9989	0.5251E-01	620.74	0.8459E-04	0.6941E-02	0.2017E-03
3.4889	0.5390E-01	614.61	0.8770E-04	0.6815E-02	0.1856E-03
2.9635	0.5252E-01	611.55	0.8588E-04	0.6602E-02	0.1582E-03
2.5095	0.5528E-01	607.47	0.9100E-04	0.6509E-02	0.1332E-03
1.9995	0.6495E-01	604.40	0.1075E-03	0.6199E-02	0.1042E-03
1.4945	0.6910E-01	599.30	0.1153E-03	0.5867E-02	0.8758E-04
1.0201	0.7186E-01	601.34	0.1195E-03	0.5488E-02	0.7216E-04
0.6121	0.7048E-01	598.28	0.1247E-03	0.5331E-02	0.6044E-04
0.7804	0.7463E-01	598.28	0.1178E-03	0.5028E-02	0.6137E-04
0.3979	0.8568E-01	599.30	0.1430E-03	0.4660E-02	0.4101E-04
0.1989	0.9259E-01	595.21	0.1556E-03	0.4010E-02	0.5273E-04

SAMPLE 3 CYCLE 1

STRESS PERMEABILITY DATA SUMMARY

SIGMA (MPA)	Q (CC/SEC)	DH (CM)	Q/DH (CC/SEC-CM)	MEAN D2B (CM)	DL-ROCK (CM)
0.2020	0.8015E 01	140.89	0.5689E-01	0.1648E-02	0.3084E-05
0.4162	0.6739E 01	134.77	0.5001E-01	0.2782E-02	0.9560E-05
0.5998	0.5465E -1	196.02	0.2788E-01	0.4055E-02	0.5551E-05
0.7926	0.4326E 01	207.25	0.2087E-01	0.4975E-02	0.8018E-05
0.9885	0.2960E 01	211.34	0.1401E-01	0.5808E-02	0.9251E-06
1.4598	0.1412E 01	235.84	0.5987E-02	0.7630E-02	0.3454E-04
2.0106	0.1032E 01	237.88	0.4338E-02	0.8654E-02	0.3577E-04
2.5217	0.8500E 00	227.67	0.3733E-02	0.9631E-02	0.3639E-04
3.0083	0.6831E 00	236.86	0.2884E-02	0.1036E-01	0.3485E-04
3.5132	0.6147E 00	247.07	0.2488E-02	0.1097E-01	0.3207E-04
4.0090	0.4736E 00	237.88	0.1991E-02	0.1152E-01	0.3145E-04
5.0066	0.3825E 00	242.99	0.1574E-02	0.1247E-01	0.3330E-04
6.9897	0.3234E 00	241.97	0.1337E-02	0.1376E-01	0.4317E-04
10.0164	0.2239E 00	237.88	0.9412E-03	0.1609E-01	0.6507E-04
15.0200	0.2032E 00	274.64	0.7399E-03	0.1689E-01	0.1224E-03
19.9899	0.1700E 00	298.12	0.5702E-03	0.1805E-01	0.1733E-03
25.0118	0.1451E 00	329.77	0.4400E-03	0.1905E-01	0.2214E-03
30.0032	0.9121E-01	306.28	0.2978E-03	0.1997E-01	0.2664E-03
25.0302	0.9328E-01	331.81	0.2811E-03	0.1973E-01	0.2217E-03
20.0021	0.9536E-01	346.10	0.2755E-03	0.1945E-01	0.1687E-03
15.0077	0.9950E-01	364.48	0.2730E-03	0.1909E-01	0.1218E-03
10.0072	0.1016E-01	366.52	0.2772E-03	0.1859E-01	0.6846E-04
7.0050	0.1078E 00	368.56	0.2925E-03	0.1817E-01	0.4040E-04
5.0066	0.1078E 00	364.48	0.2958E-03	0.1780E-01	0.2652E-04
4.0090	0.1057E 00	354.27	0.2984E-03	0.1755E-01	0.2189E-04
3.4826	0.1202E 00	394.09	0.3050E-03	0.1742E-01	0.1758E-04
2.9991	0.1182E 00	385.92	0.3063E-03	0.1725E-01	0.1758E-04
2.5003	0.1223E 00	380.81	0.3212E-03	0.1705E-01	0.1665E-04
1.9831	0.1306E 00	387.96	0.3366E-03	0.1676E-01	0.1326E-04
1.5148	0.1451E 00	384.90	0.3770E-03	0.1631E-01	0.1264E-04
0.9977	0.2094E 00	375.71	0.5573E-03	0.1558E-01	0.9560E-05
0.7926	0.2405E 00	371.63	0.6472E-03	0.1517E-01	0.8943E-05
0.6029	0.3441E 00	362.44	0.9494E-03	0.1462E-01	0.9868E-05
0.3764	0.5224E 00	365.50	0.1429E-02	0.1374E-01	0.1018E-04
0.1806	0.1548E 01	368.56	0.4200E-02	0.1165E-01	0.1264E-04

SAMPLE 3 CYCLE 2

STRESS PERMEABILITY DATA SUMMARY

SIGMA (MPA)	Q (CC/SEC)	DH (CM)	Q/DH (CC/SEC-CM)	MEAN D2B (CM)	DL-ROCK (CM)
0.2142	0.6375E 00	295.05	0.2161E-02	0.4061E-02	0.4934E-05
0.4040	0.3643E 00	370.60	0.9830E-03	0.5014E-02	0.3392E-05
0.5968	0.2653E 00	397.15	0.6680E-03	0.5775E-02	0.9251E-06
0.8171	0.2011E 00	385.92	0.5211E-03	0.6394E-02	0.4317E-05
1.0221	0.1638E 00	390.00	0.4200E-03	0.6817E-02	0.3700E-05
1.5148	0.1119E 00	398.17	0.2810E-03	0.7579E-02	0.1850E-05
2.0014	0.9121E-01	412.46	0.2211E-03	0.8052E-02	0.2159E-05
2.5278	0.8707E-01	467.59	0.1862E-03	0.8446E-02	0.1234E-05
3.0144	0.7877E-01	481.89	0.1635E-03	0.8729E-02	0.4626E-05
3.5040	0.7255E-01	474.74	0.1528E-03	0.8978E-02	0.3082E-06
3.9814	0.6012E-01	475.76	0.1264E-03	0.9213E-02	0.3700E-05
5.0128	0.5390E-01	481.89	0.1119E-03	0.9610E-02	0.8326E-05
6.9897	0.4008E-01	477.80	0.6100E-04	0.1097E-01	0.5304E-04
9.9980	0.2902E-01	475.76	0.8388E-04	0.1024E-01	0.2375E-04
15.0414	0.1907E-01	472.70	0.4034E-04	0.1182E-01	0.1079E-03
20.0144	0.1384E-01	467.59	0.2960E-04	0.1256E-01	0.1610E-03
25.0026	0.1033E-01	455.34	0.2269E-04	0.1324E-01	0.2097E-03
30.0123	0.7225E-02	443.09	0.1631E-04	0.1393E-01	0.2606E-03
24.9996	0.6700E-02	412.46	0.1624E-04	0.1368E-01	0.2146E-03
20.0205	0.6350E-02	442.07	0.1436E-04	0.1336E-01	0.1656E-03
15.0108	0.6174E-02	420.63	0.1468E-04	0.1294E-01	0.1163E-03
10.0041	0.6218E-02	411.44	0.1511E-04	0.1239E-01	0.6322E-04
6.9928	0.7444E-02	433.90	0.1716E-04	0.1195E-01	0.3269E-04
5.0128	0.8058E-02	433.90	0.1857E-04	0.1155E-01	0.1789E-04
4.0029	0.8233E-02	421.65	0.1953E-04	0.1130E-01	0.1326E-04
3.5102	0.8233E-02	431.86	0.1906E-04	0.1116E-01	0.1665E-04
3.0022	0.8933E-02	436.97	0.2044E-04	0.1099E-01	0.1203E-04
2.5094	0.8933E-02	433.90	0.2059E-04	0.1080E-01	0.8943E-05
1.9923	0.1068E-01	422.67	0.2527E-04	0.1052E-01	0.8634E-05
1.5026	0.1279E-01	428.80	0.2983E-04	0.1016E-01	0.1048E-04
0.9915	0.1559E-01	426.76	0.3653E-04	0.9532E-02	0.1079E-04
0.8018	0.1935E-01	452.28	0.4278E-04	0.9158E-02	0.1018E-04
0.5876	0.2626E-01	452.28	0.5806E-04	0.8626E-02	0.9560E-05
0.4040	0.4837E-01	422.67	0.1144E-03	0.7827E-02	0.8943E-05
0.1897	0.2280E 00	452.28	0.5041E-03	0.6008E-02	0.8943E-05

SAMPLE 3 CYCLE 3

STRESS PERMEABILITY DATA SUMMARY

SIGMA (MPA)	Q (CC/SEC)	DH (CM)	Q/DH (CC/SEC-CM)	MEAN D2B (CM)	DL-ROCK (CM)
0.2050	0.2218E 00	486.99	0.4554E-03	0.3889E-02	0.5859E-05
0.4193	0.1016E 00	482.91	0.2104E-03	0.5089E-02	0.4009E-05
0.5937	0.6426E-01	477.80	0.1345E-03	0.5642E-02	0.3392E-05
0.8079	0.3870E-01	477.80	0.8100E-04	0.6237E-02	0.6476E-05
0.9946	0.2488E-01	466.57	0.5332E-04	0.6622E-02	0.6476E-05
1.5118	0.1575E-01	467.59	0.3368E-04	0.7380E-02	0.8018E-05
1.9984	0.1078E-01	466.57	0.2310E-04	0.7826E-02	0.4934E-05
2.5094	0.8189E-02	455.34	0.1789E-04	0.8165E-02	0.7401E-05
3.0175	0.7225E-02	457.39	0.1580E-04	0.8447E-02	0.8943E-05
3.5132	0.5824E-02	458.41	0.1270E-04	0.8670E-02	0.9251E-05
4.0090	0.4905E-02	442.07	0.1110E-04	0.8909E-02	0.1974E-04
4.9913	0.4423E-02	449.22	0.9846E-05	0.9234E-02	0.2251E-04
6.9316	0.3591E-02	440.03	0.8161E-05	0.9799E-02	0.3916E-02
10.0286	0.3328E-02	453.30	0.7342E-05	0.1061E-01	0.6723E-04
15.0016	0.3022E-02	473.72	0.6379E-05	0.1128E-01	0.1252E-03
20.0450	0.2277E-02	403.28	0.5646E-05	0.1194E-01	0.1758E-03
25.0179	0.2102E-02	398.17	0.5279E-05	0.1255E-01	0.2291E-03
30.0093	0.2014E-02	387.96	0.5191E-05	0.1313E-01	0.2803E-03
24.9965	0.2233E-02	398.17	0.5608E-05	0.1293E-01	0.2319E-03
19.9746	0.2058E-02	397.15	0.5182E-05	0.1261E-01	0.1829E-03
15.0138	0.2365E-02	383.88	0.6161E-05	0.1218E-01	0.1304E-03
10.0255	0.2584E-02	359.37	0.7190E-05	0.1166E-01	0.7925E-04
7.0050	0.2584E-02	353.25	0.7315E-05	0.1122E-01	0.5119E-04
4.9994	0.2890E-02	347.12	0.8326E-05	0.1084E-01	0.3731E-04
3.9814	0.3065E-02	361.42	0.8481E-05	0.1059E-01	0.3176E-04
3.5285	0.3190E-02	361.42	0.8602E-05	0.1046E-01	0.2991E-04
2.9960	0.3722E-02	442.07	0.8419E-05	0.1028E-01	0.2991E-04
2.4880	0.4335E-02	427.78	0.1013E-04	0.1009E-01	0.2930E-04
1.9923	0.1082E-01	414.51	0.2610E-04	0.9825E-02	0.2868E-04
1.5332	0.1209E-01	430.84	0.2806E-04	0.9498E-02	0.2930E-04
0.9977	0.1603E-01	437.99	0.3660E-04	0.8900E-02	0.2837E-04
0.7865	0.1866E-01	461.47	0.4044E-04	0.8522E-02	0.2683E-04
0.6059	0.2488E-01	453.30	0.5489E-04	0.8024E-02	0.2930E-04
0.4040	0.5390E-01	451.26	0.1194E-03	0.7224E-02	0.2837E-04
0.2112	0.1845E 00	452.28	0.4079E-03	0.5708E-02	0.2930E-04

SAMPLE 4 CYCLE 1

STRESS PERMEABILITY DATA SUMMARY

SIGMA (MPA)	Q (CC/SEC)	DH (CM)	Q/DH (CC/SEC-CM)	MEAN D2B (CM)	DL-ROCK (CM)
0.2037	0.8379E 01	67.38	0.1243E 00	0.1980E-02	0.2868E-04
0.3920	0.5783E 01	72.49	0.7978E-01	0.4954E-02	0.2991E-04
0.6188	0.8379E 01	189.90	0.4412E-01	0.6606E-02	0.5551E-05
0.8032	0.6284E 01	209.29	0.3002E-01	0.7539E-02	0.1018E-04
0.9954	0.5191E 01	207.25	0.2505E-01	0.8355E-02	0.1789E-04
1.5142	0.4554E 01	253.20	0.1799E-01	0.1026E-01	0.3053E-04
2.0061	0.3962E 01	282.80	0.1401E-01	0.1149E-01	0.3670E-04
2.5019	0.3324E 01	299.14	0.1111E-01	0.1245E-01	0.4564E-04
2.9785	0.3051E 01	337.93	0.9028E-02	0.1321E-01	0.5520E-04
3.5127	0.2596E 01	333.85	0.7776E-02	0.1385E-01	0.4965E-04
4.0085	0.2216E 01	339.98	0.6518E-02	0.1442E-01	0.7247E-04
5.0015	0.1791E 01	355.29	0.5041E-02	0.1537E-01	0.8511E-04
7.0138	0.1305E 01	358.35	0.3642E-02	0.1670E-01	0.1048E-03
10.0115	0.9715E 00	446.16	0.2177E-02	0.1819E-01	0.3639E-04
15.0115	0.6193E 00	442.07	0.1401E-02	0.1978E-01	0.1912E-04
20.0077	0.4189E 00	451.26	0.9238E-03	0.2086E-01	0.1283E-03
24.9885	0.2964E 00	458.41	0.6466E-03	0.2192E-01	0.4872E-04
29.9769	0.2280E 00	468.62	0.4865E-03	0.2254E-01	0.2720E-03
25.0154	0.2156E 00	466.57	0.4621E-03	0.2238E-01	0.3485E-04
20.0038	0.2177E 00	474.74	0.4586E-03	0.2175E-01	0.1906E-03
15.0231	0.2218E 00	463.51	0.4785E-03	0.2121E-01	0.1835E-03
10.0346	0.2529E 00	467.59	0.5409E-03	0.2056E-01	0.1382E-03
6.9831	0.2757E 00	460.45	0.5988E-03	0.2001E-01	0.1163E-03
5.0038	0.3027E 00	453.30	0.6678E-03	0.1954E-01	0.1018E-03
3.9892	0.3296E 00	449.22	0.7337E-03	0.1921E-01	0.9590E-04
3.5050	0.2985E 00	395.11	0.7555E-03	0.1903E-01	0.9159E-04
3.0015	0.3068E 00	388.98	0.7887E-03	0.1880E-01	0.8974E-04
2.5058	0.3379E 00	390.00	0.8664E-03	0.1815E-01	0.8357E-04
2.0100	0.3814E 00	379.79	0.1004E-02	0.0814E-01	0.8110E-04
1.4912	0.4312E 00	365.50	0.1180E-02	0.1758E-01	0.7925E-04
1.0031	0.5763E 00	359.37	0.1604E-02	0.1672E-01	0.7987E-04
0.7994	0.7297E 00	349.16	0.2090E-02	0.1615E-01	0.8049E-04
0.5957	0.9826E 00	328.75	0.2989E-02	0.1534E-01	0.8172E-04
0.3997	0.1958E 01	376.73	0.5197E-02	0.1399E-01	0.8172E-04
0.2114	0.4053E 01	343.04	0.1181E-01	0.1162E-01	0.8172E-04

SAMPLE 4 CYCLE 2

STRESS PERMEABILITY DATA SUMMARY

SIGMA (MPA)	Q (CC/SEC)	DH (CM)	Q/DH (CC/SEC-CM)	MEAN D2B (CM)	DL-ROCK (CM)
0.2114	0.7741E 00	234.82	0.3297E-02	0.5973E-02	0.1203E-04
0.3997	0.7286E 00	328.75	0.2216E-02	0.8037E-02	0.1049E-04
0.6111	0.6603E 00	462.49	0.1428E-02	0.9326E-02	0.1604E-04
0.8032	0.5659E 00	492.10	0.1150E-02	0.1011E-01	0.1943E-04
1.0108	0.3731E 00	502.31	0.7428E-03	0.1074E-01	0.2251E-04
1.5065	0.3296E 00	515.58	0.6393E-03	0.1168E-01	0.3207E-04
2.0023	0.2778E 00	519.66	0.5346E-03	0.1231E-01	0.3947E-04
2.4942	0.2467E 00	518.64	0.4757E-03	0.1277E-01	0.4379E-04
2.9939	0.2239E 00	521.71	0.4292E-03	0.1313E-01	0.4811E-04
3.5165	0.2114E 00	522.73	0.4044E-03	0.1344E-01	0.5242E-04
3.9892	0.9536E-01	557.44	0.1711E-03	0.1382E-01	0.5890E-04
5.0038	0.8706E-01	533.96	0.1630E-03	0.1419E-01	0.6969E-04
7.0177	0.8292E-01	523.75	0.1583E-03	0.1485E-01	0.8542E-04
10.0115	0.7463E-01	505.37	0.1477E-03	0.1556E-01	0.1052E-03
15.0231	0.7463E-01	514.56	0.1450E-03	0.1647E-01	0.1415E-03
20.0038	0.6772E-01	506.39	0.1337E-03	0.1717E-01	0.1776E-03
25.0307	0.6081E-01	499.24	0.1218E-03	0.1781E-01	0.2189E-03
29.9962	0.6772E-01	494.14	0.1370E-03	0.1837E-01	0.2572E-03
24.9962	0.7877E-01	490.06	0.1607E-03	0.1802E-01	0.2226E-03
20.0192	0.8084E-01	479.85	0.1685E-03	0.1760E-01	0.1785E-03
14.9962	0.8499E-01	488.01	0.1742E-03	0.1710E-01	0.1403E-03
10.0154	0.8914E-01	483.93	0.1842E-03	0.1647E-01	0.1030E-03
6.9831	0.2280E-01	485.97	0.4692E-04	0.1596E-01	0.7864E-04
5.0192	0.2280E-01	488.01	0.4672E-04	0.1553E-01	0.6538E-04
4.0008	0.2280E-01	488.01	0.4672E-04	0.1524E-01	0.5551E-04
3.5127	0.2695E-01	483.93	0.5569E-04	0.1506E-01	0.5427E-04
3.0015	0.3524E-01	478.83	0.7360E-04	0.1485E-01	0.5366E-04
2.4904	0.2280E-01	483.93	0.4711E-04	0.1459E-01	0.4934E-04
1.9946	0.3317E-01	475.76	0.6972E-04	0.1426E-01	0.4872E-04
1.4988	0.7463E-01	472.70	0.1579E-03	0.1377E-01	0.4626E-04
0.9992	0.2218E 00	473.72	0.4682E-03	0.1295E-01	0.4502E-04
0.7994	0.2384E 00	489.03	0.4875E-03	0.1246E-01	0.4533E-04
0.6149	0.2467E 00	469.64	0.5253E-03	0.1181E-01	0.4286E-04
0.4074	0.6426E 00	478.83	0.1342E-02	0.1070E-01	0.3701E-04
0.1998	0.1867E 01	476.78	0.3916E-02	0.8102E-02	0.3824E-04

SAMPLE 4 CYCLE 1

STRESS PERMEABILITY DATA SUMMARY

SIGMA (MPA)	Q (CC/SEC)	DH (CM)	Q/DH (CC/SEC-CM)	MEAN D2B (CM)	DL-ROCK (CM)
0.2037	0.8379E 01	67.38	0.1243E 00	0.1980E-02	0.2868E-04
0.3920	0.5783E 01	72.49	0.7978E-01	0.4954E-02	0.2991E-04
0.6188	0.8379E 01	189.90	0.4412E-01	0.6606E-02	0.5551E-05
0.8032	0.6284E 01	209.29	0.3002E-01	0.7539E-02	0.1018E-04
0.9954	0.5191E 01	207.25	0.2505E-01	0.8355E-02	0.1789E-04
1.5142	0.4554E 01	253.20	0.1799E-01	0.1026E-01	0.3053E-04
2.0061	0.3962E 01	282.80	0.1401E-01	0.1149E-01	0.3670E-04
2.5019	0.3324E 01	299.14	0.1111E-01	0.1245E-01	0.4564E-04
2.9785	0.3051E 01	337.93	0.9028E-02	0.1321E-01	0.5520E-04
3.5127	0.2596E 01	333.85	0.7776E-02	0.1385E-01	0.4965E-04
4.0085	0.2216E 01	339.98	0.6518E-02	0.1442E-01	0.7247E-04
5.0015	0.1791E 01	355.29	0.5041E-02	0.1537E-01	0.8511E-04
7.0138	0.1305E 01	358.35	0.3642E-02	0.1670E-01	0.1048E-03
10.0115	0.9715E 00	446.16	0.2177E-02	0.1819E-01	0.3639E-04
15.0115	0.6193E 00	442.07	0.1401E-02	0.1978E-01	0.1912E-04
20.0077	0.4189E 00	451.26	0.9238E-03	0.2086E-01	0.1283E-03
24.9885	0.2964E 00	458.41	0.6466E-03	0.2192E-01	0.4872E-04
29.9769	0.2280E 00	468.62	0.4865E-03	0.2254E-01	0.2720E-03
25.0154	0.2156E 00	466.57	0.4621E-03	0.2238E-01	0.3485E-04
20.0038	0.2177E 00	474.74	0.4586E-03	0.2175E-01	0.1906E-03
15.0231	0.2218E 00	463.51	0.4785E-03	0.2121E-01	0.1835E-03
10.0346	0.2529E 00	467.59	0.5409E-03	0.2056E-01	0.1382E-03
6.9831	0.2757E 00	460.45	0.5988E-03	0.2001E-01	0.1163E-03
5.0038	0.3027E 00	453.30	0.6678E-03	0.1954E-01	0.1018E-03
3.9892	0.3296E 00	449.22	0.7337E-03	0.1921E-01	0.9590E-04
3.5050	0.2985E 00	395.11	0.7555E-03	0.1903E-01	0.9159E-04
3.0015	0.3068E 00	388.98	0.7887E-03	0.1880E-01	0.8974E-04
2.5058	0.3379E 00	390.00	0.8664E-03	0.1815E-01	0.8357E-04
2.0100	0.3814E 00	379.79	0.1004E-02	0.0814E-01	0.8110E-04
1.4912	0.4312E 00	365.50	0.1180E-02	0.1758E-01	0.7925E-04
1.0031	0.5763E 00	359.37	0.1604E-02	0.1672E-01	0.7987E-04
0.7994	0.7297E 00	349.16	0.2090E-02	0.1615E-01	0.8049E-04
0.5957	0.9826E 00	328.75	0.2989E-02	0.1534E-01	0.8172E-04
0.3997	0.1958E 01	376.73	0.5197E-02	0.1399E-01	0.8172E-04
0.2114	0.4053E 01	343.04	0.1181E-01	0.1162E-01	0.8172E-04

SAMPLE 4 CYCLE 2

STRESS PERMEABILITY DATA SUMMARY

SIGMA (MPA)	Q (CC/SEC)	DH (CM)	Q/DH (CC/SEC-CM)	MEAN D2B (CM)	DL-ROCK (CM)
0.2114	0.7741E 00	234.82	0.3297E-02	0.5973E-02	0.1203E-04
0.3997	0.7286E 00	328.75	0.2216E-02	0.8037E-02	0.1049E-04
0.6111	0.6603E 00	462.49	0.1428E-02	0.9326E-02	0.1604E-04
0.8032	0.5659E 00	492.10	0.1150E-02	0.1011E-01	0.1943E-04
1.0108	0.3731E 00	502.31	0.7428E-03	0.1074E-01	0.2251E-04
1.5065	0.3296E 00	515.58	0.6393E-03	0.1168E-01	0.3207E-04
2.0023	0.2778E 00	519.66	0.5346E-03	0.1231E-01	0.3947E-04
2.4942	0.2467E 00	518.64	0.4757E-03	0.1277E-01	0.4379E-04
2.9939	0.2239E 00	521.71	0.4292E-03	0.1313E-01	0.4811E-04
3.5165	0.2114E 00	522.73	0.4044E-03	0.1344E-01	0.5242E-04
3.9892	0.9536E-01	557.44	0.1711E-03	0.1382E-01	0.5890E-04
5.0038	0.8706E-01	533.96	0.1630E-03	0.1419E-01	0.6969E-04
7.0177	0.8292E-01	523.75	0.1583E-03	0.1485E-01	0.8542E-04
10.0115	0.7463E-01	505.37	0.1477E-03	0.1556E-01	0.1052E-03
15.0231	0.7463E-01	514.56	0.1450E-03	0.1647E-01	0.1415E-03
20.0038	0.6772E-01	506.39	0.1337E-03	0.1717E-01	0.1776E-03
25.0307	0.6081E-01	499.24	0.1218E-03	0.1781E-01	0.2189E-03
29.9962	0.6772E-01	494.14	0.1370E-03	0.1837E-01	0.2572E-03
24.9962	0.7877E-01	490.06	0.1607E-03	0.1802E-01	0.2226E-03
20.0192	0.8084E-01	479.85	0.1685E-03	0.1760E-01	0.1785E-03
14.9962	0.8499E-01	488.01	0.1742E-03	0.1710E-01	0.1403E-03
10.0154	0.8914E-01	483.93	0.1842E-03	0.1647E-01	0.1030E-03
6.9831	0.2280E-01	485.97	0.4692E-04	0.1596E-01	0.7864E-04
5.0192	0.2280E-01	488.01	0.4672E-04	0.1553E-01	0.6538E-04
4.0008	0.2280E-01	488.01	0.4672E-04	0.1524E-01	0.5551E-04
3.5127	0.2695E-01	483.93	0.5569E-04	0.1506E-01	0.5427E-04
3.0015	0.3524E-01	478.83	0.7360E-04	0.1485E-01	0.5366E-04
2.4904	0.2280E-01	483.93	0.4711E-04	0.1459E-01	0.4934E-04
1.9946	0.3317E-01	475.76	0.6972E-04	0.1426E-01	0.4872E-04
1.4988	0.7463E-01	472.70	0.1579E-03	0.1377E-01	0.4626E-04
0.9992	0.2218E 00	473.72	0.4682E-03	0.1295E-01	0.4502E-04
0.7994	0.2384E 00	489.03	0.4875E-03	0.1246E-01	0.4533E-04
0.6149	0.2467E 00	469.64	0.5253E-03	0.1181E-01	0.4286E-04
0.4074	0.6426E 00	478.83	0.1342E-02	0.1070E-01	0.3701E-04
0.1998	0.1867E 01	476.78	0.3916E-02	0.8102E-02	0.3824E-04

SAMPLE 5 CYCLE 2

STRESS PERMEABILITY DATA SUMMARY

SIGMA (MPA)	Q (CC/SEC)	DH (CM)	Q/DH (CC/SEC-CM)	MEAN D2B (CM)	DL-ROCK (CM)
0.2226	0.2239E 00	455.34	0.4917E-03	0.2541E-03	0.1233E-05
0.4213	0.1202E 00	470.66	0.2554E-03	0.3450E-02	0.2158E-05
0.6014	0.8292E-01	477.80	0.1735E-03	0.4003E-02	0.3392E-05
0.8478	0.5804E-01	467.59	0.1241E-03	0.4596E-02	0.5242E-05
1.0148	0.4457E-01	467.59	0.9532E-04	0.4884E-02	0.8018E-05
1.5208	0.3234E-01	478.83	0.6754E-04	0.5667E-02	0.1079E-04
2.0057	0.2653E-01	495.16	0.5358E-04	0.6216E-02	0.1018E-04
2.4985	0.2239E-01	502.31	0.4457E-04	0.6688E-02	0.1357E-04
2.9966	0.1990E-01	501.29	0.3970E-04	0.7073E-02	0.1634E-04
3.5106	0.1741E-01	491.08	0.3545E-04	0.7424E-02	0.1511E-04
4.0113	0.1515E-01	466.57	0.3247E-04	0.7728E-02	0.1573E-04
4.9996	0.1266E-01	453.30	0.2793E-04	0.8262E-02	0.2004E-04
7.0159	0.1068E-01	465.55	0.2294E-04	0.9106E-02	0.3207E-04
10.0072	0.8977E-02	475.76	0.1887E-04	0.1004E-01	0.4780E-04
15.0015	0.85393-02	551.31	0.1549E-04	0.1115E-01	0.9097E-04
19.9958	0.7007E-02	545.19	0.1285E-04	0.1203E-01	0.1431E-03
23.5832	0.5912E-02	537.02	0.1011E-04	0.1262E-01	0.1721E-03
20.0017	0.5912E-02	509.42	0.1160E-04	0.1233E-01	0.1397E-03
15.0121	0.6218E-02	508.43	0.1223E-04	0.1170E-01	0.9683E-04
9.9992	0.7182E-02	519.66	0.1382E-04	0.1082E-01	0.5921E-04
6.9920	0.8145E-02	509.45	0.1599E-04	0.1004E-01	0.4009E-04
4.9996	0.1060E-01	528.85	0.2004E-04	0.9295E-02	0.3176E-04
3.9981	0.1270E-01	523.75	0.2425E-04	0.8808E-02	0.2683E-04
3.5079	0.1274E-01	490.06	0.2600E-04	0.8535E-02	0.2344E-04
2.9966	0.1336E-01	476.78	0.2802E-04	0.8198E-02	0.2374E-04
2.5011	0.1480E-01	473.72	0.3124E-04	0.7830E-02	0.2004E-04
2.0030	0.1647E-01	445.13	0.3700E-04	0.7376E-02	0.1604E-04
1.4917	0.2764E-01	538.04	0.5137E-04	0.6811E-02	0.1264E-04
0.9777	0.4146E-01	536.00	0.7735E-04	0.6030E-02	0.8326E-05
0.8001	0.4561E-01	532.94	0.8558E-04	0.5667E-02	0.6784E-05
0.6067	0.6634E-01	523.75	0.1267E-03	0.5202E-02	0.8018E-05
0.3948	0.1265E 00	533.96	0.2369E-03	0.4499E-02	0.5242E-05
0.2014	0.3151E 00	512.52	0.6148E-03	0.3411E-02	0.1851E-05

REPORT OF: TEST OF GRANITE CORES

PROJECT: MATERIAL CHECK

DATE: March 20, 1973

REPORTED TO: Cold Spring Granite Co.
202 South Third Ave.
Cold Spring, MN 56320
Attn: Joe Peters

FURNISHED BY:
COPIES TO:

LABORATORY NO. 8-631A

IDENTIFICATION Charcoal Gray; West of St. Cloud, Minnesota

BULK DENSITY (ASTM:C97-47)

Type of Specimens	2" x 2" x 2" cubes		
Sample Number	1	2	3
Bulk Specific Gravity	2.72	2.72	2.72
Bulk Density (pcf)	170.9	170.9	170.9
Average Bulk Density (pcf)		170.9	

ABSORPTION (ASTM:C97-47)

Type of Specimens	2" x 2" x 2" cubes		
Sample Number	1	2	3
Absorption (%)	0.12	0.13	0.12
Average Absorption (%)		0.12	

COMPRESSION STRENGTH (ASTM:C170-50)

Type of Specimens	2" x 2" x 2" cubes		
Condition at Test	Oven dry		
Sample Number	1	2	3
Compressive strength (psi)	28,100	33,400	33,500
Average Compressive Strength (psi)		21,670	

MODULUS OF RUPTURE (ASTM:C99-52)

Type of Specimens	Approximate 4" x 2 1/4" x 8"prisms		
Condition at Test	Oven dry		
Span Length	7 inches		
Sample Number	1	2	3
Modulus of Rupture (psi)	2025	2010	1980
Average Modulus of Rupture (psi)		2005	

REMARKS

The above specimens were submitted to the laboratory and received here on February 21, 1973.

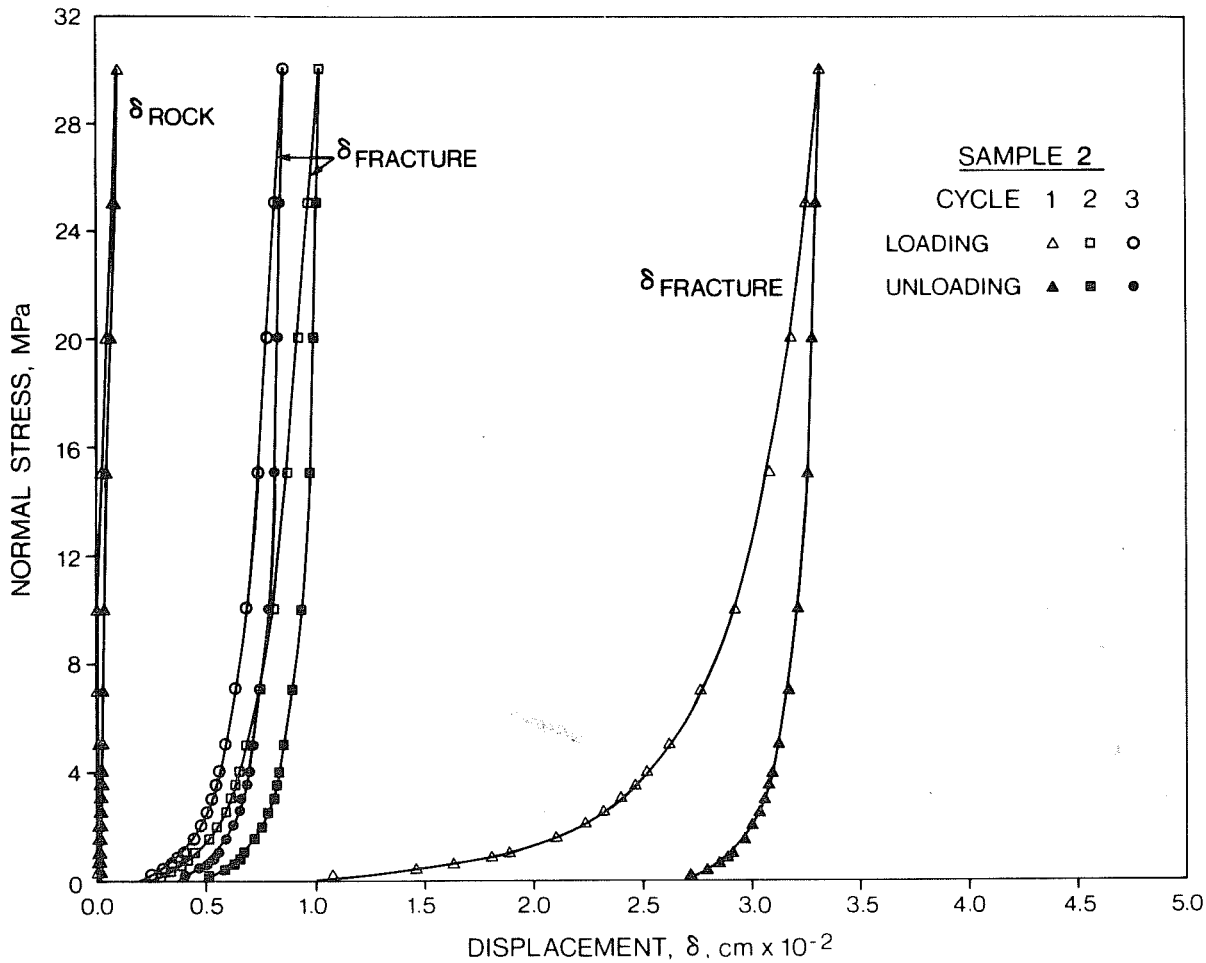

XBL 846-2221

Fig. B.1. Fracture and rock displacement as a function of normal stress, sample 2, cycles 1, 2, and 3.

This report is part of a cooperative Swedish-American project supported by the U.S. Department of Energy and/or the Swedish Nuclear Fuel Supply Company. Any conclusions or opinions expressed in this report represent solely those of the author(s) and not necessarily those of The Regents of the University of California, the Lawrence Berkeley Laboratory, the Department of Energy, or the Swedish Nuclear Fuel Supply Company.

Reference to a company or product name does not imply approval or recommendation of the product by the University of California or the U.S. Department of Energy to the exclusion of others that may be suitable.

TECHNICAL INFORMATION DEPARTMENT
LAWRENCE BERKELEY LABORATORY
UNIVERSITY OF CALIFORNIA
BERKELEY, CALIFORNIA 94720